AD NUMBER

**AD840743**

LIMITATION CHANGES

TO:

**Approved for public release; distribution is unlimited.**

FROM:

**Distribution authorized to U.S. Gov't. agencies and their contractors; Critical Technology; JUL 1968. Other requests shall be referred to Air Force Technical Application Center, Washington, DC. This document contains export-controlled technical data.**

AUTHORITY

**usaf ltr, 25 jan 1972**

AFTAC Project No. VELA T/8701/ASD
ARPA Order No. 624
ARPA Program Code No. 7F10

# FINAL REPORT
# OCEAN-BOTTOM SEISMOGRAPH PRODUCTION AND GULF OF MEXICO DATA ANALYSIS

Prepared by

Edgar G. BeAbout  Hugh K. Harris  R. Fred Howard
Benjamin F. Kimler  William A. Johnson

Benjamin F. Kimler, Program Manager
Telephone: 1-214-238-4701

TEXAS INSTRUMENTS INCORPORATED
Science Services Division
P.O. Box 5621
Dallas, Texas 75222

| | |
|---|---|
| Date of Contract: | 31 August 1967 |
| Contract Expiration Date: | 31 July 1968 |
| Amount of Contract: | $499,800 |

## ACKNOWLEDGMENT

This research was supported by the
ADVANCED RESEARCH PROJECTS AGENCY
Nuclear Test Detection Office
under Project VELA UNIFORM
and accomplished under the technical direction of the
AIR FORCE TECHNICAL APPLICATIONS CENTER
Contract No. F33657-68-C-0242



31 July 1968

AFTAC Project No. VELA T/8701/ASD
ARPA Order No. 624
ARPA Program Code No. 7F10

# FINAL REPORT
# OCEAN-BOTTOM SEISMOGRAPH PRODUCTION AND GULF OF MEXICO DATA ANALYSIS

Prepared by

Edgar G. BeAbout  Hugh K. Harris  R. Fred Howard
Benjamin F. Kimler  William A. Johnson

Benjamin F. Kimler, Program Manager
Telephone: 1-214-238-4701

TEXAS INSTRUMENTS INCORPORATED
Science Services Division
P.O. Box 5621
Dallas, Texas 75222

| | |
|---|---|
| Date of Contract: | 31 August 1967 |
| Contract Expiration Date: | 31 July 1968 |
| Amount of Contract: | $499,800 |

## ACKNOWLEDGMENT

This research was supported by the
ADVANCED RESEARCH PROJECTS AGENCY
Nuclear Test Detection Office
under Project VELA UNIFORM
and accomplished under the technical direction of the
AIR FORCE TECHNICAL APPLICATIONS CENTER
Contract No. F33657-68-C-0242

31 July 1968

## ABSTRACT

Six additional Ocean-Bottom Seismographs, similar in design and functionally interchangeable with existing units, were produced. Results of testing the new units showed that system performance is not measurably affected by the unit modifications and that the replacement Hall-Sears seismometer package is operationally similar to the EV-17 but is more dependable.

Shallow bottom sediments in the test area are highly layered, supporting several propagation modes. Shear velocities vary rapidly in these shallow sediments. Very low-velocity Rayleigh-type wave motion is observed from explosions, following refracted arrivals and higher-velocity normal modes; these low-velocity arrivals are probably dispersive Stoneley waves. Signal energy on the horizontals immediately following the refracted arrivals is a combination of leaking modes and shear modes. The dominant ambient noise appears to be isotropic and of low velocity; this results from unusually well-defined shallow mud layers and may serve to explain much of the difference between ocean-bottom and land recordings.

TABLE OF CONTENTS



APPENDIXES



LIST OF TABLES

List of Illustrations

List of Illustrations (contd)

BLANK PAGE

# SECTION I

# INTRODUCTION AND SUMMARY

Contract F33657-68-C-0242 provides for the production and testing of six additional Ocean-Bottom Seismographs (OBS) which are to be similar in design and functionally interchangeable with existing units. This work is part of a continuing program of Ocean-Bottom Seismological Measurements under the VELA UNIFORM research effort sponsored by the Advanced Research Projects Agency.

Before going into production, a field-testing program was undertaken to check out some of the proposed modifications. The key item to be evaluated was a replacement 3-component seismometer package. As a result of the tests, an Engineering Change Notice was forwarded to the monitoring agency recommending the use of a different seismometer package in the new units. The field tests also produced some significant seismological data worthy of additional analysis, which were added to the contract as Task e. Section II of this report covers this analysis work.

Upon approval of the engineering changes to the sensor package, the six new units were fabricated. Individual components were tested before assembly into the system. Tests included

- Pressure testing to 12,000 psi of beacon light, hydrophones, and bottom plugs
- Various electrical tests of all sonar receivers, radio transmitters, clocks, and amplifiers
- Shake-table testing of a representative seismometer package

After assembly, each OBS unit was given a thorough system test; then all six new units were placed in a cold-storage chamber set at 2°C for a 30-day environmental operations check.

The final task was updating and rewriting the operations manual. The following paragraphs describe various tasks of the work statement in the order in which they were performed.

## A. DEEP-WATER TESTS

### 1. Objective

The 1967 Gulf of Mexico tests investigated Ocean-Bottom Seismograph modifications to decrease the overall resonant character of the records and to improve the sensor-package leveling ability and performance. Actual sea tests were performed to confirm the reliability of the new seismometer package, to experiment with various coupling configurations, and to check system correlation between units planted in a close array.

Improved leveling and performance were to be obtained by using a Geo Space 3-component sensor package, with individual sensors arranged on a vertical axis.

Improvements in the coupling between the sensor and the sphere by using various silicon rubber pastes were planned. This change also was intended to improve the leveling ability of the sensor. Increased coupling to the ocean floor was to be gained through increased anchor weight and by placing circular feet 1 ft in diameter on the anchor legs.

No modifications of the recording or release mechanisms were made; however, a buoy, rope, and chain were attached to the anchor to insure retrieval of the units.

Three drops of four units each were scheduled. Modifications were interchanged between units to insure that any improvements or deleterious effect on the recorded data could be attributed solely to the modifications.

Ocean-current velocity and direction were measured during each recording period to correlate ocean-current data with the recordings.

## 2. Operations

Tests were conducted between 19 October and 11 November 1967, 75 mi southeast of Galveston, Texas, in the Gulf of Mexico. The M/V JUPITER, a 150-ft long by 33-ft beam quad-diesel vessel, was used instead of the M/V VIRGO, the vessel used in the Aleutian Islands Experiments, because of her previous commitments.

The drop area selected had a water depth of 200 ft and was far enough from cultural features to prevent man-made noises from contaminating the records. The water depth was determined by a free-fall weight and wire-rope measurement. A bottom profile was not made because the ship's fathometer transducer was inoperative; however, an over-the-side transducer was used to make spot depth measurements.

Navigation utilized Loran A, radar, and deadreckoning. Accurate navigation was not required except to locate all drops in the same area. Marker buoys were used to relocate the drop zone. Each of the two Loran-A lines (3H0, 3H1) was accurate to ±1/2 mi but, because of the small angle of intersection, a Loran fix could be in error by as much as 10 mi. A radar fix on an active drilling rig 17 mi away was used as an additional checkpoint. One deadreckoning run of 8 hr in calm seas missed the marker buoys by 1 min (1/10 mi) of the original estimated arrival time. Marker buoys were located on a subsequent run in heavy seas by using the 3H1 Loran-A line as a course and traveling up and down this line for 1 mi from the deadreckoning location. The buoy was located on the third pass. The drop-1 marker buoys (styrofoam) were lost in a storm, and marker buoys for drops 2 and 3 were located approximately 1.5 mi southeast of drop 1.

Core samples taken at the drop locations showed the bottom to be blue clay, shells, and sand.

Radio communications were maintained with TI Dallas through the TI commercial station at Berwick, Louisiana, and through the ITT terminal in Galveston. Fading conditions limited the Berwick contacts to early morning, and the Galveston contacts were limited by the heavy traffic load carried by that station. On several occasions, communications were relayed through the TI ship M/V CECIL GREEN to Berwick and then to Dallas.

To have concurrent recording periods, four people simultaneously reset all clocks, with WWV recorded on only one unit. No attempt was made to maintain precise time (±0.1 sec) on the units or to time the 33-lb detonations accurately.

3. Conditions

All units were moored to prevent possible loss of a unit. Decoupling from the mooring was accomplished by attaching a chain to the anchor. The chain itself was anchored by a 100-lb weight. Figures I-1, I-2, and I-3 show the overall mooring system. In case of recall-system failure, the unit and anchor were retrieved using the 1-in. rope. Units were dropped in 200 ft of water. Figure I-4 shows the approximate configuration around the marker buoy. Exact distances between units are not known, however, minimum separation is estimated to be 50 ft and maximum separation about 400 ft. Oceanographic survey reports show the water temperature to be 19°C (±2°).

a. Drop 1

The recording period for drop 1 was from 1600Z on 21 October to 1600Z on 23 October. Seas and weather were calm through the entire recording period. Two 33-1/2-lb charges were detonated 1 mi from the units. The first shot was 30 ft deep at 1745Z on 22 October, and the second was 60 ft deep at 1758Z on 22 October. While the units were on the bottom, a seismic (explosive) crew in the area detonated a shot approximately every 2 min.

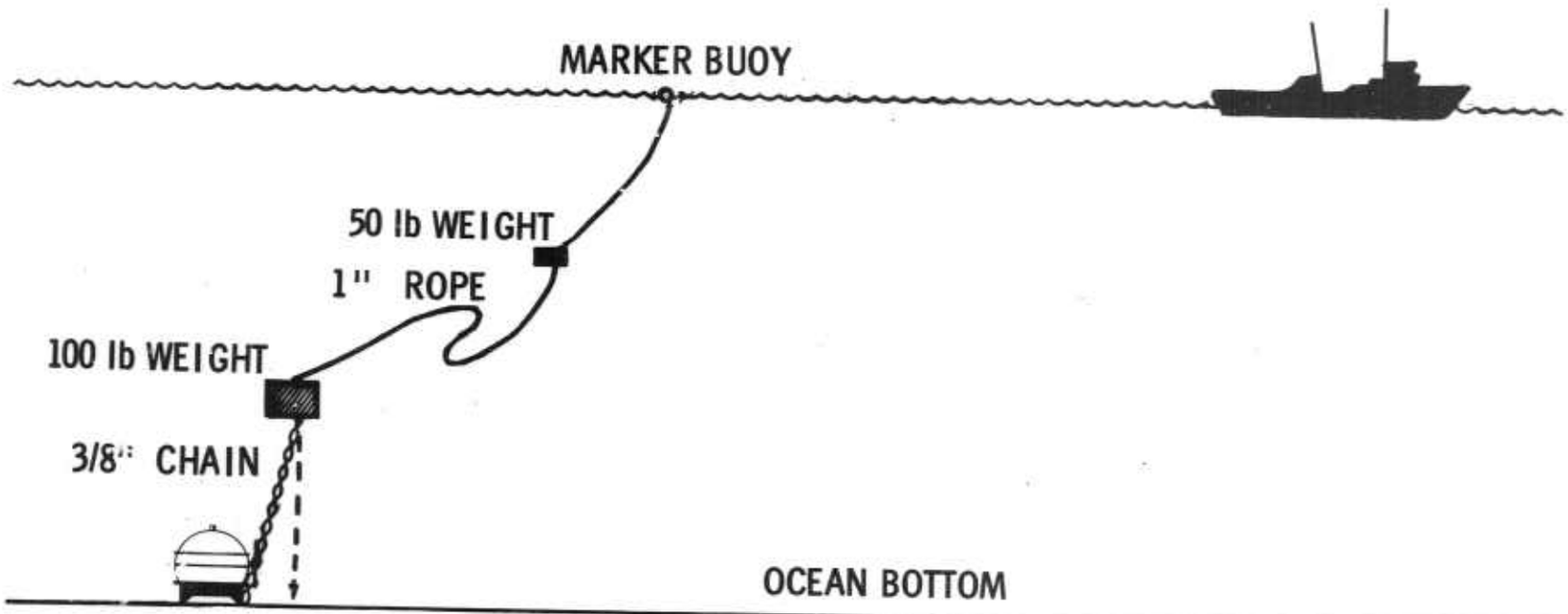


Figure I-1. Drop 1 Instrument Configuration

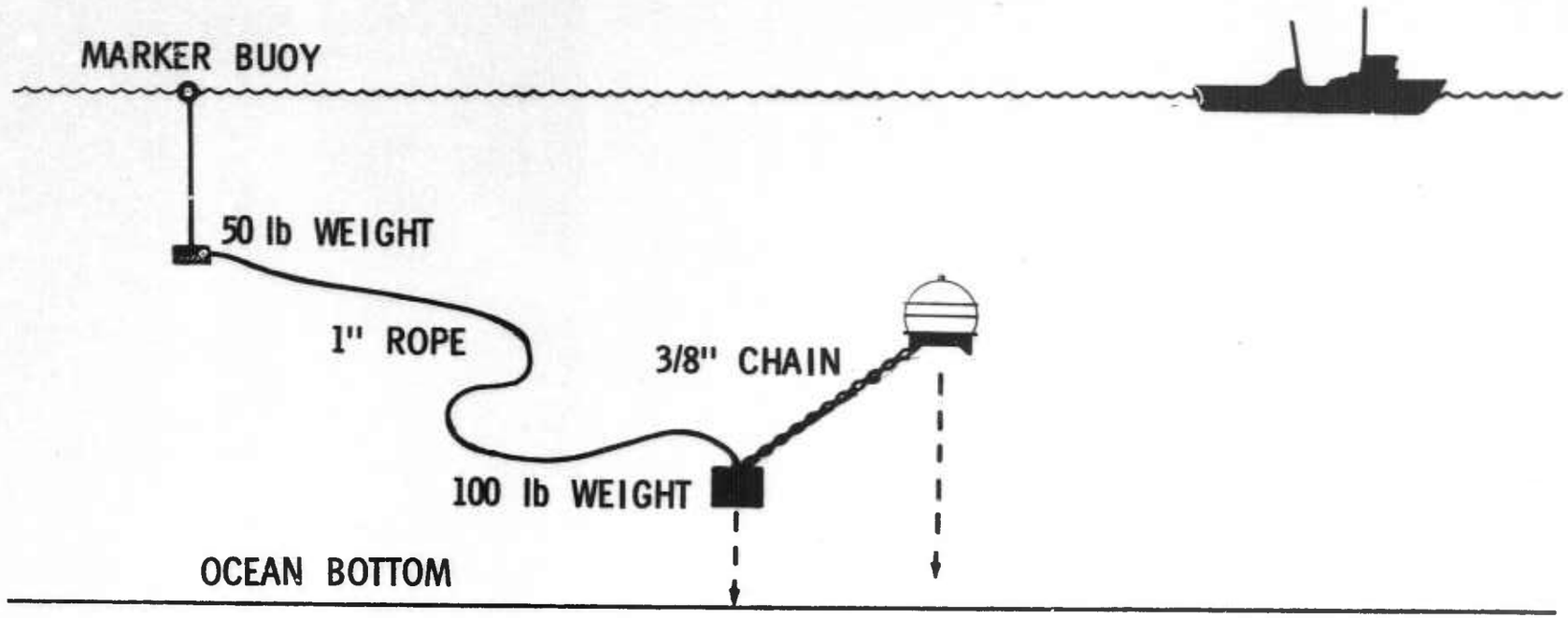


Figure I-2. Drop 2 Instrument Configuration

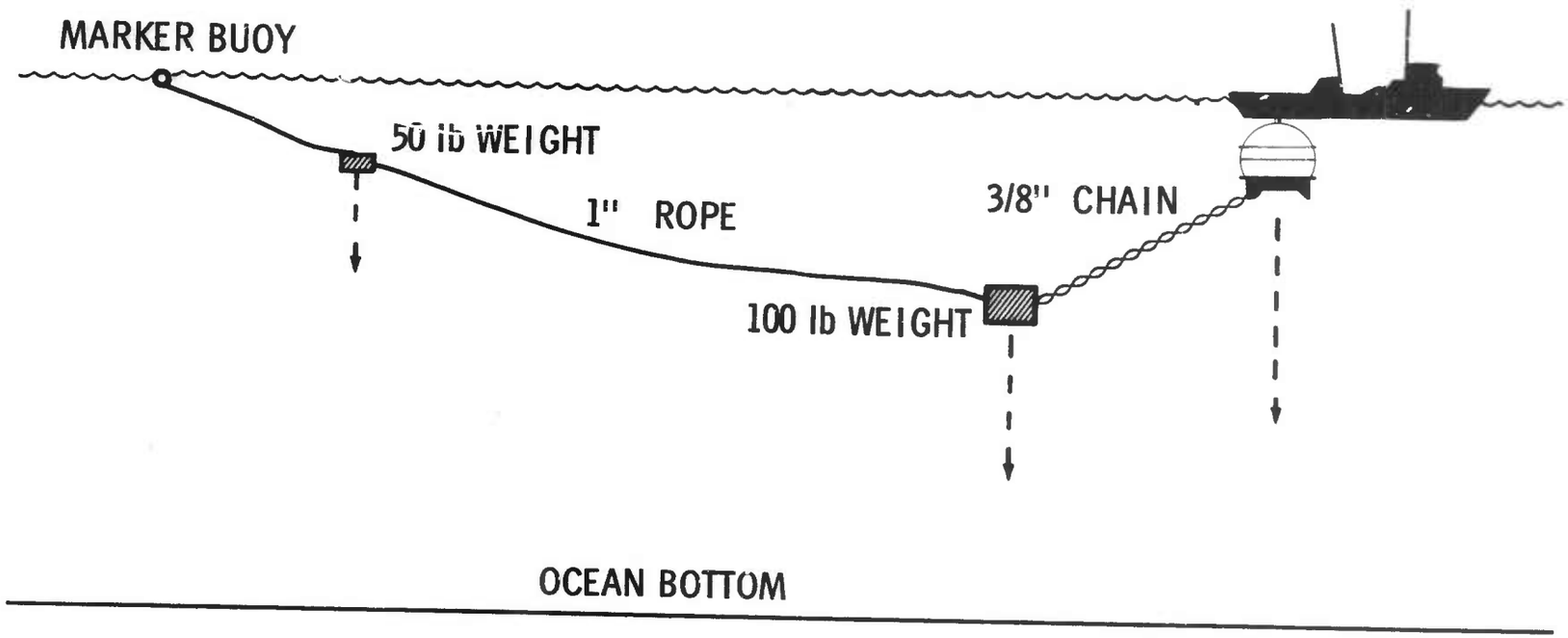


Figure I-3. Drop 3 Instrument Configuration

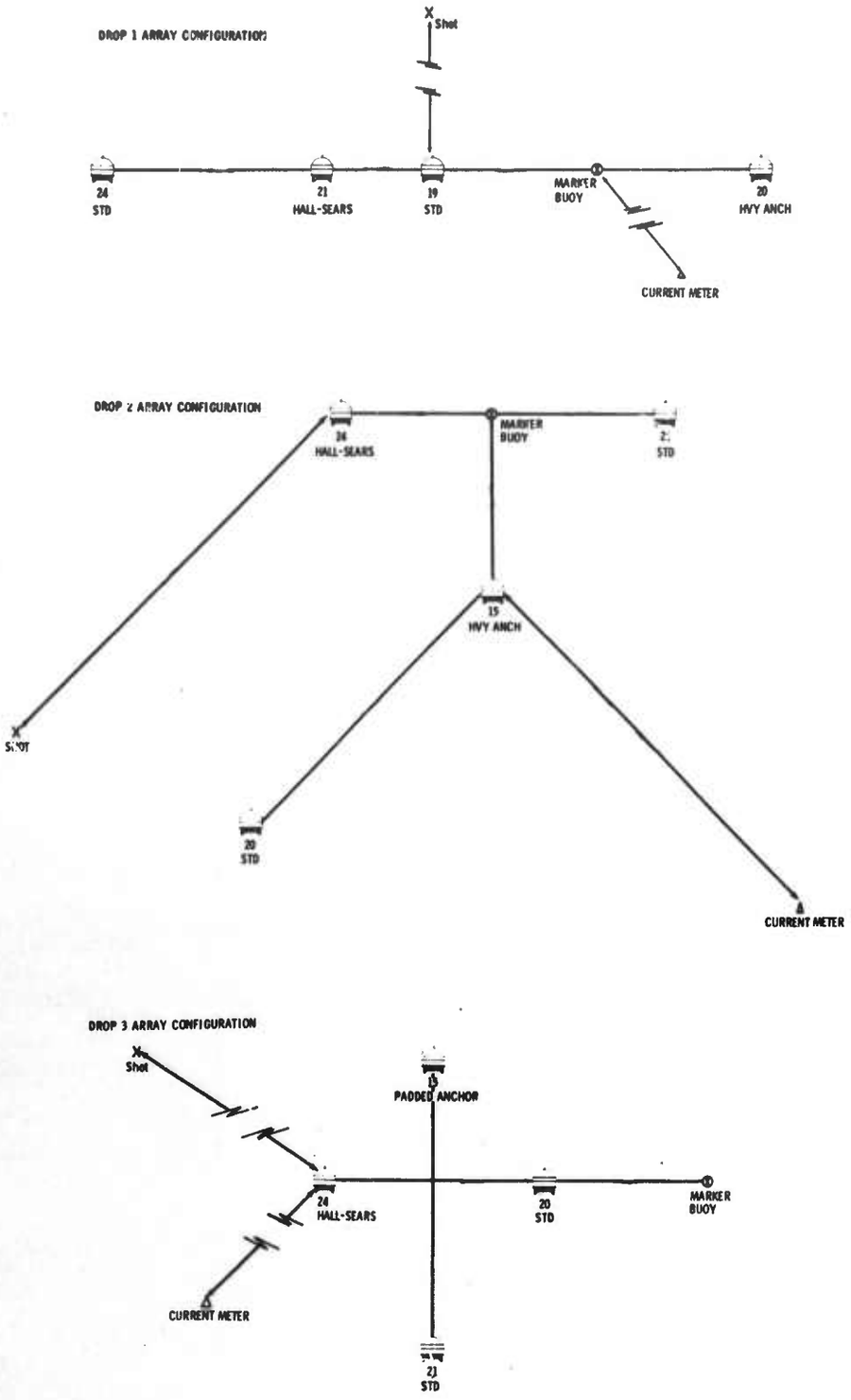


Figure I-4. Approximate Location of Units Around Marker Buoy (minimum separation between units is about 50 ft, and maximum separation is about 400 ft)

b. Drop 2

The recording period for drop 2 was from 1625Z on 27 October to 1400Z on 29 October. A frontal system passed through the drop zone at 1815Z on 27 October, with winds from 10 to 15 knots and seas of 5 to 6 ft. The disturbance continued until 0200Z on 28 October. Seas for the remainder of the recording period remained at 3 to 4 ft. Two 33-1/3-lb charges were detonated 1/4 mi from the units. The first shot was at 1616Z on 28 October at a 30-ft depth, and the second was at 1626Z on 28 October at a 7-ft depth. A sparker seismic crew mapped the area and came within 4 mi of the units.

c. Drop 3

The recording period for drop 3 was from 1530Z on 2 November to 1300Z on 4 November. Seas were calm until 1630Z, 3 November, when a frontal passage increased the seas from 3 to 6 ft. Winds increased to 40 knots during the next 12 hr with seas of 12 to 15 ft which persisted to the end of the recording period. Two 66-2/3-lb charges were detonated at 200 ft from the units. The first shot was at 1450Z on 3 November at a 30-ft depth, and the second was at 1502Z on 3 November at a 7-ft depth.

4. Performance

a. Drop 1

The OBS unit was launched first, followed by chain, weights, rope, and buoy. No difficulty was experienced with the launch; however, the possibility of the mooring chain and weights falling directly onto the unit was immediately apparent (Figure I-1).

Sonar recall was attempted on all units. Unit 21 responded immediately, and unit 20 responded after approximately 10 min. Units 19 and 24 did not respond to 2 hr of sonar sounding at various power levels and ship positions.

All units were in the immediate vicinity of the ship and were located visually. Batteries had been removed from the beacon lights because of insufficient water depth to activate the pressure turn-off switch. The radio transmitter operated immediately on unit 21 but did not operate on any of the other units until they were on deck.

Units 21 and 20 released normally and were recovered without difficulty. Unit 24 (with anchor) was retrieved from the bottom by using the buoy line; however, the unit broke from the anchor and was retrieved by normal procedures from the floating position. Unit 19 (with anchor) was retrieved from the bottom with the buoy line and deliberately released from the anchor by manually breaking the release fuse wire. The unit then was recovered normally from the floating position.

b. Drop 2

Buoy, rope, chain, and weights were launched preceding the OBS unit in an attempt to keep the chain away from the units (Figure I-2).

All units were released by the Bulova clock at the preset time. The beacon lights were disconnected as in drop 1. All the transmitters operated properly while the units were floating in the water in spite of relatively heavy seas.

Unit 20 was recovered without difficulty. Unit 24 went under the ship, and its light was destroyed. External leads were broken during recovery on unit 15. The bail on unit 21 was broken as the ship rolled during recovery.

c. Drop 3

Buoy, rope, chain, and weights were launched and towed by the ship prior to release of the OBS unit (Figure I-3). This technique undoubtedly increased the uncertainties in the estimated spacing of the instruments.

All units were released by the Bulova clock at the preset time. Transmitters for units 15 and 21 were operating properly in heavy seas. The unit-20 transmitter was inoperative, and the unit was visually sighted approximately 5 hr after the release time. The unit-24 transmitter began operating after an unknown period (several days), and the unit was located 7 days after the release time. It is unknown whether unit 24 was on the bottom or on the surface for this 7-day period; however, all power had been turned off at the backup-clock release time. All units were recovered without damage.

5. Observations

A 3° to 5° tilt toward the heavy battery side of the sphere resulted when the units settled into the clay ocean floor. Clay markings on the anchors after retrieval (including those modified) indicate that the blue clay covered approximately two-thirds of the anchor.

The silicon rubber pastes remained in a more pliable state in the Gulf of Mexico than that experienced during the Aleutian Islands Experiment. This pliable state permitted the sensor packages to relevel by the time the lids were removed after recovery, and it can be reasonably assumed that this ease of leveling also existed on the Gulf floor.

Insufficient ocean-current data were obtained to correlate the current effects on the seismic data. The 28 hr of recording obtained during drop 3 indicated that ocean-current speed never exceeded 0.06 knots.

6. Operational Conclusions and Recommendations

The deep-water tests result in the following conclusions and recommendations.

- OBS units can be moored without contaminating the seismic records by decoupling the mooring through a chain.

- To insure nearly 100 percent anchor-release probability, the release fuse wire can be electrically fired from the surface when using a buoyed system.
- A pressure switch, paralleling the transmitter salt-water short system, is needed to insure that the transmitter will operate upon surfacing. (Note: This has been accomplished under a parallel effort for Contract No. F33657-68-C-0875.)
- A corrosive link should be incorporated in the release mechanism to insure anchor release if the electrical system should fail.
- Low-value pressure switches should be provided to permit use of the beacon light in shallow-drop locations.
- The anchor weight could be increased without difficulty; however, the circular anchor feet are not recommended for general use. The current track system used for movement of the OBS units aboard ship would be unusable in conjunction with the circular feet.
- The mixture of silicon compound and bouncing putty proved more pliable and easier to handle than the bouncing putty alone.

## B. PRODUCTION OF OCEAN-BOTTOM SEISMOGRAPHS

The six new OBS units designated as the Mark V models were to be operationally compatible and interchangeable with the existing units produced under previous programs. The primary modification which was dictated by previous field experience and then tested in the Gulf of Mexico was the substitution of the HS-10 seismometer package for the EV-17. This modification was justified through an engineering-evaluation and field-tests report to AFTAC according to an Engineering Change Notice dated 19 January 1968. Other modifications were minor and resulted in no loss of interchangeability. These minor changes included the substitution of a different semiconductor network (used in the clocks) to replace a discontinued type, use of a new-

model transmitter board which increased the reliability of the radio beacon over the manufacturer's older model, and use of a new-model operational amplifier replacing the older discontinued type. Most of the fabrication and manufacture was performed within Texas Instruments facilities in Dallas, Texas. The one large outside purchase was the 41-in.-diameter spun aluminum spheres. These were produced by Phoenix Products of Milwaukee, Wisconsin.

The 30-day Ocean-Bottom Seismograph (Figures I-5 and I-6) is described as a completely self-contained, free-fall, unattended, untethered, retrievable seismograph system capable of recording seismic information continuously for 30 days at depths to 25,000 ft. Units are designed to provide a maximum of 40 days' bottom time and up to 2 weeks of beacon signaling after surfacing.

Data sensors for the OBS consist of a 3-component (one vertical and two horizontal) velocity-type seismometer system and a pressure-change sensing hydrophone. All four sensors are input to TI Model RA-6 amplifiers and then to trilevel (x1, x10, and x100) operational amplifiers, thus producing 12 data channels which are recorded on a slow-speed (0.0075) ips) 14-channel magnetic tape recorder. A digital time code and a 12.5-pps tape-speed reference signal are recorded on the two remaining tape channels. The digital clock which supplies these last two signals also may be programmed to release the OBS from the bottom at any desired day from 1 to 40 after reset.

The OBS is released by burning a short length of steel fuse wire in the spring-loaded release mechanism. Upon release, the 335-lb expendable anchor is detached, and the buoyant instrument package rises to the surface. Normally, release is accomplished by sonar command; however, if this system should fail, either the digital clock or the backup clock may effect release at a programmed time.

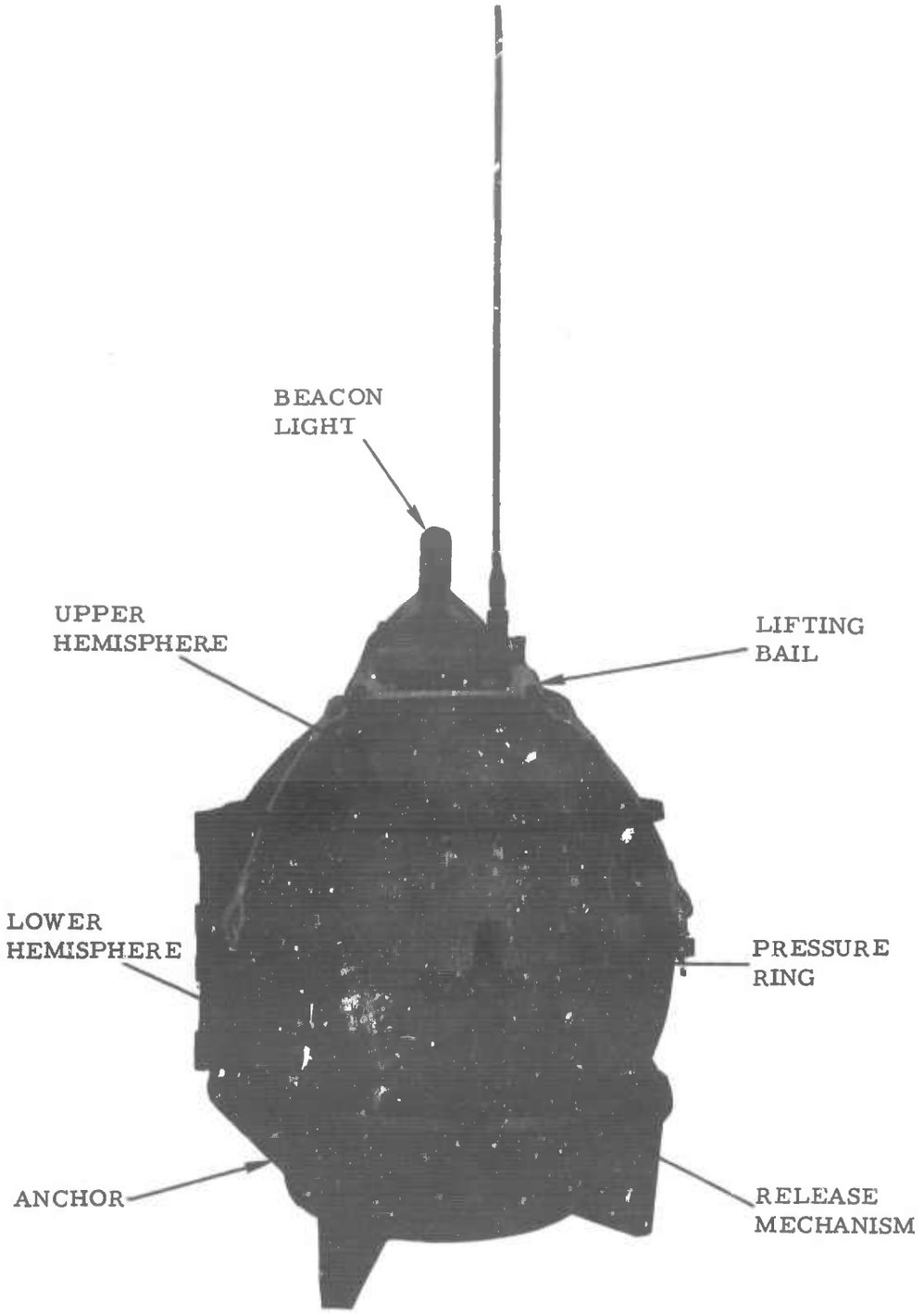


Figure I-5. External View of 30-Day Ocean-Bottom Seismograph

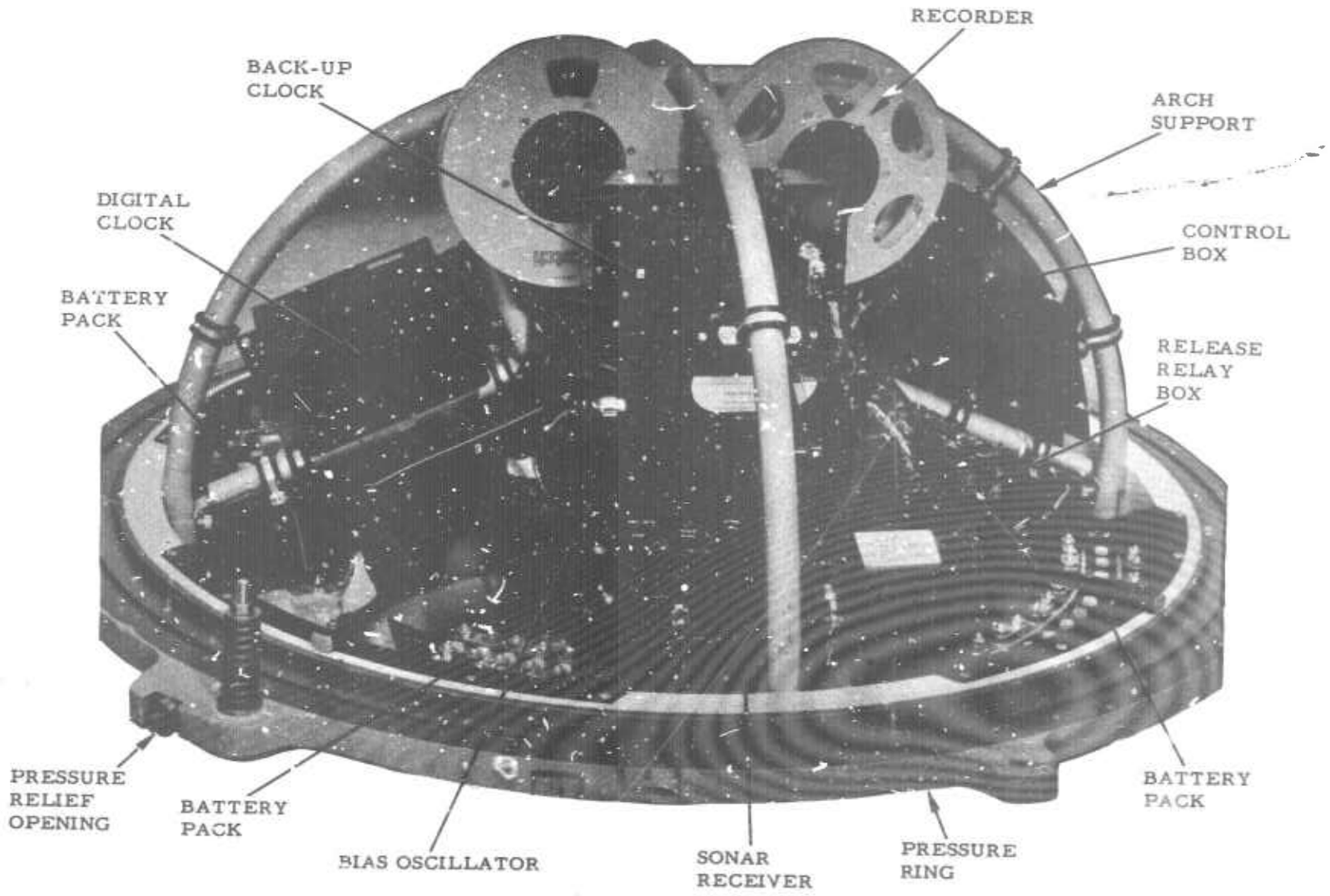


Figure I-6. Internal 30-Day Ocean-Bottom Seismograph Instrumentation

Upon surfacing, a flashing beacon light and a pulsed radio beacon are turned on automatically. The harness and bail assembly design provides for easy attachment of a snap hook for overhead lifting.

Appendix A gives electrical and mechanical specifications of the OBS.

## C. TESTING OF OCEAN-BOTTOM SEISMOGRAPHS

A complete test of an OBS unit consists of an operational drop to near-maximum-specification depths for a period in excess of 30 days. All environmental factors (pressure, time, temperature, currents, corrosion, weather, and wave and implantation motion) and all the stresses of physically handling the unit are present only in such a test. Since it is not feasible to drop a unit without some testing, subsystems and completed units are subjected to simulated tests which approximate the environmental conditions. It is therefore necessary and appropriate to devise and specify tests which can be performed in the laboratory during the manufacturing cycle. This is also a good manufacturing procedure and complies with the quality-assurance program that is an inherent part of TI's production processes.

A unit-test-specification drawing is part of the required assembly drawings on each subsystem or "black box." Appendix B gives a list of the applicable unit-test drawings. The unit-test-specification drawing shows the test configuration, lists the test equipment required, and details the test parameters to be checked. Whenever a voltage, current, frequency, etc., must be measured, the test specification shows the nominal value and gives the permissible tolerance limits. With each unit-test drawing is a reproducible unit-test data sheet. The unit-test technician completes the data sheet as he checks the subassembly. After completion, the data sheet is filed with the permanent record file of the OBS system to which the subassembly becomes a part. This permanent file is available in the TI plant at any time.

In addition to the unit-test specifications, complete OBS system test procedures and special procedures such as shake-table tests or 30-day environmental tests are provided.

The majority of the unit tests are readily performed on the laboratory workbench using standard test equipment and instrumentation. These tests check such parameters as amplification, voltage or current readings, output power, frequency, sonar coding, sensitivity, and polarity to prove proper operation of the units.

A few of the unit tests require special equipment. These tests are described in the following paragraphs.

1. Pressure Testing of Bottom Plugs, Beacon Lights, Hydrophones

Bottom plugs were tested in a TI pressure chamber. Plugs were attached to a specially designed test fixture and subjected to pressures of 12,000 psi while outputs of the Mecca terminals were monitored for electrical leakage. The slightest amount of water leakage would be indicated immediately on the monitor.

Beacon lights and hydrophones were too large for the TI test chamber. A larger test chamber at Jet Research Corporation was utilized to test these two units. Beacon lights were tested for operation to 12,000 psi without water leakage. The hydrophone test is more complicated. Operation of the hydrophone is dependent upon both mechanical and electrical characteristics. Pressure changes on the crystals (mechanical energy) are transduced to electrical output. Output characteristics are dependent upon the rate of change and impedance. The impedance changes with the mechanical coupling of crystals (capacitance) and the resistance between terminals. These parameters were recorded while testing under pressures to 12,000 psi. All test results are on file in the permanent record book.

2. Shake-Table Testing

The unit tested was one of the new HS-10 3-component seismometer packages. Tests were conducted using GFE equipment at Geotechnical Corporation and were limited to the vertical component only. Results of these tests were submitted in an earlier report.[1] Results of these tests, together with other electrical and mechanical comparisons, provided the technical justification to recommend that the HS-10 seismometers be substituted for the EV-17 seismometers. Concurrence with this recommendation was received.

3. 30-Day Environmental Test

It is impossible to simulate all the environmental forces which act upon the units, but temperature and time can be simulated. A refrigerated trailer van of the type used to transport fresh produce was leased and parked at the TI manufacturing facility. The van, 40 ft long by 8 ft wide, carried its own refrigeration plant and thermostat controls for temperature regulation. The temperature was set to 36°F, equivalent to average ocean-bottom temperatures of approximately 2°C. A chart recorder continuously recorded the inside temperature of the van.

The six new OBS units were modified so that important test points could be monitored. In addition, a standard time signal was fed into each unit from the central timing system. Thus, each OBS clock had a common standard time against which it could be calibrated. External monitoring consisted of

- Daily recorder motor current measurements and recording
- Daily sample strips of clock output
- A single vertical component output for observation of noise levels
- Temperature

At the beginning of the test, all systems were reset simultaneously and then sealed. Amplifier attenuation controls were set much higher than normal due to the noise level of the test chamber. However, the seismic level often was higher than the saturation level of the tape.

At the end of the 30-day test, all tapes were transcribed to 16-mm film which was inspected for system operation. A sample ensemble of film was spliced and forwarded to the AFTAC project officer, along with an evaluation of all the test results.

At this time, all six new OBS units were given a final check before inspection and acceptance by the Government.

## D. PREPARATION OF OPERATIONS MANUAL

The many modifications and engineering changes in the OBS units during the past 2 years necessitated a complete revision of the operations manual. The manual contains operating and maintenance information for the OBS and auxiliary shipboard equipment required for OBS support during field operations. All three OBS configurations (Mark III, Mark IV, and Mark V) are included in this manual, and the information presented pertains to all configurations unless otherwise noted. The manual does not attempt to duplicate the instructions and operations included in vendor manuals supplied with auxiliary systems, e.g., Precision Instruments tape recorder, Honeywell Visicorder, various power supplies, Cadre transmitters, WWV receivers, automatic direction-finder equipment, Collins transceiver, precision depth recorders, Omega-VLF navigation system, and other similar gear. An effort is made to maintain a file of vendor manuals.

The manual, in addition to an introductory section, includes sections on theory of operations, system test and calibration, operating instructions, and schematic diagrams. The manual is written so that a technician with minimum training can operate the system and so that a good technician has all the information needed to understand and maintain every part of the system. All parts of the circuitry can be traced through the circuit diagrams and schematics. For convenience, all drawings have been reduced to a maximum size of 11 by 17 in. The very liberal use of many figures and pictorials makes the manual easy to understand and use.

# SECTION II

# ANALYSIS OF GULF DATA

## A. INTRODUCTION AND SUMMARY

Analysis of digitized data samples from the Gulf of Mexico recordings was undertaken to evaluate the seismic performance of the various OBS units. Principal objectives of the analysis included

- Evaluating total system performance in terms of seismic validity
- Comparing the performance of the Hall-Sears and the EV-17 3-component seismometer packages
- Determining the effect of various unit modifications on system performance
- Defining system instrument noise levels and the usable seismic spectrum

Following the system evaluation, an effort was made to model the signal and noise characteristics measured by the four units and to obtain from the model a consistent interpretation of the various observations.

Both system performance and seismic modeling employed spectral analysis of signal energy density and noise power density. This method yields amplitude and coherence as a function of frequency, thus allowing a fairly direct investigation of the modal content and the directionality of waves traversing the instrument-array site. In addition, rather extensive visual analysis of signal recordings obtained from nearby geophysical exploration operations was conducted. Dispersion models were fit to the observed data.

In general, the data were well-recorded. Noise levels were appreciably higher than those in the Aleutian Islands: visual measurements from film for drop 1 indicated peak noise levels at about 1 Hz of approximately 0.5-micron ground motion as opposed to 0.1 to 0.2 microns in the Aleutian Islands. During drops 2 and 3, noise levels were from 3 to 6 db higher than during drop 1; the increase was apparently related to local storm fronts. With the exception of the pressure channels, the x10 and x100 channels were generally overdriven; thus, the x1 channels were used for analysis.

Two major instrumental problems were noted: gain variations in certain channels (possibly related to the switching connections) and some difficulty in leveling the EV-17 horizontal instruments. Bottom slope was estimated at 5° in the vicinity. No problems were experienced with the Hall-Sears seismometers; however, amplifier adjustments inadvertently resulted in an overall response curve significantly different from the EV-17 above 1.0 Hz. Otherwise, the Hall-Sears system was more dependable. The heavy anchor, padded anchor, and different silastic modifications produced no measurable change in unit performance.

The quality of the seismic data is generally excellent. Noise power-density measurements indicate that most of the recorded energy is concentrated between 0.5 and 3.0 Hz. Below 0.5 Hz, ambient noise is greatly attenuated by the system response; recorded energy appears to be nonseismic. Peak power is concentrated in the 1.0- to 1.25-Hz range. Above 1.25 Hz, noise power decreases exponentially and approaches system noise levels again above 3.0 Hz.

Both signal and noise analyses suggest that the shallow mud sediments are highly layered, supporting several propagation modes over short distances. Signal analysis reveals the presence of a very-low-velocity

Rayleigh-type wave (500 fps near 1.5 Hz) appearing primarily on the vertical-component instruments. For wavelengths much smaller than the layer thicknesses of the semiconsolidated (i.e., fairly rigid) sedimentary beds underlying the soft mud veneer at the water-earth interface, this mode of propagation is identical to the dispersed Stoneley wave described by Davies.[2] A study of digitized noise data obtained from the four OBS units also suggests that the predominant vertical-component noise is propagating with a surprisingly low velocity. Pressure-vertical amplitude ratios and interunit coherences indicate isotropic noise around 1 Hz, with a phase velocity on the order of 800 fps.

Because of the short wavelengths and the isotropic nature of the noise, seismometer spacings were generally too large for measurable interunit coherence. An exception was drop 1, where both pressure and vertical instruments indicated coherent energy.

Intraunit pressure-vertical coherences were high for all units, with 90° phase shifts observed between pressure and vertical. A 180° phase shift was observed between the Hall-Sears and the EV-17 vertical-component instruments. Improper polarization of the EV-17, resulting from ambiguous polarity tests during instrumentation checkout, caused the phase shift.

Horizontal-component noise (and signal) was modal and complex. A large part of the horizontal noise component appears to consist of Love-mode energy, and vertical-horizontal coherence was correspondingly low. During drops 2 and 3, a considerable amount of high-frequency energy (4.0 to 6.0 Hz) was detected on the units nearest the ship. This energy attenuated rapidly with distance and is believed to be directional Love-mode energy produced by the ship. In addition to the low-velocity Rayleigh-type signal, higher-velocity Love- and Rayleigh-mode energy was observed on the horizontals. The distribution of modal energy is strongly affected by the seismic source, and there has been no attempt to derive these experimental results theoretically.

In summary, the seismometers performed well, particularly the Hall-Sears. Even on the x1 channels, system noise levels were appreciably down from recording levels (with the exception of Px 1). The data are seismically valid and interpretable in a spatial sense. Particular insight into the validity of the horizontal recording is obtained from the combined analysis of the noise samples and the set of short-range shot recordings.

The modal character of the data traces indicates the presence of well-defined layers of unconsolidated sediments in the top 300 ft of the oceanic crust. With regard to differences in OBS observations and standard land observations, a better understanding of the role and importance of modal propagation of seismic energy through these very soft (low-rigidity) sediments becomes essential.

## B. PREPARATION OF THE DATA ENSEMBLE

The analysis program was conducted using data recorded in the Gulf of Mexico with an array of four OBS units. The units were dropped three different times, all in the same approximate area (Figure II-1). Two-day recording periods were obtained for each drop. As a part of the experiment, two chemical explosions were detonated during each drop at distances varying from 200 ft to 10,000 ft from the array.

Additionally, numerous signals resulting from detonations set off by a nearby seismic exploration crew were recorded and used in the signal analysis because of their generally good signal-to-noise ratios. Resulting seismic profiles also are shown in Figure II-1. An x-y plot of the seismic profiles in Lambert coordinates, with individual profile shot locations, is presented in Figure II-2 and may be used to determine shot-to-OBS array distances.

Modifications were made to certain instruments prior to each drop (Figure II-3). Unit 19 was damaged during drop-1 recovery operations, and unit 15 was substituted. Modifications were switched between units before each drop so that unit-related effects could be separated from operational changes related to the modifications.

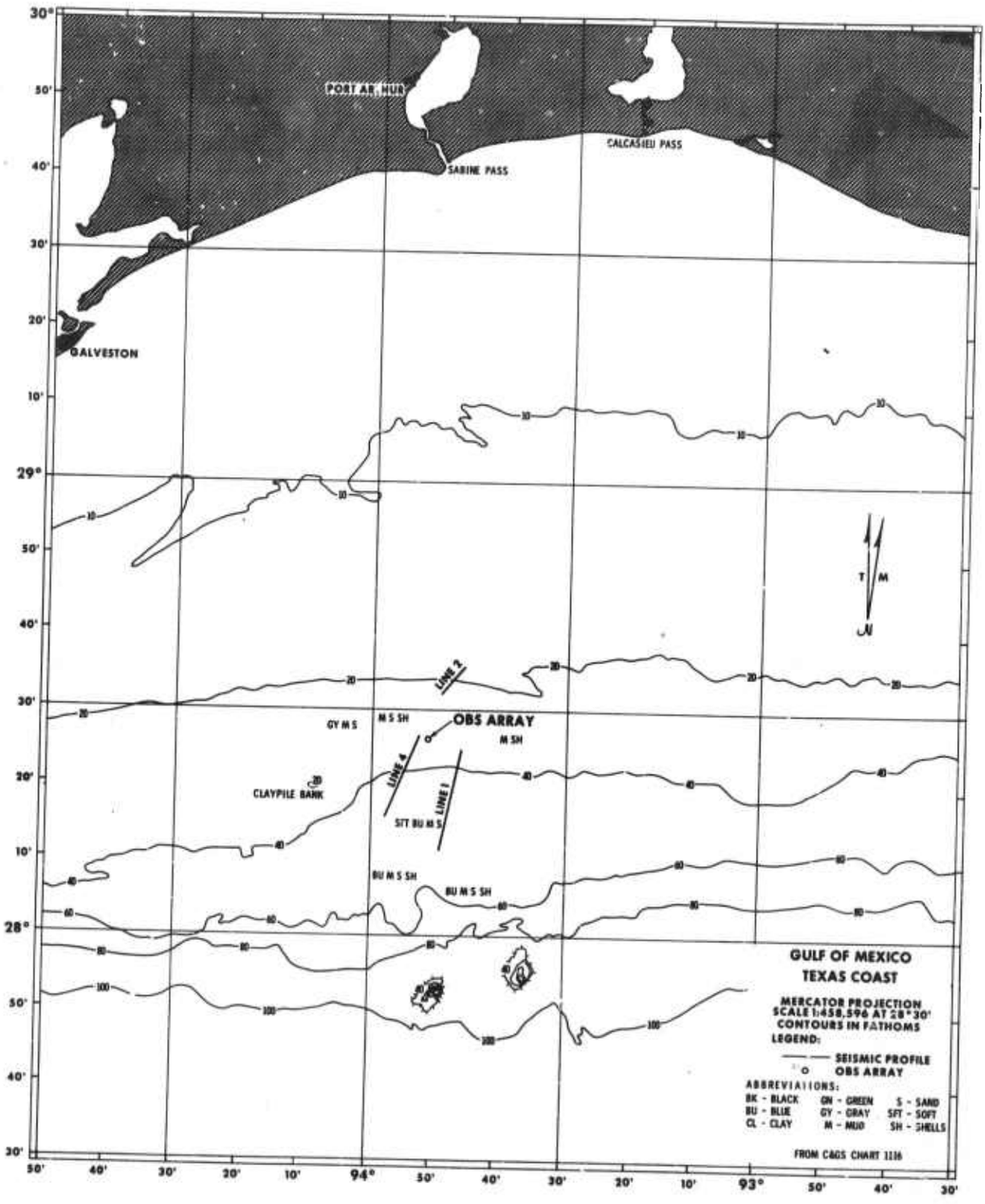


Figure II-1. Gulf Coast Instrument and Seismic Profile Locations

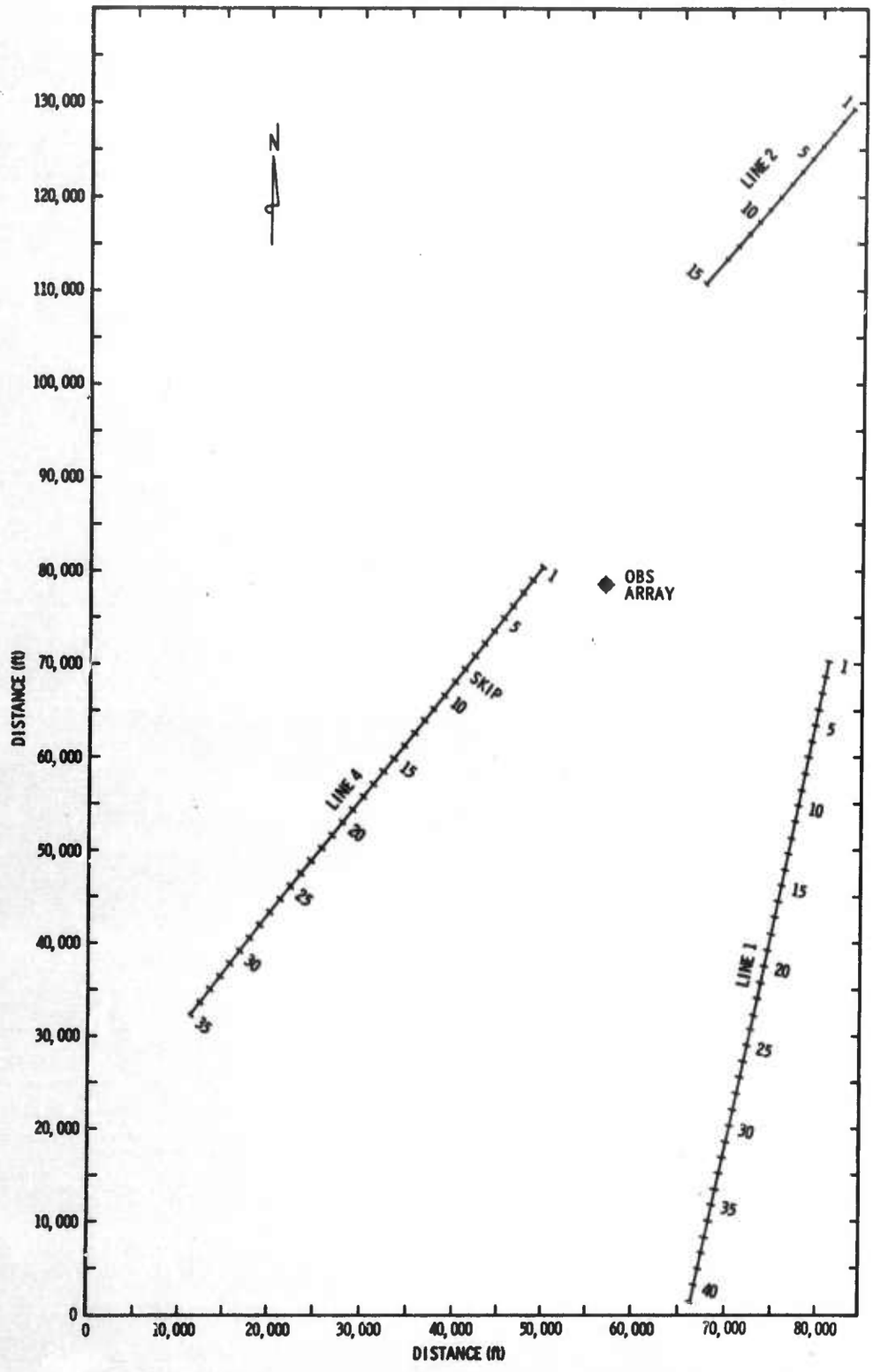


Figure II-2. x-y Plot of Seismic Profiles in Lambert Coordinates

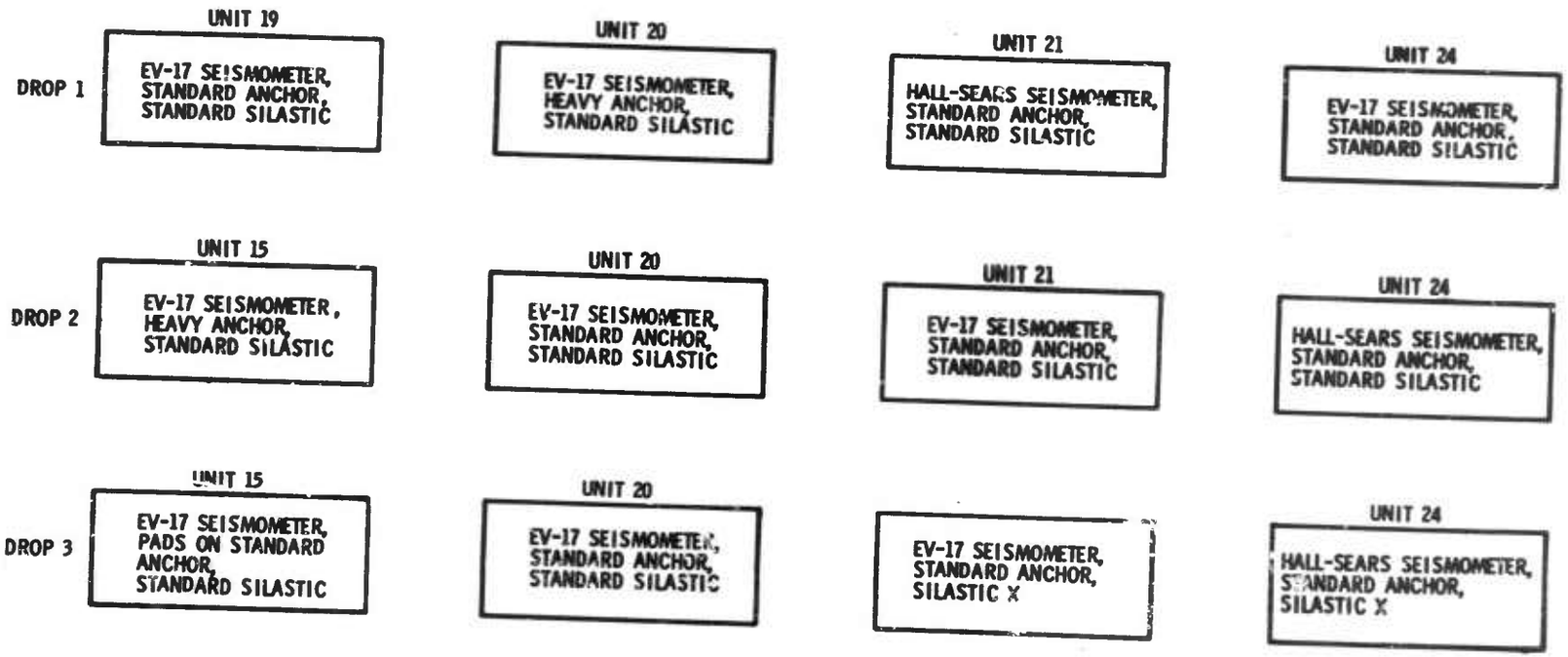


Figure II-3. Gulf Coast Experiment Instrument Modifications

Two data samples were selected for digital analysis from each drop. Each sample represented approximately 6 min of data and included a signal from one of the explosive detonations. The signal in each case was preceded by enough data to obtain an estimate of the ambient noise. Table II-1 summarizes the digitized data ensemble. Listed sample times are relative to the quoted unit reset time.

These data samples were field-recorded at 0.0075 ips. During the analog-to-digital transcription process, playback was at 0.234 ips, resulting in a 0.03125-sec digital sampling interval (32 samples/sec) and a Nyquist, or folding, frequency of 16.0 Hz. Initial examination of the digital data revealed an unusually high level of system noise, which was traced to the transcription equipment. Some preliminary processing and analysis was conducted using these data.

Most of the noise and signal energy appeared to be located below 6 Hz; thus, a 2-to-1 resampling appeared to be advantageous. Following modifications to the transcription equipment, the data ensemble was redigitized at a 16 sample/sec rate, yielding a 0.0625/sec sample interval and a folding frequency of 8.0 Hz. Antialias filters using a 6.0-Hz corner frequency and a 35-db/octave rolloff rate were applied to the data before digitization.

A library of permanent playbacks of the data ensemble was compiled. In addition, direct analog playbacks were made for many additional signals from the seismic exploration program. Processing data gates were determined, and considerable visual analysis was conducted from these playbacks.

## C. EVALUATION OF UNIT PERFORMANCE

Figure II-4 presents a flow chart of the data analysis program.

For purposes of discussion, analysis results are grouped into two categories: ambient noise analysis and signal analysis. The conclusions and observations are based on the study of several hundred spectra and coherences; therefore, in the interest of brevity, only a representative few are shown in illustration and support of the points under discussion.

## Table II-1

## GULF COAST DIGITIZED DATA ENSEMBLE

| Unit | Drop | Event | Sample Time d | Hr | Min | Sec | Unit Reset | Remarks | Noise Gated (min) | "P" Phase Signal Gate (sec) | "Rayleigh Wave" Gate (sec) |
|---|---|---|---|---|---|---|---|---|---|---|---|
| 24 | 1 | 1 | 00 | 07 | 38 | 30 | 1300 GCT | $H_2$ bad | 3.0 | 12 | 17 |
| | | 2 | 01 | 00 | 26 | 30 | 10-21-67 | $H_2$ bad | 3.0 | | |
| | 2 | 1 | 01 | 04 | 41 | 30 | 1130 GCT | | 3.1 | | |
| | | 2 | 01 | 04 | 51 | 30 | 10-27-67 | | 3.1 | | |
| | 3 | 1 | 01 | 01 | 46 | 30 | 1255 GCT | | 2.2 | | |
| | | 2 | 01 | 01 | 59 | 30 | 11-2-67 | | 2.2 | | |
| 21 | 1 | 1 | 00 | 07 | 38 | 30 | 1300 GCT | | 3.0 | 12 | 17 |
| | | 2 | 01 | 00 | 26 | 30 | 10-21-67 | | 3.0 | | |
| | 2 | 1 | 01 | 04 | 41 | 30 | 1130 GCT | $H_2$ bad | 3.1 | | |
| | | 2 | 01 | 04 | 51 | 30 | 10-27-67 | $H_2$ bad | 3.1 | | |
| | 3 | 1 | 01 | 01 | 45 | 30 | 1256 GCT | P & Z bad | 2.2 | | |
| | | 2 | 01 | 01 | 58 | 30 | 11-2-67 | | 2.2 | | |
| 20 | 1 | 1 | 00 | 07 | 38 | 30 | 1300 GCT | | 3.0 | 12 | 17 |
| | | 2 | 01 | 00 | 26 | 30 | 10-21-67 | | 3.0 | | |
| | 2 | 1 | 01 | 04 | 41 | 30 | 1130 GCT | | 3.1 | | |
| | | 2 | 01 | 04 | 51 | 30 | 10-27-67 | | 3.1 | | |
| | 3 | 1 | 01 | 01 | 46 | 30 | 1255 GCT | $H_1$ bad | 2.2 | | |
| | | 2 | 01 | 01 | 59 | 30 | 11-2-67 | | 2.2 | | |
| 19 | 1 | 1 | 00 | 07 | 38 | 30 | 1300 GCT | Unit damaged | 3.0 | 12 | 17 |
| | | 2 | 01 | 00 | 26 | 30 | 10-21-67 | during recovery | 3.0 | | |
| 15 | 2 | 1 | 01 | 04 | 41 | 30 | 1130 GCT | Z and $H_2$ recording channels switched | 3.1 | | |
| | | 2 | 01 | 04 | 51 | 30 | 10-27-67 | | 3.1 | | |
| | 3 | 1 | 01 | 01 | 44 | 30 | 1257 GCT | $H_2$ traces: 2, 6 & 10 | 3.1 | | |
| | | 2 | 01 | 01 | 57 | 30 | 11-2-67 | Z traces: 4, 8 & 12 | 3.1 | | |

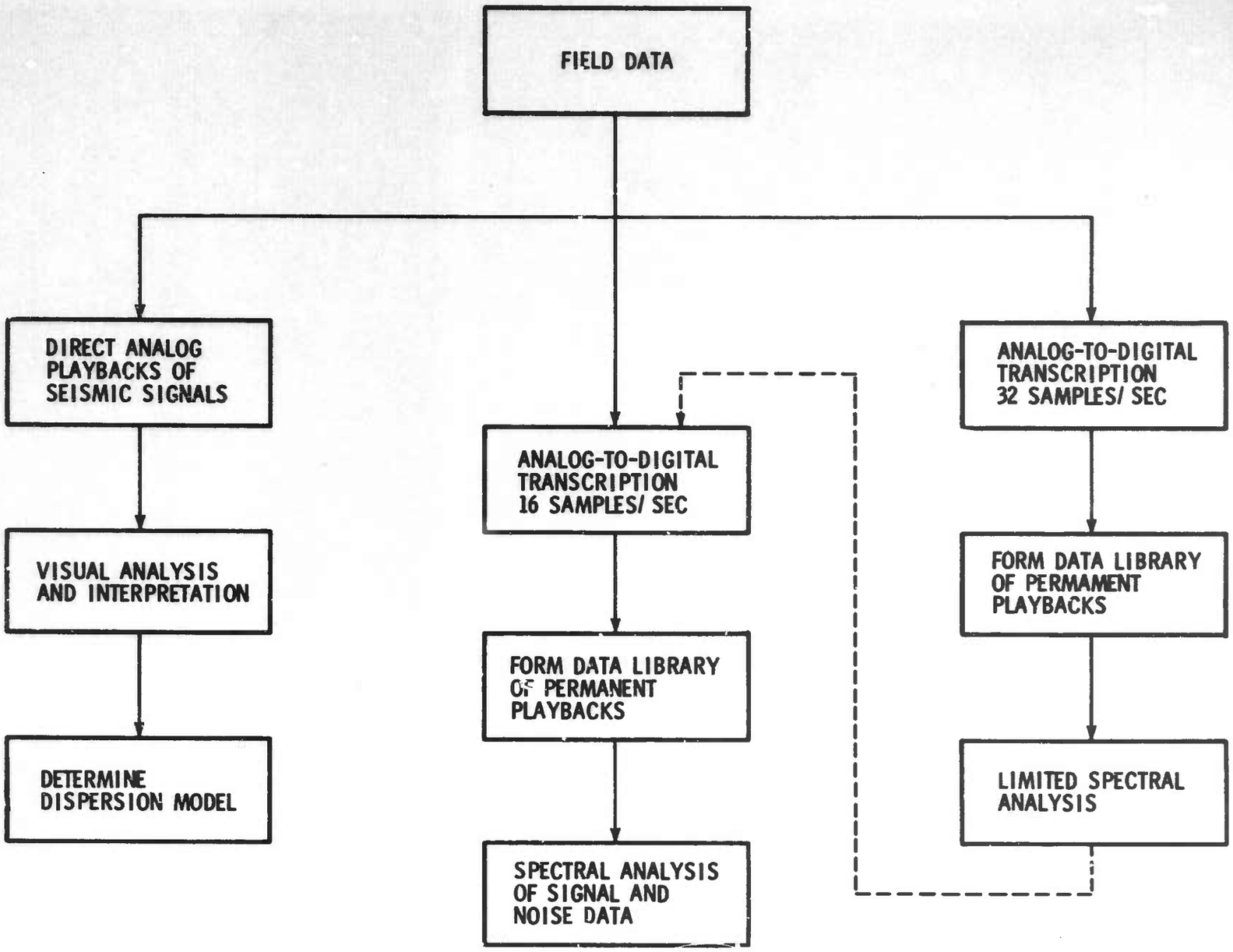


Figure II-4. Data Processing and Analysis Flow Chart

Appendix C presents a discussion of the mathematical approaches used in the spectral analysis.

1. Ambient Noise Analysis

a. Noise Spectra

Noise power-density spectra were computed for two data samples from each drop. In each case, spectra were obtained for the vertical (V x 1), pressure (P x 10), upper horizontal ($H_1$ x 1) and lower horizontal ($H_2$ x 1) of each unit. The noise samples represent simultaneous recordings at each unit. (Table II-1 gives the sample lengths.)

Figure II-5 shows noise power-density spectral levels observed with the unit-20 vertical-component instrument during the three drops. Superimposed on the figure are two curves representing estimates of the system noise levels. The relatively wide, shaded curve defines the extremes of system noise introduced by the analog-to-digital transcription equipment as measured on the x1 channels with no input to the playback heads. The second curve, broader than the ambient noise spectra, is an indirect estimate of total system noise resulting from examination of low-level or inoperable traces.

Between 0.5 and 3.0 Hz, the curves reflect valid seismic data. A noise power peak is seen in the 1.0- to 1.25-Hz range, with energy decaying exponentially above 1.25 Hz. Peak noise levels during drops 2 and 3 are roughly 6 db above those for drop 1 at peak power; the increased levels apparently are the result of strong frontal activity along the coast. Attenuation below 1.0 Hz is due primarily to instrument responses (Figure II-6). The Hall-Sears amplifiers were inadvertently misadjusted during impedance-matching changes, resulting in an amplitude response below the EV-17 response at frequencies above 1.0 Hz.

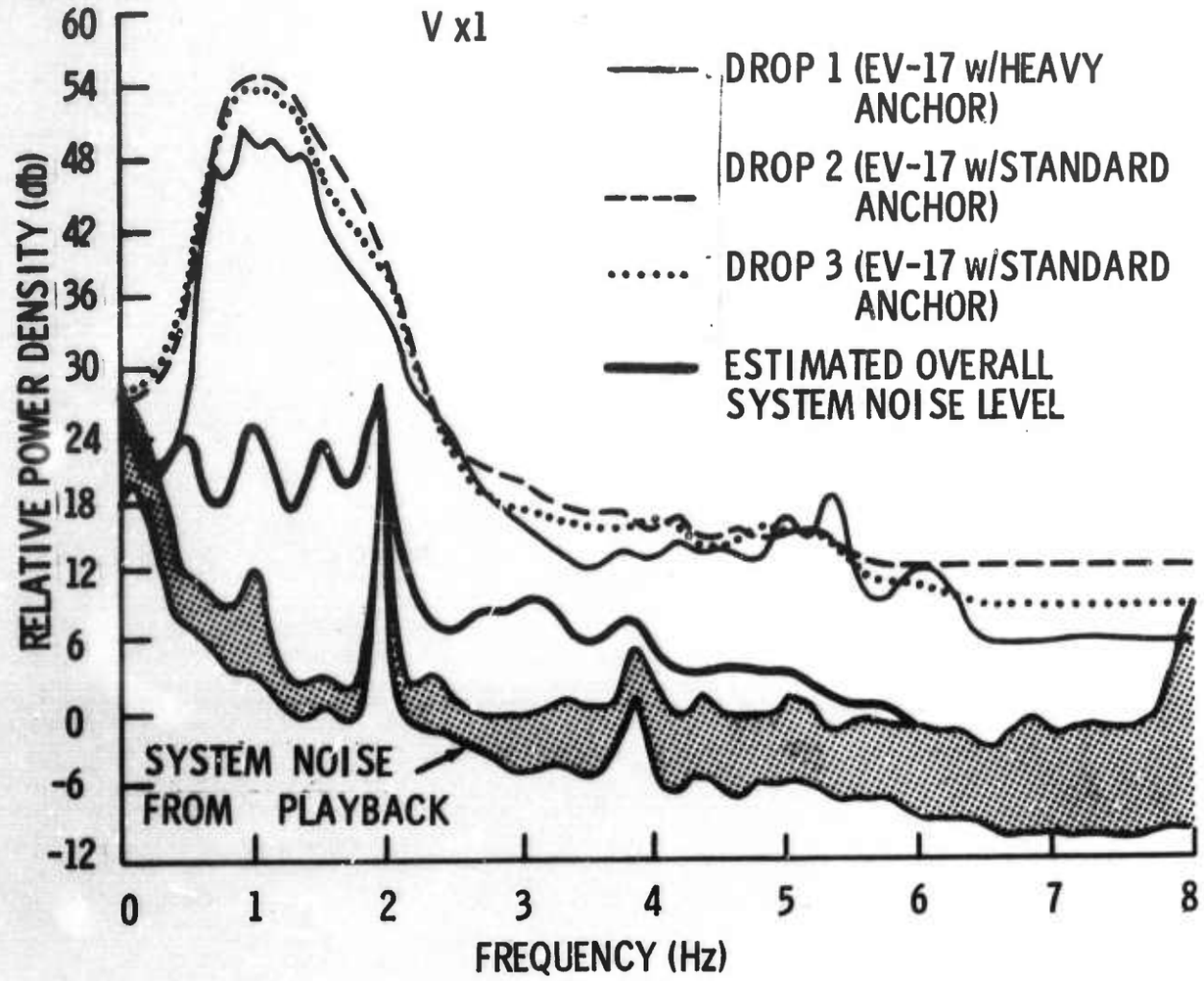


Figure II-5. Noise Spectra: Unit 20, Drops 1, 2, and 3

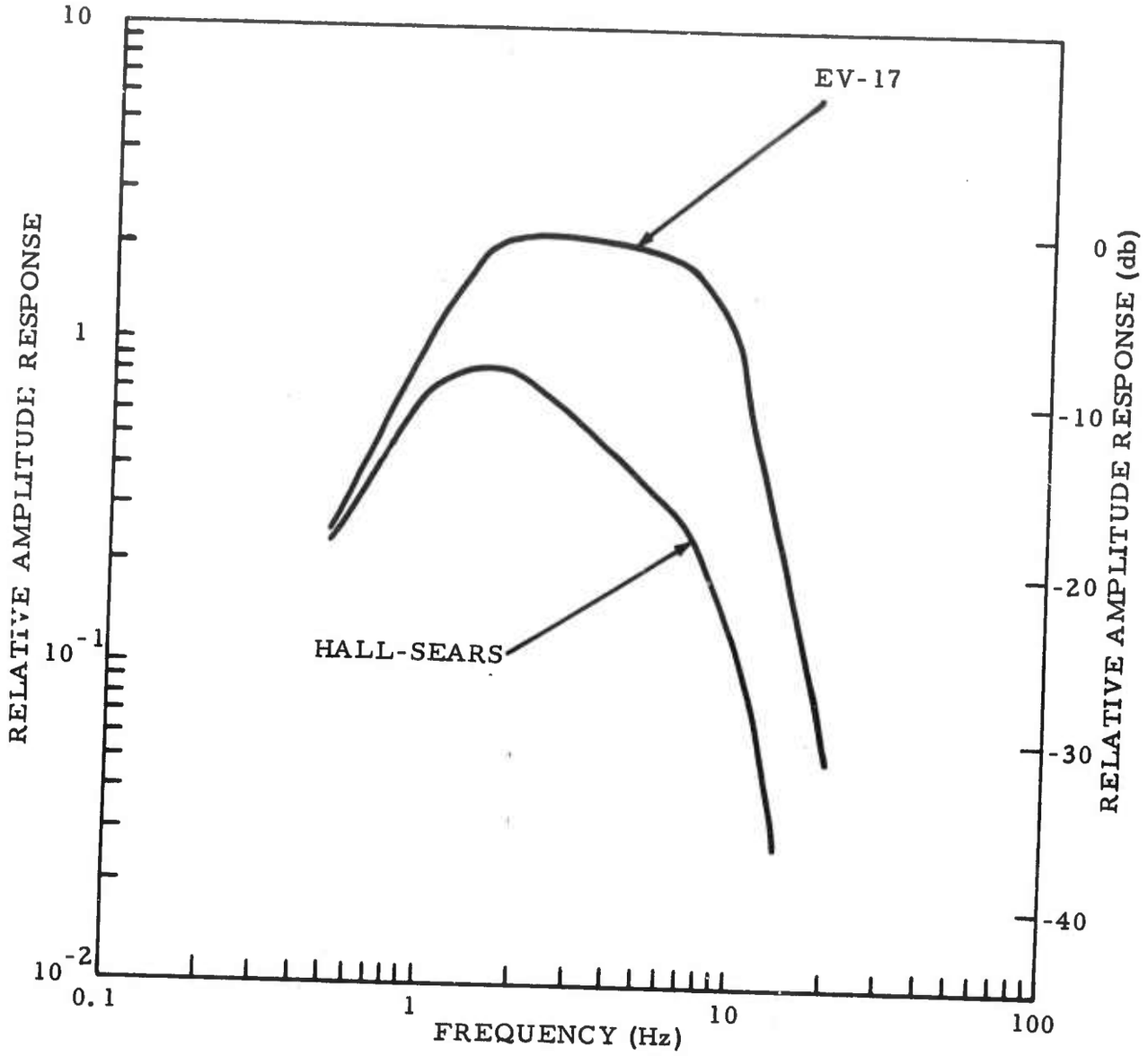


Figure II-6. Instrument Response Curves for Hall-Sears and EV-17 Seismometer Packages

Figure II-7 shows superimposed noise spectra from the four components of unit 19 (EV-17) for sample 2 from drop 1. This direct comparison of component spectra illustrates the lower noise levels seen at peak power on the horizontals. Analysis of noise coherence (presented later) suggests that the vertical component represents primarily low-velocity Rayleigh-type energy, while the horizontal component represents a mixture of Love-mode and Rayleigh-mode energy. The low-velocity waves comprising the vertical noise field are not significant contributors to the horizontal noise field. If the source mechanism favors excitation of predominantly vertical-amplitude particle motion around 1 Hz, the 3- to 6-db reduction of horizontal power-density levels displayed in Figure II-7 is a reasonable result. At the higher frequencies (3.0 to 6.0 Hz), considerable horizontal-component energy is seen. Analysis suggests that this is directional Love-mode energy, possibly from the marine geophysical exploration ship underway at approximately 1.8-mi distance.

Figure II-8 presents the power-density spectra obtained for drop 1, sample 2; spectra for like components from each unit are overlaid. For each set of curves, a 30-db reference level is shown. The space-stationarity of the spectra is very apparent. Also evident is the difference between the Hall-Sears and EV-17 responses. The performance of the unit appears not to be affected by the heavy anchor (unit 20), possibly because the OBS spheres were supported by mud to some extent. Again, considerable energy, apparently from the ship, is concentrated at 5.5 Hz on the horizontals. This peak is not seen in the other drop-1 noise sample; at that time, the ship was approximately 5 mi distant.

Figures II-9 and II-10 present spectra in the same format from drop 2, sample 1, and drop 3, sample 2, respectively. Higher noise levels are evident for these drops. Again, the heavy anchor (unit 15, drop 2) does not appear to have altered unit performance. The high level of noise concentrated between 5.0 and 7.0 Hz on unit-20 horizontals is believed to be directional energy from the ship, which was anchored very close to unit 20 during drop 2.

This energy is apparently attenuated rapidly with distance and is horizontally polarized. Similarly, this energy is seen on the horizontals for both units 15 and 21 during drop 3 when the ship was reported to have bee anchored nearest these units. The padded anchor and different silastic do not appear to have affected unit performances.

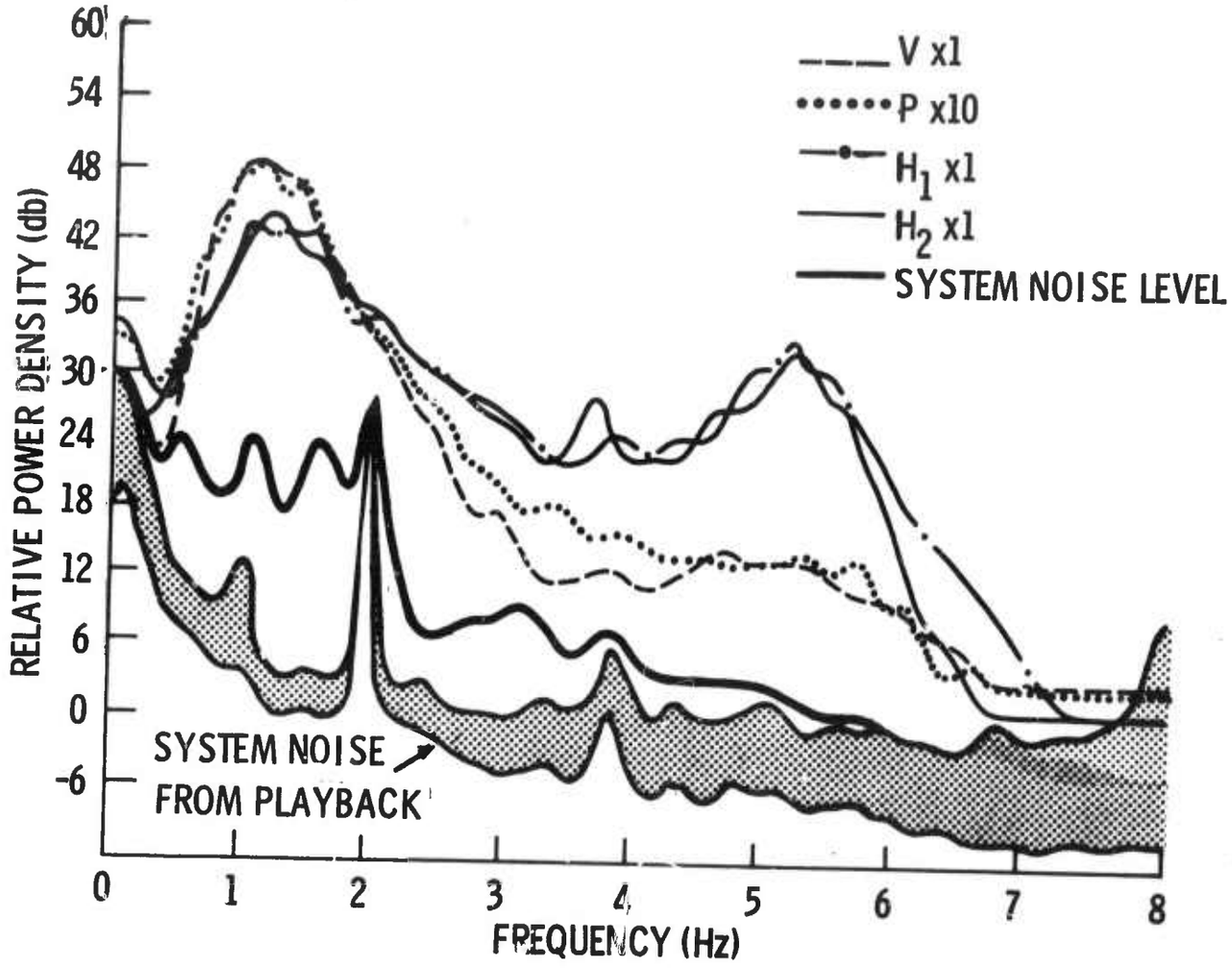


Figure II-7. V, P, $H_1$, and $H_2$ Noise Spectra: Unit 19, Drop 1, Sample 2

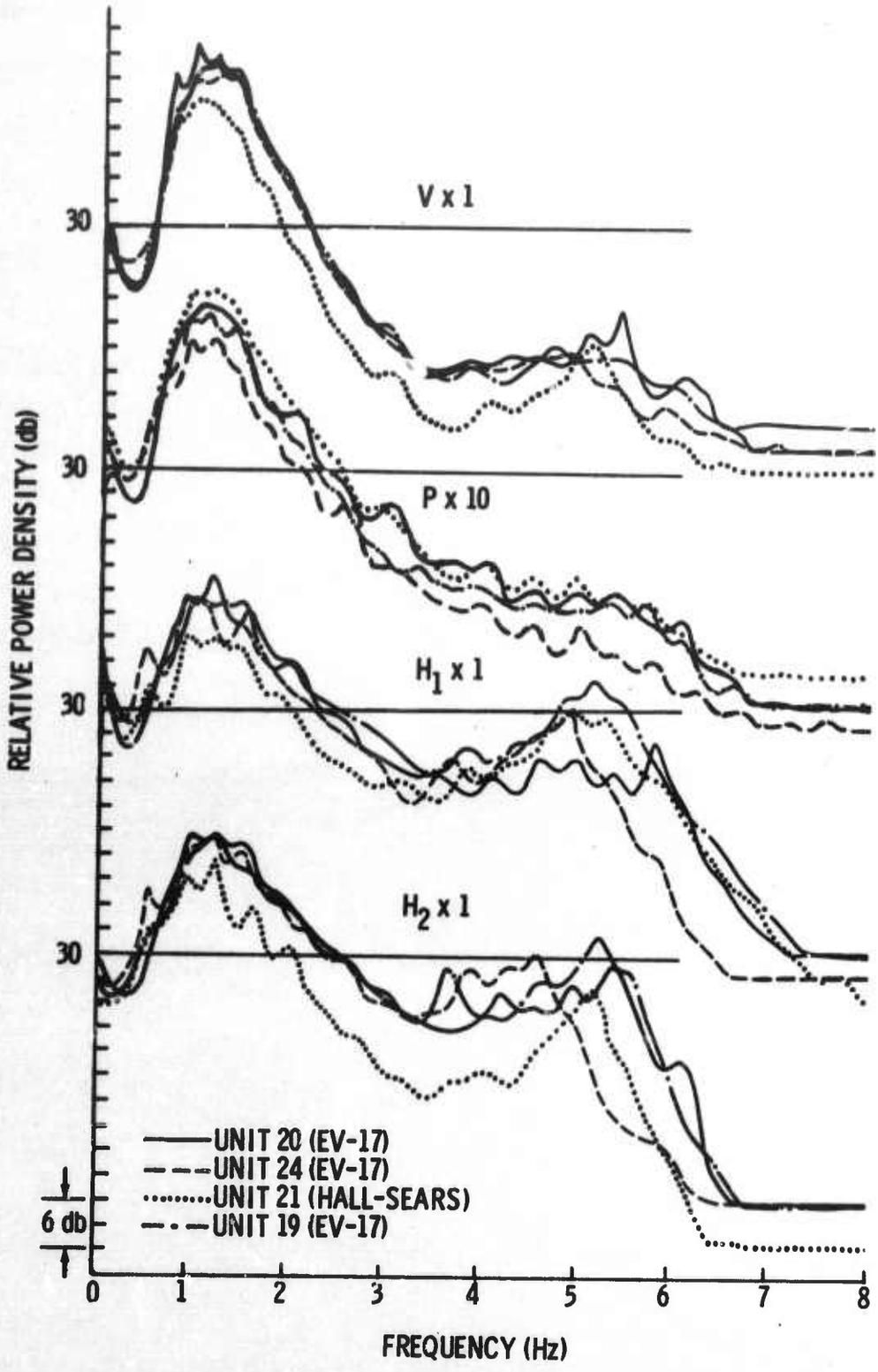


Figure II-8. Component Noise Spectra: Drop 1, Sample 2

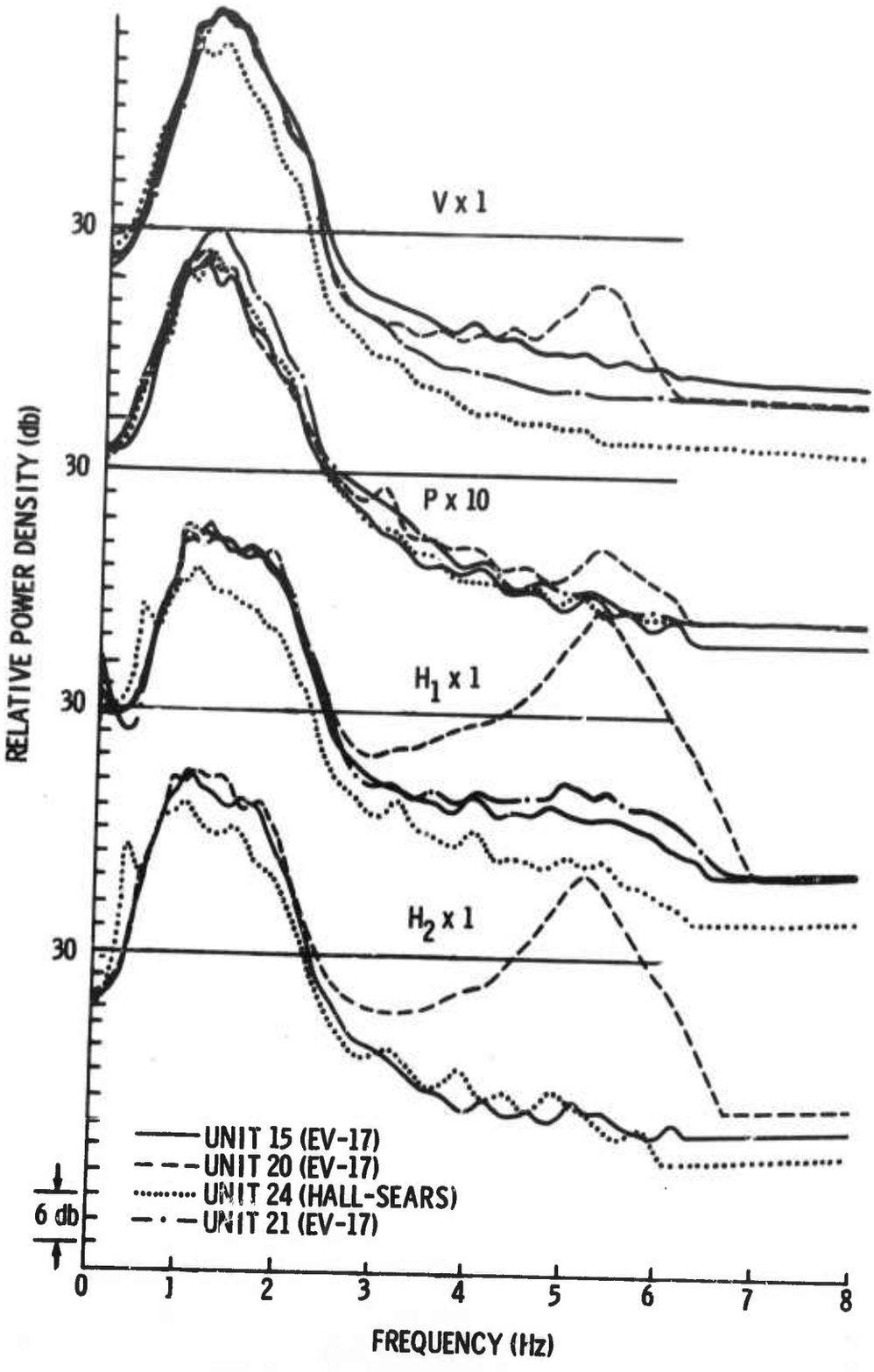


Figure II-9. Component Noise Spectra: Drop 2, Sample 1

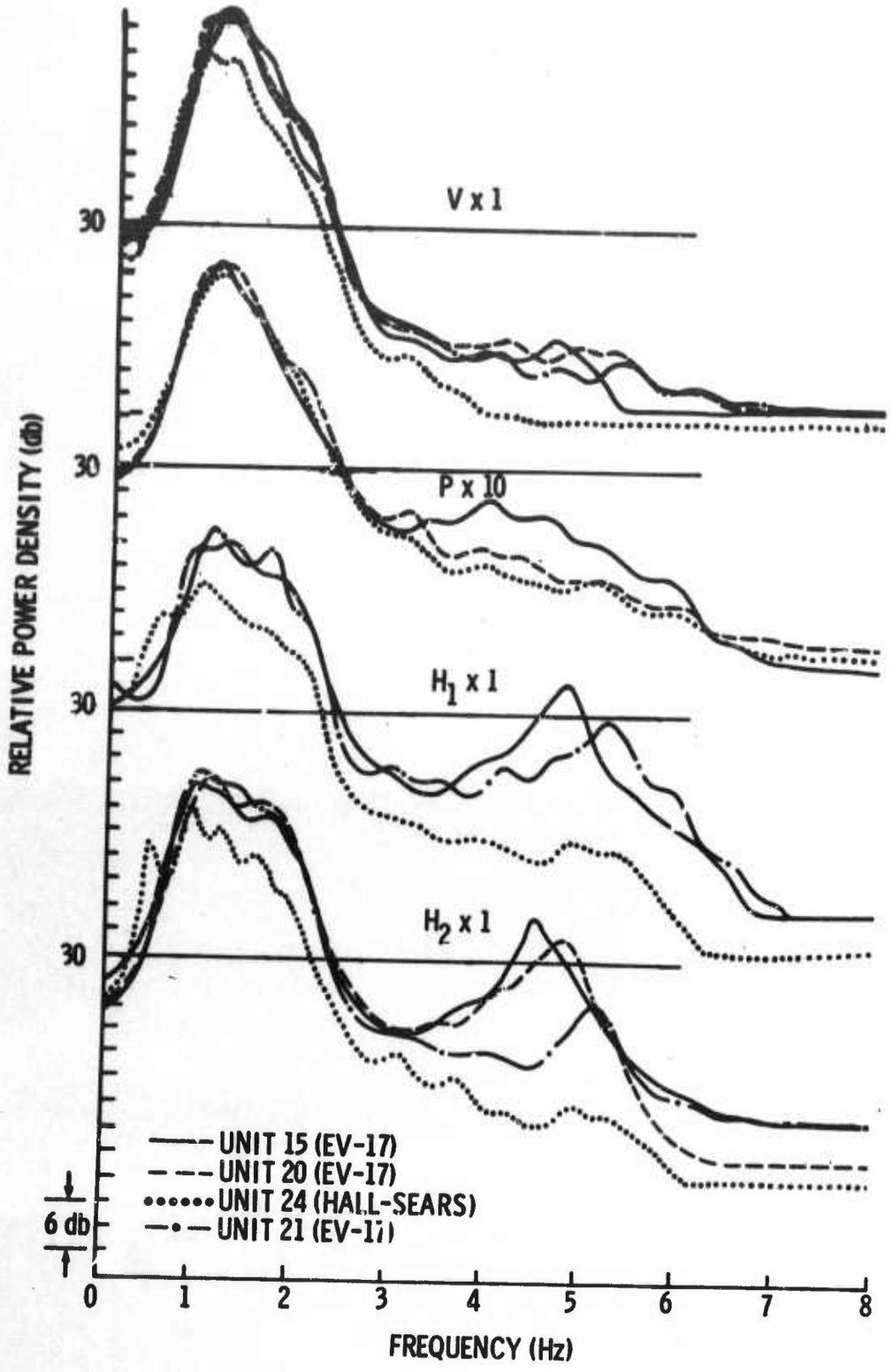


Figure II-10. Component Noise Spectra: Drop 3, Sample 2

b. Spectral Ratios

The ratio of spectra as a function of frequency provides additional insight into operational behavior. Various spectral ratios were analyzed, particularly to determine whether unit modifications significantly influenced unit performance.

Figure II-11 shows ratios of spectra computed for drop 1, sample 1, which is typical of other samples. No appreciable difference is detected for unit 20 (EV-17 with the heavy anchor) and unit 19 (a standard EV-17) relative to unit 24 (another standard EV-17 within the seismic range of 0.5 to 3.0 Hz). The response difference encountered with the Hall-Sears is quite evident; the Hall-Sears is effectively 6-db down between 1.0 and 2.0 Hz. At higher frequencies, system noise levels are high compared to the ambient noise level and, therefore, the differences in the spectral levels predicted by the response curves are not observable.

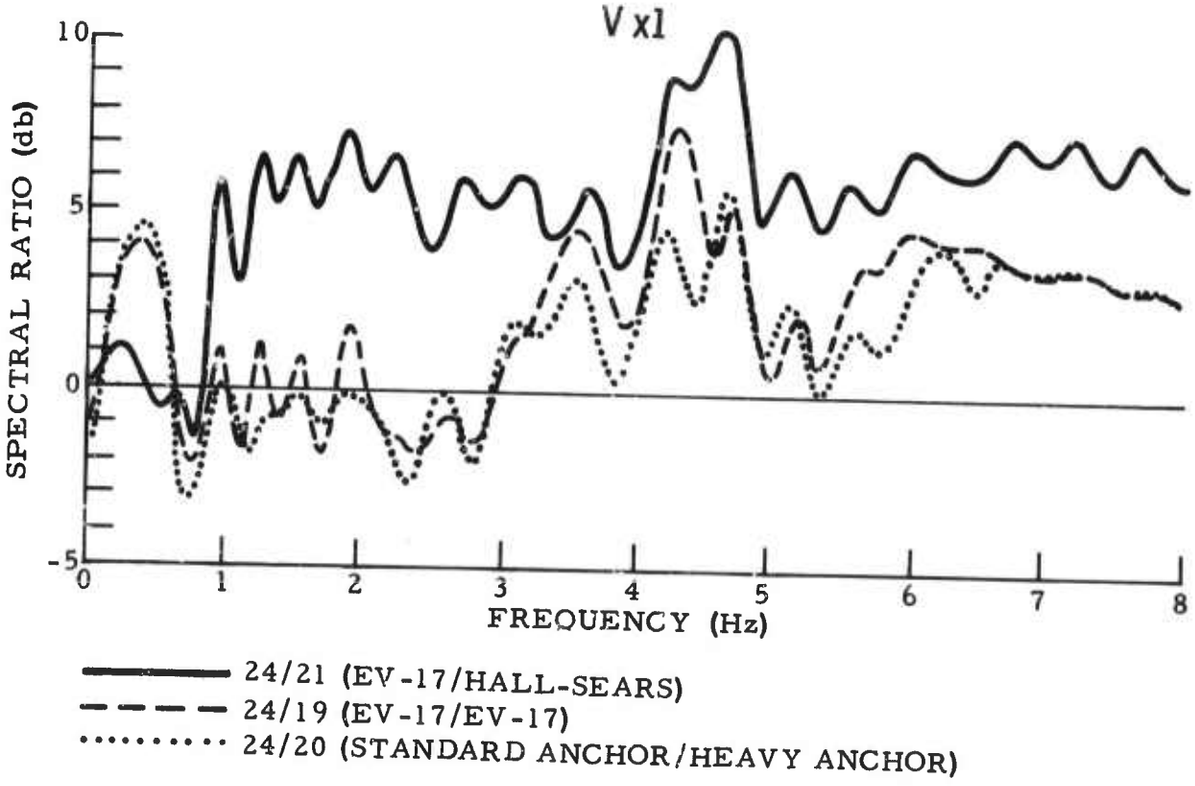


Figure II-11. Interunit Spectral Ratios: Vertical x1 Component, Drop 1, Sample 1

Figure II-12 illustrates P x 1/P x 10 and P x 100/P x 10 ratios for spectra from drop 1, sample 2; all four units are shown. A direct measure of the relative amplifier gains as a function of frequency is indicated in this manner. Relative to the P x 10 trace, all P x 100 channels are within 3 to 4 db of the theoretical factor of 10 differences (20 db) above 0.5 Hz. However, the P x 1 channels do not show the desired 20-db separation except marginally between 1.0 and 2.0 Hz; this is due to contamination of the P x 1 channel with system noise (both OBS-generated and laboratory-generated noise during playback and digitization). For this reason, the P x 10 channel was used in the data analysis. An estimate of total system noise as a function of frequency is possible from these ratios.

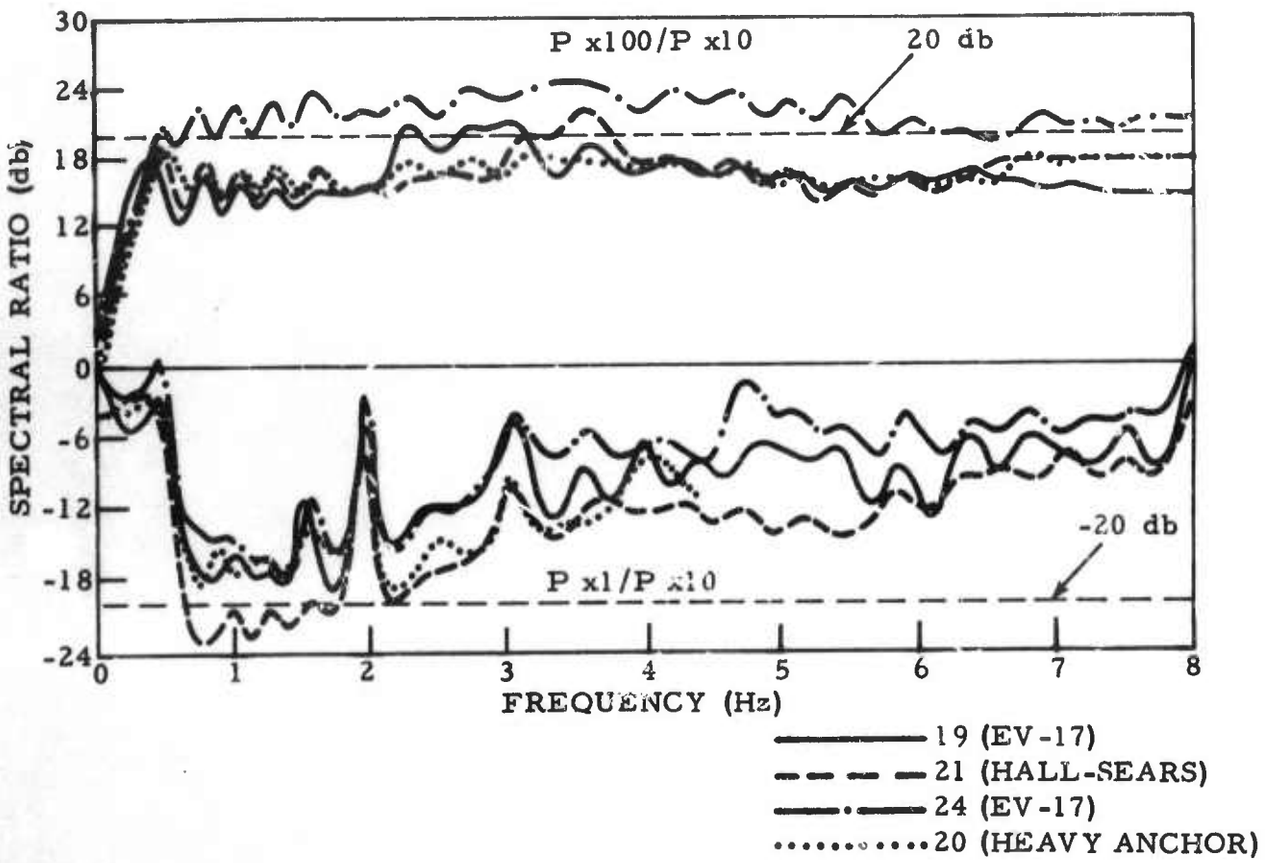


Figure II-12. Intraunit Spectral Ratios: P x 1/P x 10 and P x 10/P x 100, Drop 1, Sample 2

Figure II-13 shows ratios of the x1/x10 channels for the vertical, upper, and lower horizontals of each unit. Generally, these are better behaved than the P x 1, illustrating that these x1 channels are usable. The improper V x 1/V x 10 ratio for unit 24 is the result of a bad V x 10 amplifier gain. Interestingly, the trough between 3.0 and 4.0 Hz on the vertical ratios is the result of harmonic distortion of 1.0- to 1.25-Hz noise peaks resulting from clipping.

c. Noise Coherence

Coherences determined for the vertical components of the drop 1 noise field are shown in Figure II-14. Vertical-component x1 instruments from each of the four units were used. Figure II-14 also shows the coherences determined for the pressure (x10) transducers.

Both sets of curves indicate the largest coherence to be in the 0.7- to 0.8-Hz range. Below 0.7 Hz, instrument responses (which begin to roll off at 1.5 Hz) result in an appreciable decrease in seismic energy relative to system noise levels. Below 0.5 Hz, the spectra apparently are dominated by incoherent system noise, with coherence becoming negligible. Similarly, above 3.0 Hz, any coherences reflect system noise correlation in most cases. The incoherent system noise below 0.5 Hz was likely unit-related, but correlated system noise above 3.0 Hz probably was produced during the playback digitization process. Between 0.5 and 3.0 Hz, measured coherences appear to reflect seismically valid data.

The rather wide range in coherence values resulting from the various unit combinations strongly suggests that the noise field is not directional; therefore, the most plausible model appears to be that of an isotropic noise field.

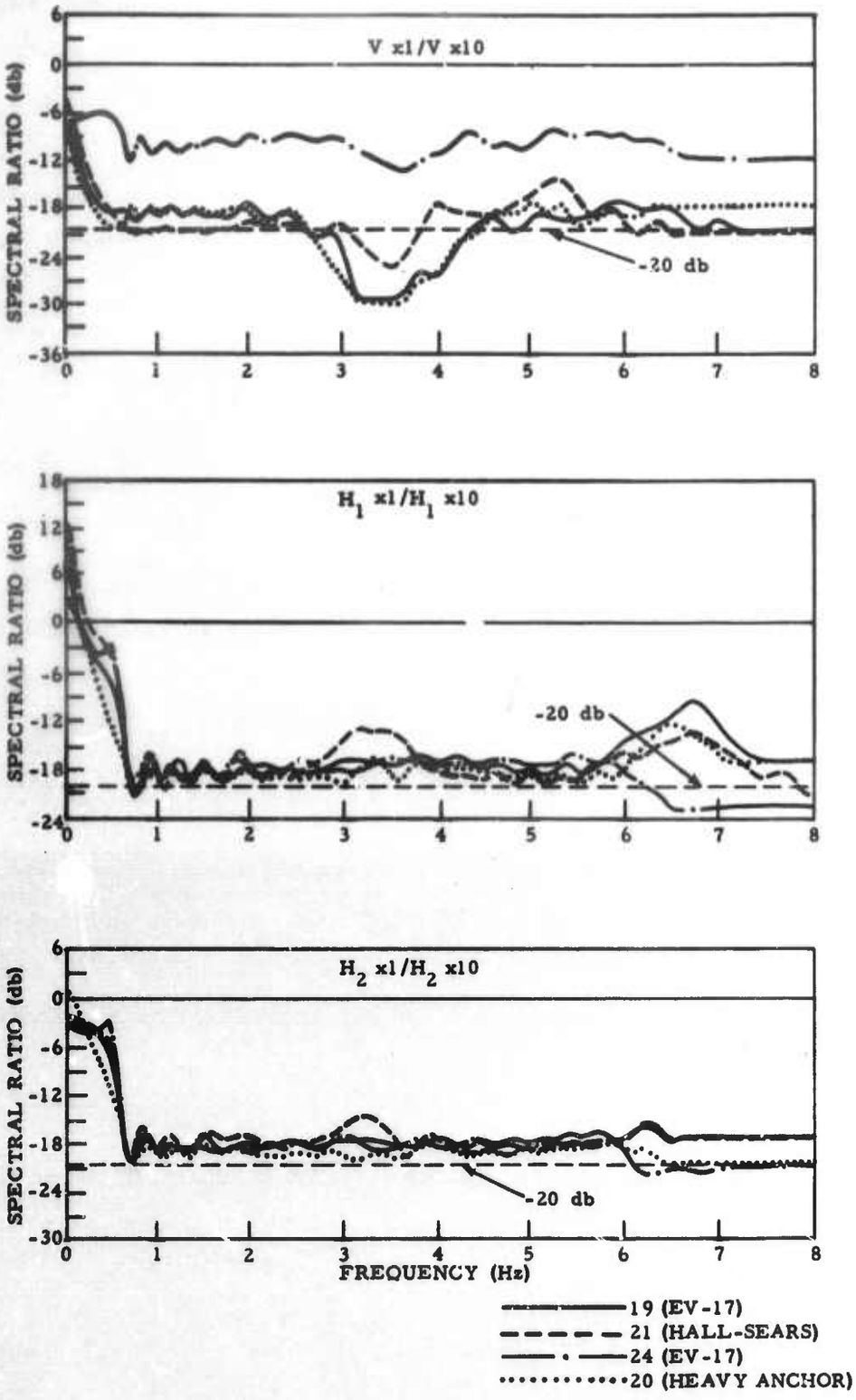


Figure II-13. Intraunit Spectral Ratios: x1/x10, V, $H_1$, and $H_2$ Components, Drop 1, Sample 2

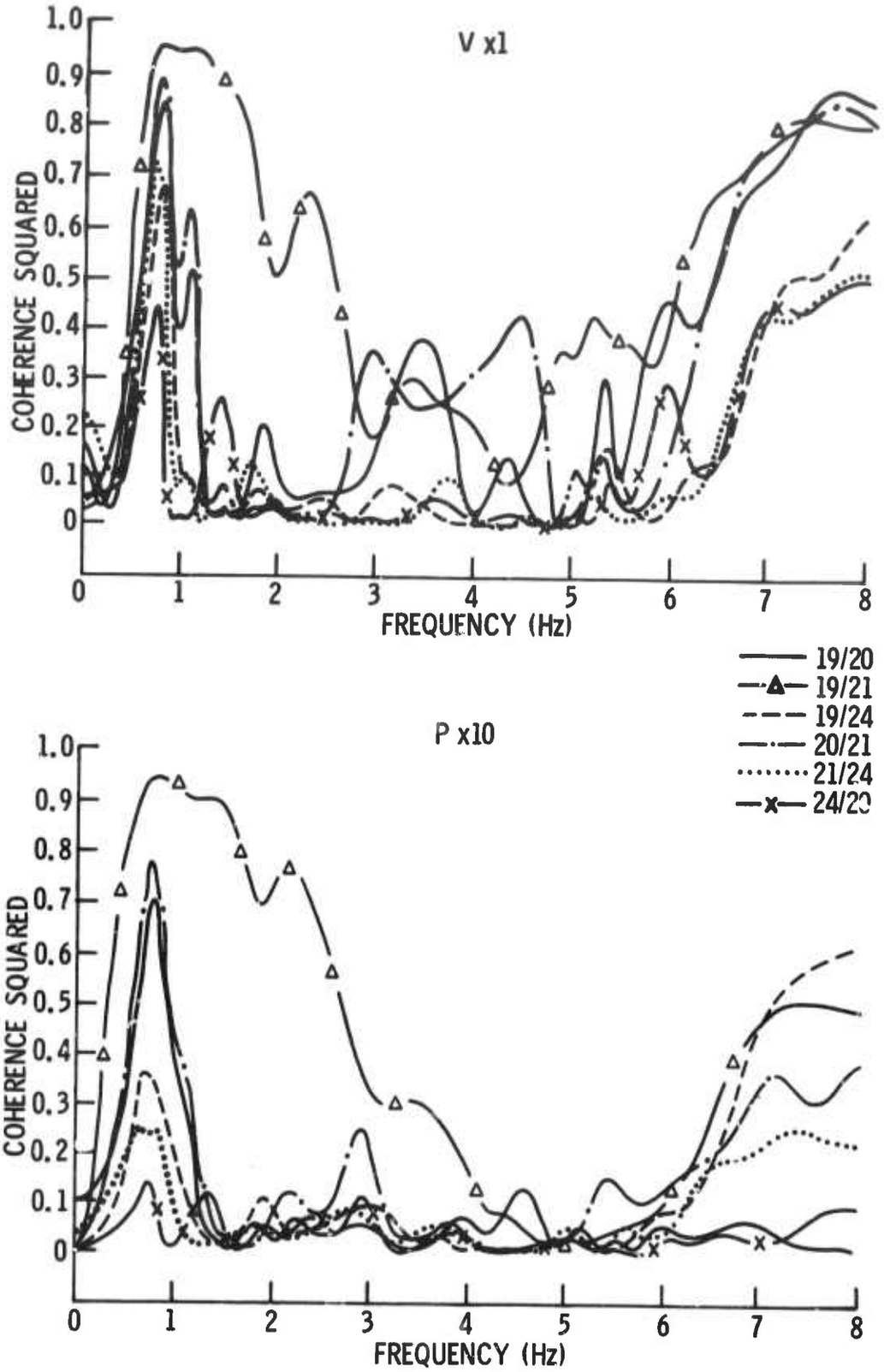


Figure II-14. Interunit Noise Coherence: V x 1 and P x 10, Drop 1, Sample 2

Figure II-15 illustrates the 2-channel coherence theoretically expected for constant-velocity isotropic noise with vertical-component instruments. The abscissa ($d/\lambda$) represents the ratio of the spacing between seismometers (d) to wavelength ($\lambda$). The theoretical coherence for isotropic noise of a given velocity is essentially a zero-order Bessel function and approaches a null as the spacing between instruments approaches one-third of a wavelength. In general, large spacing between seismometers will directly reduce anticipated coherences.

The coherences obtained here suggest that the seismometer spacings are relatively large compared to the dominant seismic wavelenght, with the exception of units 19 and 21 (which appear to be located very close to each other). While relative unit positions are not known exactly, approximate locations are available (Figure I-4). These suggest a surprisingly low phase velocity for the isotropic component of the noise field.

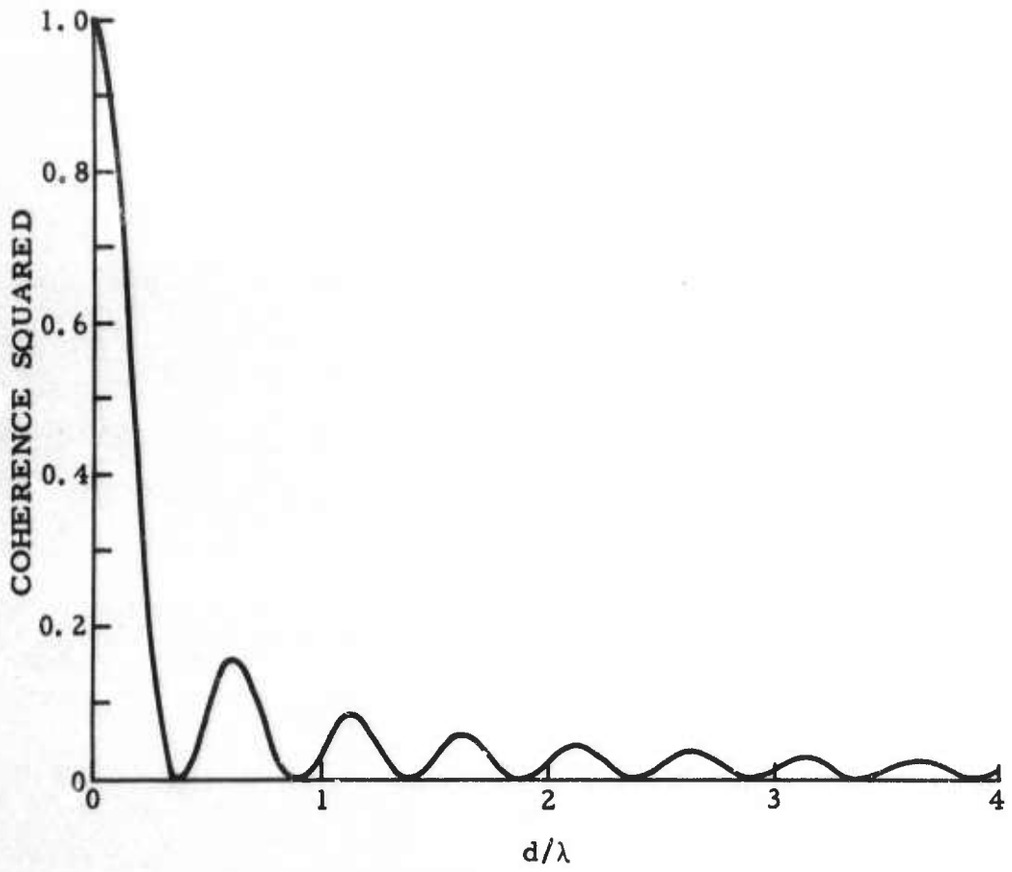


Figure II-15. Theoretical 2-Channel Coherence for Isotropic Noise, Vertical Component

Similar coherence measurements were made for a second noise sample taken from drop-1 data. Results are essentially the same, with the exception of measurements involving unit 20; these reflect complete lack of correlation across the frequency band. An explanation for this behavior is not now available, but the problem is believed to be related to the specific data sample from unit 20 (possibly a tape speed variation) rather than with the unit in general or with the postulated noise model.

Analysis of signal data (presented later) shows that the shots excited a dispersive, very low velocity mode with a phase velocity of about 620 fps at 1.3 Hz. Both the frequency band and the amplitude relationships among components for this mode were similar to that observed for the noise. This information, combined with the coherences shown, strongly suggests that the predominant noise is propagating at low velocity (about 620 fps).

The coherence data can be used to check the field-estimated locations. Assuming an isotropic noise field and a propagation velocity of 620 fps, then the separation between units, d, can be calculated from

$$2\pi f \frac{d}{V} = 2.4$$

where

f is the frequency of the first null in the coherence

V is the velocity of propagation

2.4 is the value of the first null in a zero-order Bessel function

Solving for component pairs gives a minimum separation (units 19 and 21) of 40 to 90 ft, and a maximum separation (units 24 and 20) of 240 to 400 ft (Figure II-16). These values and the relative positions of the units are consistent with field information.

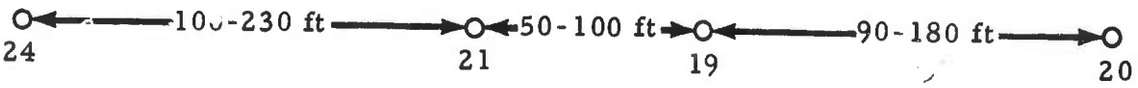


Figure II-16. Calculated Unit Locations

Interunit coherences between verticals and between pressure instruments were also computed for noise samples from drops 2 and 3. With minor exceptions, coherences were negligible, suggesting larger unit spacings during these drops. Operational conditions also substantiate these conclusions since field estimates of unit locations are approximations made from visual buoy sightings without benefit of reference points. Adverse weather conditions during drops 2 and 3 also reduced the reliability of these estimates.

Coherences computed between the pressure (x10) and vertical (x1) within each unit for all noise samples are illustrated for drop 1, sample 1, in Figure II-17. Very high coherence was obtained from 0.5 to approximately 1.5 Hz, which includes the bulk of the seismic energy seen. This high P/V coherence again reflects the extremely good quality of the vertical-component data. Figure II-17 also shows the relative phase angles between pressure and vertical instruments in each unit; the phase angles are derived from the cross-power term used for the coherence computation. All four units reflect a 90° phase shift between pressure and vertical instruments, which is theoretically predictable for Rayleigh-type propagation. Two anomalies appear: a 180° phase shift between the Hall-Sears and the EV-17 vertical-component instruments (caused by lead reversal on the EV-17, resulting from ambiguous polarity-test procedures); and a gradual, approximately linear phase change in unit 20 as frequency increases. This phase shift apparently is caused by a slight misalignment between the P x 10 and V x 1 recording heads. Such a misalignment results in a time shift (= $\Delta t$) between channels with a corresponding phase shift $\phi(f) = 2\pi(\Delta t)f$, yielding a phase difference which changes linearly with frequency.

From Figure II-17, an estimate of the magnitude of $\Delta t$ can be made by using the relation

$$\Delta t = \frac{\phi(f_2) - \phi(f_1)}{2\pi (f_2 - f_1)}$$

$$\Delta t = \frac{\phi(2.3) - \phi(0.5)}{2\pi (2.3 - 0.5)} = \frac{(175^\circ - 95^\circ)/57.3}{6.28(1.8)} = \frac{1.396}{11.304} = 0.123 \text{ sec}$$

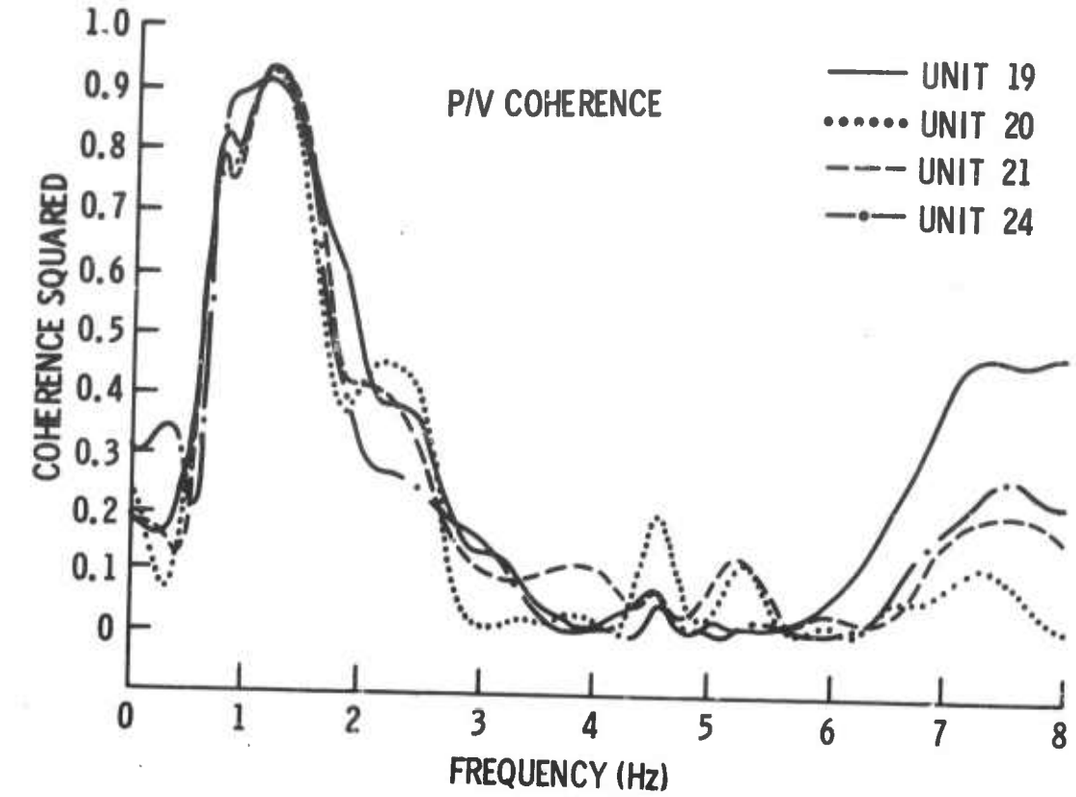


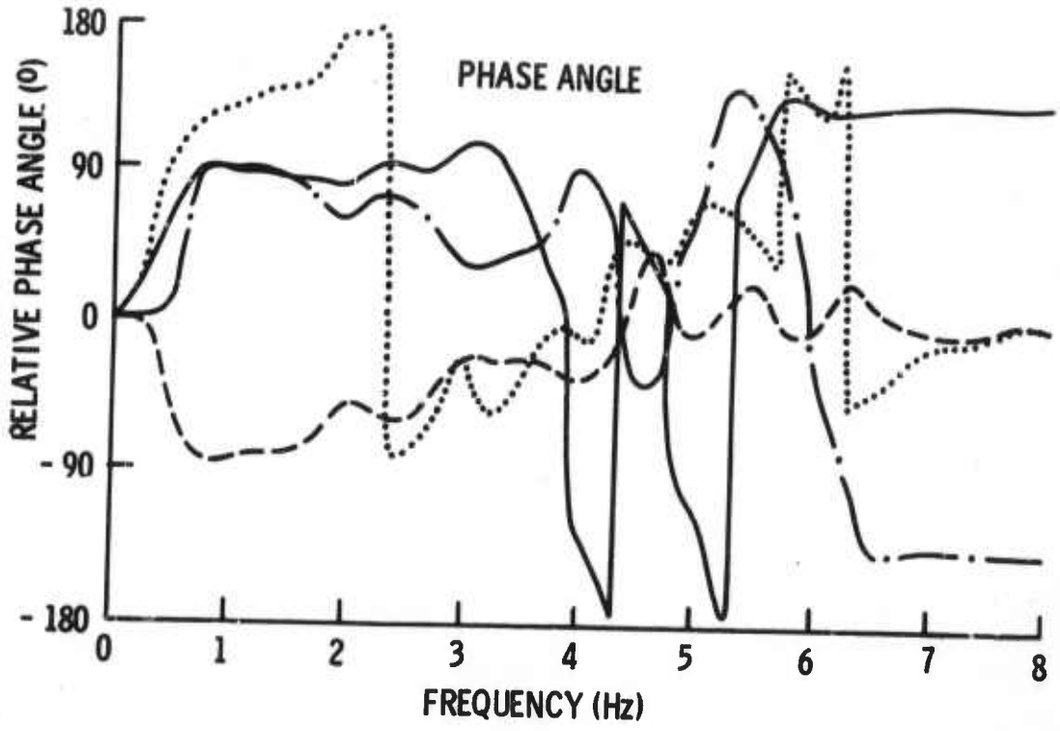


Figure II-17. Pressure/Vertical Coherence and Phase Relationships, Drop 1, Sample 1

The $\Delta t$ measured directly from field records is 0.14 sec; this is in very good agreement with the time shift just computed.

Coherences computed for vertical-horizontal pairs in each unit are negligible within the valid seismic band of 0.5 to 3.0 Hz; apparently, the horizontal motion is composed of a different combination of modes than is the vertical motion. Signal analysis (presented later) reveals the presence of several propagation modes through the shallow sediments, with one of the more important being a vertically polarized Rayleigh-type wave. The postulation is that the vertical component of the isotropic noise consists mainly of this low-velocity surface wave. Lower horizontal-component power-density levels (6 to 9 db), relative to the vertical, support such a model of the seismic noise field. The energy seen on the horizontals can be explained as a combination of both shear- and Love-mode energy.

Coherences between the upper horizontals ($H_1$ x1) and between the lower horizontals ($H_2$ x1) are shown in Figure II-18, a and b, respectively, for drop 1, sample 2. Similarly, Figure II-19 (a and b) presents coherence measurements between the upper horizontal of one unit and the lower horizontal of another. These measurements are more difficult to interpret than the vertical coherences, since the direction of orientation of the horizontals is unknown. Some horizontal alignments can be inferred, however, from the coherence functions; e.g., unit 20's upper horizontal does not correlate well with any other upper horizontal and, similarly, its lower horizontal correlates poorly with the other lower horizontals. Conversely, significant levels of coherence are observed between unit 20's upper horizontal and the other lower horizontals and between its lower horizontal and the other upper horizontals. Unit 20 appears to be oriented at right angles to the other units and this, in turn, implies that the other units are all identically oriented. Signal analysis (presented later) confirms the inferred orientation.

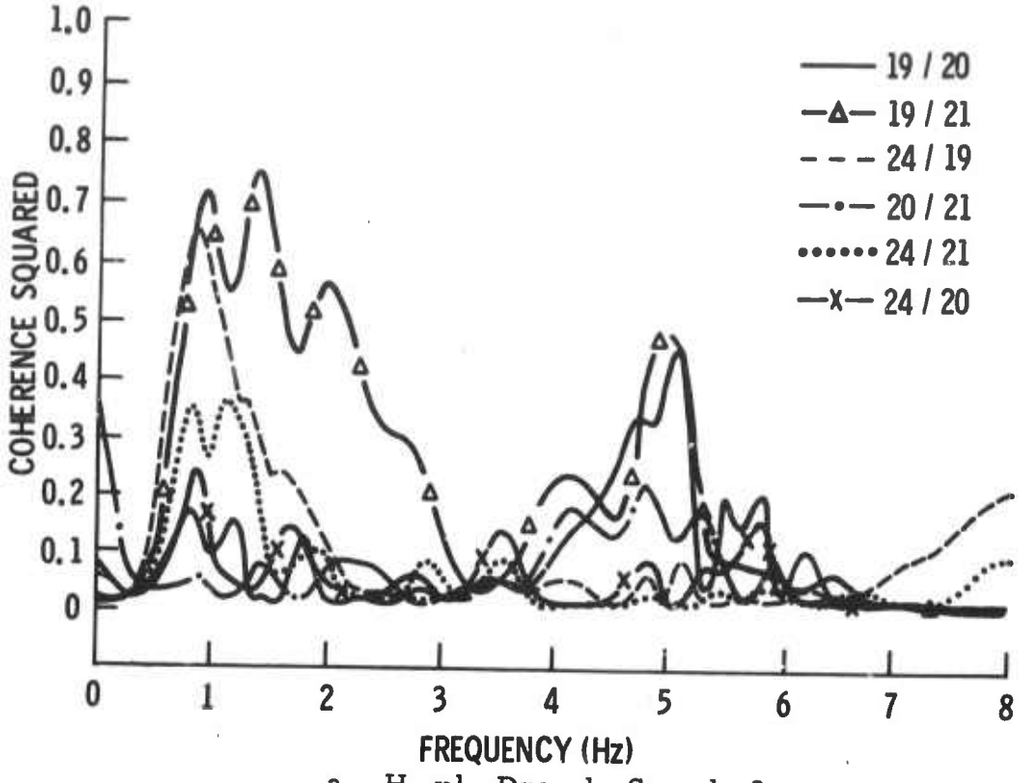


a. $H_1$ x1, Drop 1, Sample 2

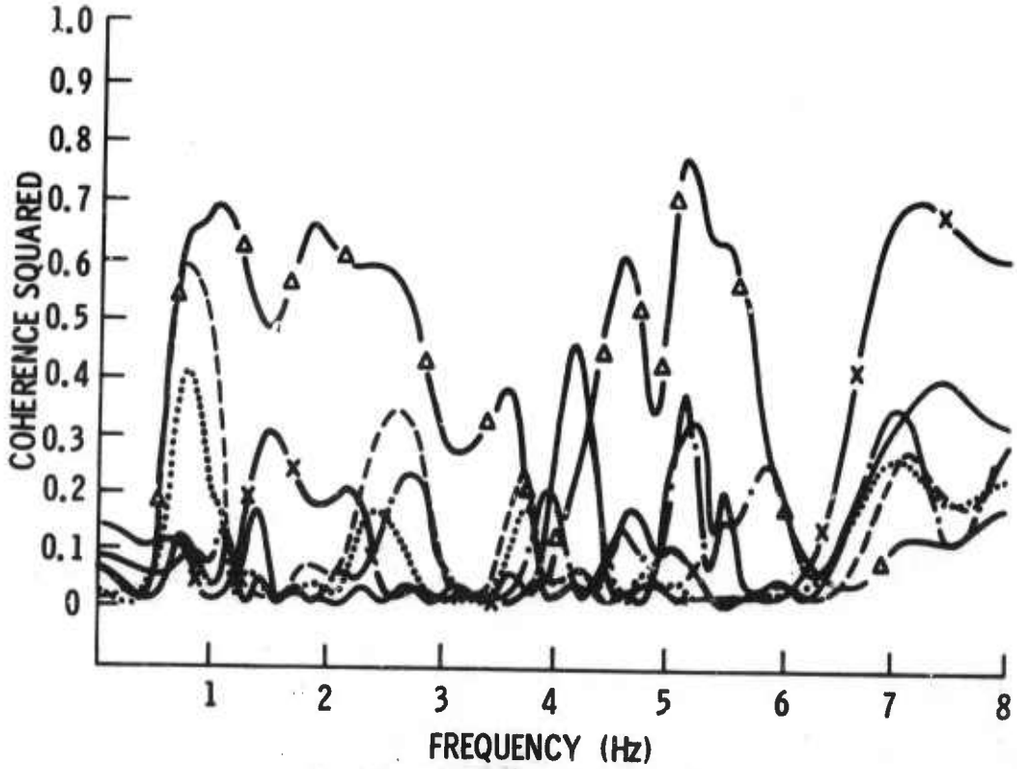


b. $H_2$ x1, Drop 1, Sample 2

Figure II-18. Interunit Coherence

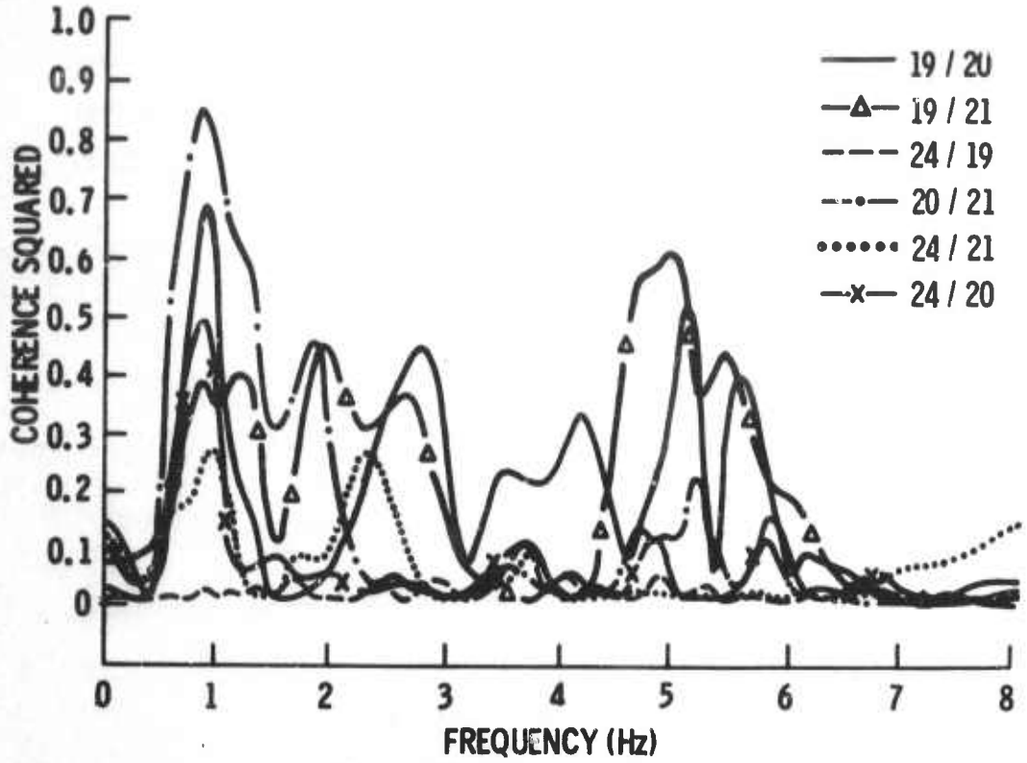


a. $H_1$ x1/$H_2$ x1, Drop 1, Sample 2

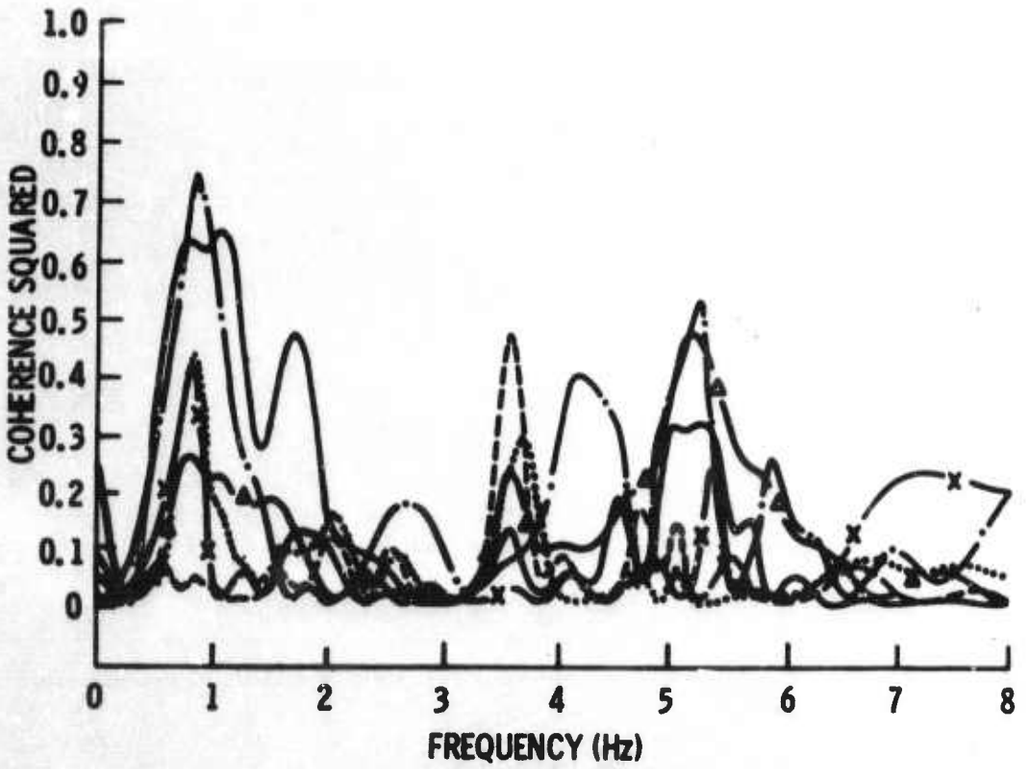


b. $H_2$ x1/$H_1$ x1, Drop 1, Sample 2

Figure II-19. Interunit Coherence

Below 1.0 Hz, there are rough indications that horizontal coherence varies inversely with unit spacing, suggesting an isotropic noise field. Results are inconclusive, however, due partly to the orientation ambiguity.

An additional coherent peak, seen at approximately 5.0 Hz for certain horizontal-component pairs, is apparently Love-mode energy and may result from ship-generated directional noise; the marine exploration ship was approximately 1.8 mi distant. Strong indications of such energy were obtained during drop 3 when the TI ship (a few hundred feet from the units) changed position by running the anchor winch.

2. Analysis of Signal Data

a. Visual Analysis and Dispersion Estimates

During the field tests, low-frequency large-amplitude arrivals propagating at velocities as low as 500 fps were consistently observed following 50-lb dynamite explosions from a nearby geophysical exploration ship. In Figures II-20a and II-20b which present 21 vertical-component recordings from unit 19, these unusual phases are clearly evident; they were observed by each of the four spatially isolated units.

Figure II-21 displays 4-component (pressure, vertical, and both horizontals) recordings from each of the four OBS units for a typical explosion wavetrain. Appearing on the data traces are a number of refractions closely accompanied by a strong ringing waveform which is probably a leaking mode. Both Love- and shear-mode energy are present shortly after the leaking-mode arrivals, followed by a very low-velocity surface wave. This complex long-duration wavetrain indicates that the ocean-bottom sediments are highly layered in the drop area, which overlies the Gulf Coast geosyncline. As can be seen in Figures II-20a and II-20b the amplitude of the low-velocity arrival diminishes with source-receiver distance, and its waveform is dispersive; it has been identified as a Rayleigh-type shear wave with mode of propagation primarily controlled by the very low rigidity of the ocean-bottom sediments.

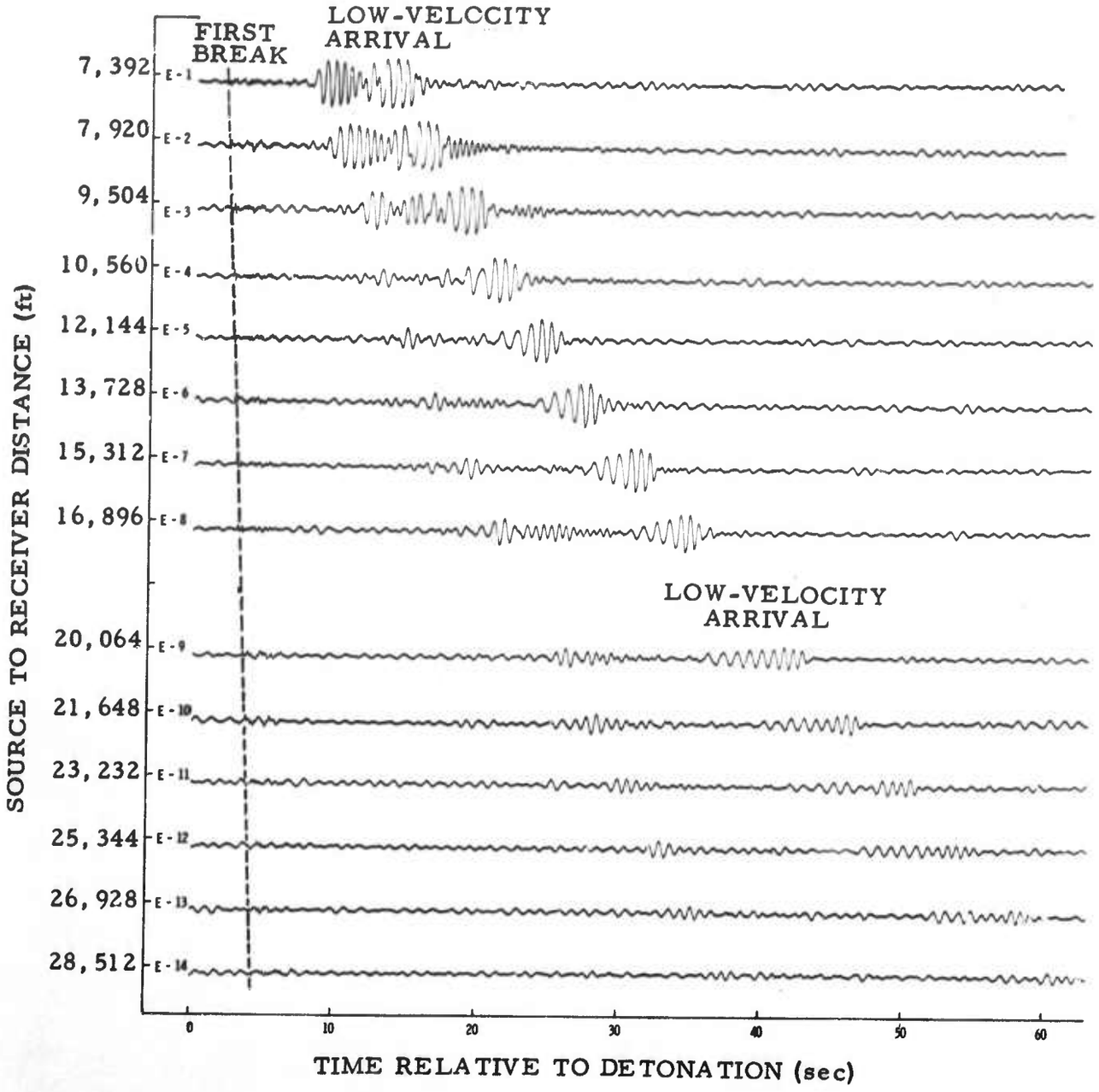


Figure II-20a. Line-4 Low-Velocity Mode, Vertical x1 Component

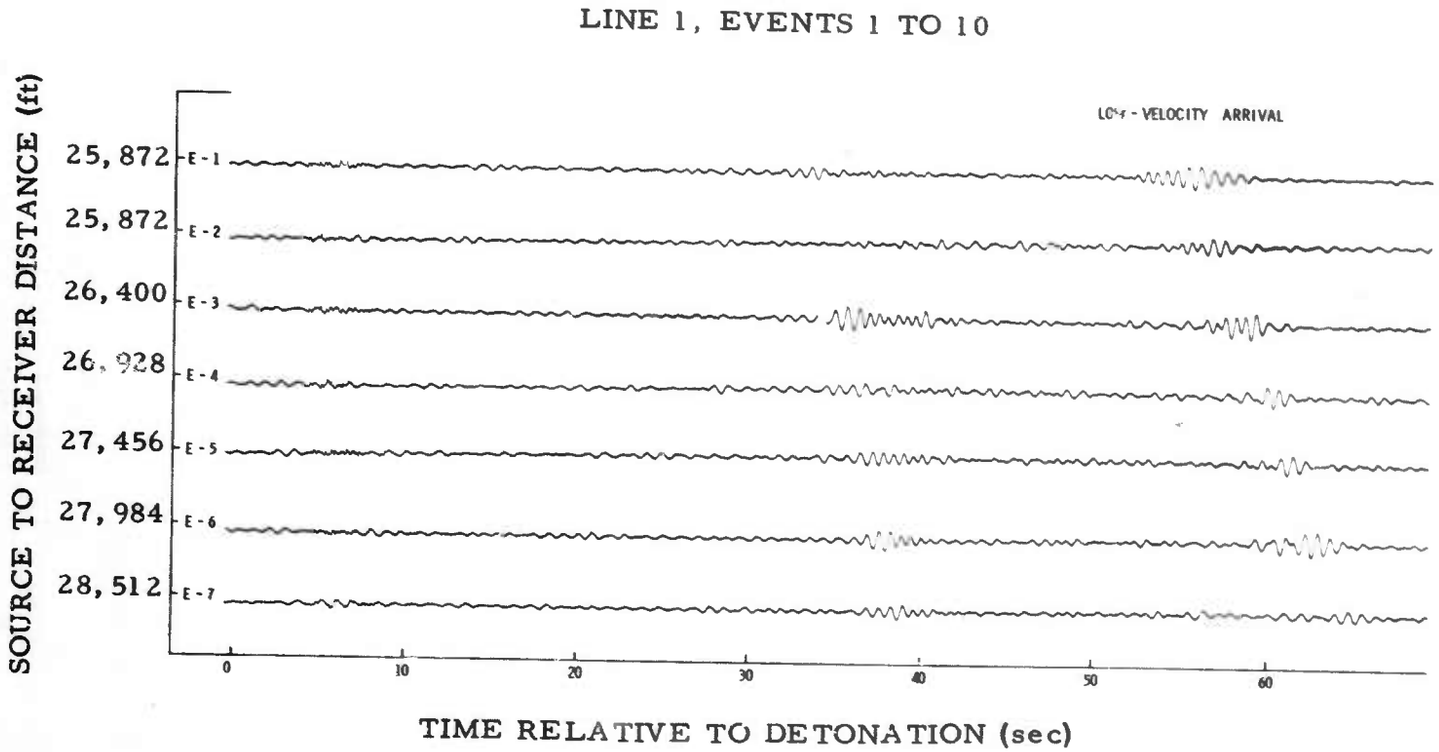


Figure II-20b. Line-1 Low-Velocity Mode, Vertical x1 Component

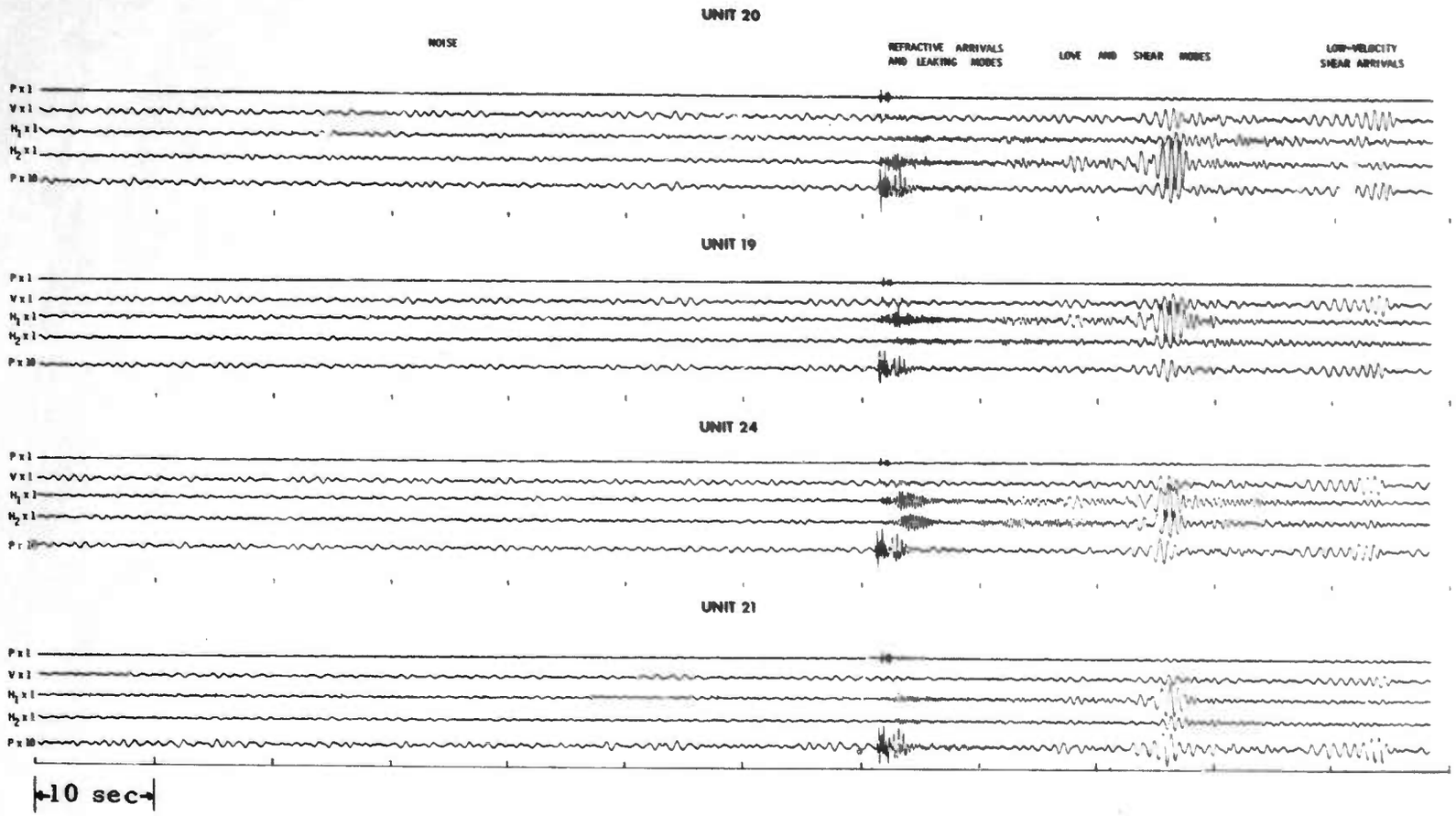


Figure II-21. Noise and Signal, Gulf Coast Sample Data

To verify the seismic source and to locate shot positions, a request for assistance was made to agents of Superior Oil Company. Through their cooperation, information was made available pertaining to the number of profiles (nine) made on 21 and 22 October; included were the number of shots per profile, the shotpoint spacing, and the endpoint coordinates of each profile. A total of 199 explosions were detonated, and all were recorded by the OBS units. The late-arriving surface wave was present only on the three nearest shot lines (1, 2, and 4); from these three, however, excellent azimuthal coverage was obtained (as can be seen in Figures II-1 and II-2).

The marine seismic exploration ship employed a Raydist-Hastings navigational system which yielded plane x, y coordinates of each of the 199 recorded shots to an accuracy of ±100 ft. For conversion to either plane or geographic coordinates, Special Publication No. 252 of the U.S. Department of Commerce, Coast and Geodetic Survey, was used. (This publication gives plane coordinates based on a Lambert conformal conic projection for the State of Texas.)

Receiver locations were less certain than the shot locations, due to the limited accuracy of navigational aids employed by the TI research ship, so recorded shots were used to determine the receiver location more accurately by triangulation. A large graphic display of shot geometry was constructed, and three pairs of recordings from the three lines (1, 2, and 4) were carefully selected. Each pair exhibited the same relative arrival times between phases and very similar amplitudes for the same refractions. Therefore, any two shots comprising a pair were very nearly equidistant from the receiver. The preservation of waveform between each of the three pairs (five recordings) is evident in Figure II-22. Adjacent shotpoints were 1760 ±100 ft apart, and the maximum error in the adjusted receiver location was less than 1000 ft. Pressure traces were used in the alignment of the first part of the explosion wavetrain, while vertical traces were used in the alignment of the last part; this was done because the various phases comprising the signal waveform did not excite the same components equally.

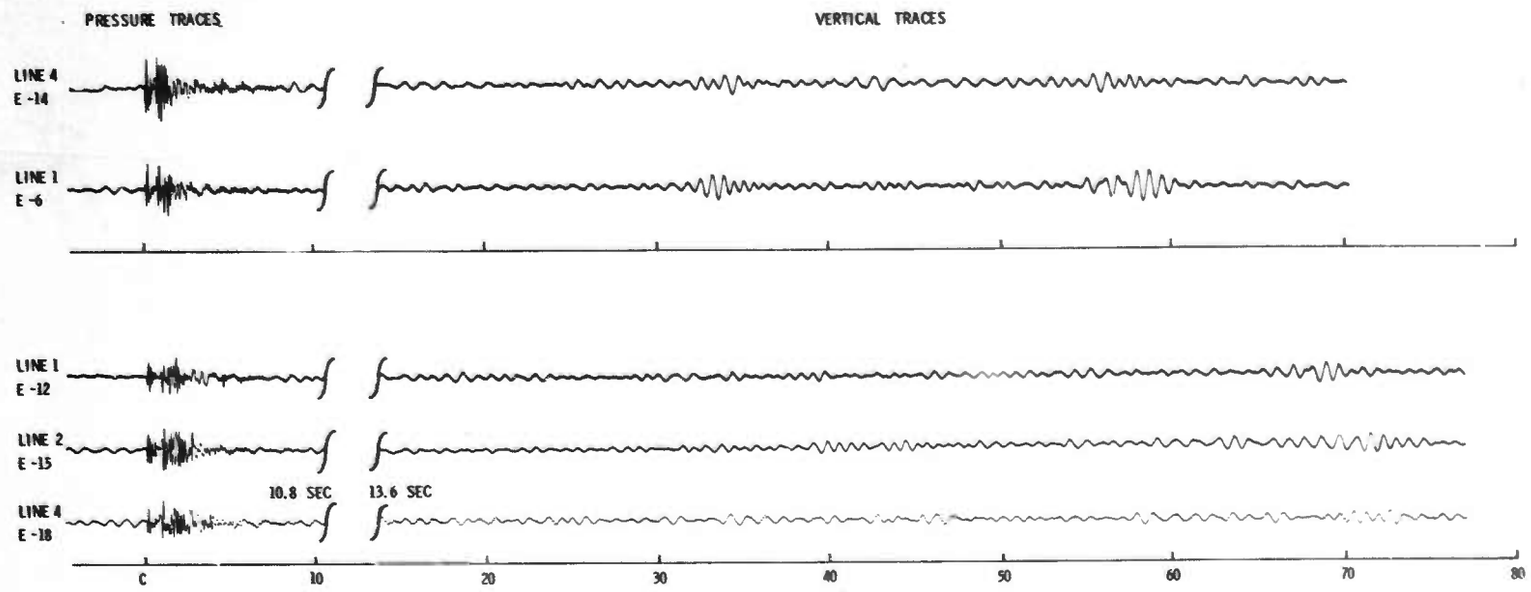


Figure II-22. Signal-Amplitude and Arrival-Time Comparison, Array Positioning (Triangulation Method)

Several such trace combinations were selected, and all yielded consistent results. In effect, a visual least-means-square fit was performed, and the receiver array location was graphically determined to be 28°26'N lat., 93°51'W long., as compared to 28°24'N lat., 93°51'W long. obtained from shipboard navigation.

A knowledge of the traveltime for the first refractive arrival was required to determine group velocities; this was obtained from a seismic refraction profile published by Ewing et al[3] for a section of the Gulf of Mexico running from Galveston, Texas, to Cartegena, Colombia. Four unreversed profiles were shot in various directions on the continental shelf and a computation made using average slopes and intercepts from all profiles to give a rough approximation of thicknesses and velocities in the general area. Profile 32 described by Ewing had geodetic coordinates of 28°09'N and 93°41'W for the receiving position — different only by 17' lat. and 10' long. from the corrected position of the OBS unit.

A crustal model in agreement with Ewing's results was constructed and is displayed in Figure II-23 with the resulting traveltime and traveltime-difference curves. Since shot times were not available on the OBS recordings, only time differences were measurable (Figure II-24). Time differences between the first break on the OBS pressure trace and the second strong refraction arrival are graphed as dots superimposed on the time-difference curves of the Ewing model (Figure II-23).

Clearly, the first arrival is a refraction from the top of the third layer of the model in Table II-2. Numerous arrivals were timed, but only the first two were fitted to the model since they were the strongest and cleanest picks on the records and since the data did not warrant the construction of a complete refraction model.

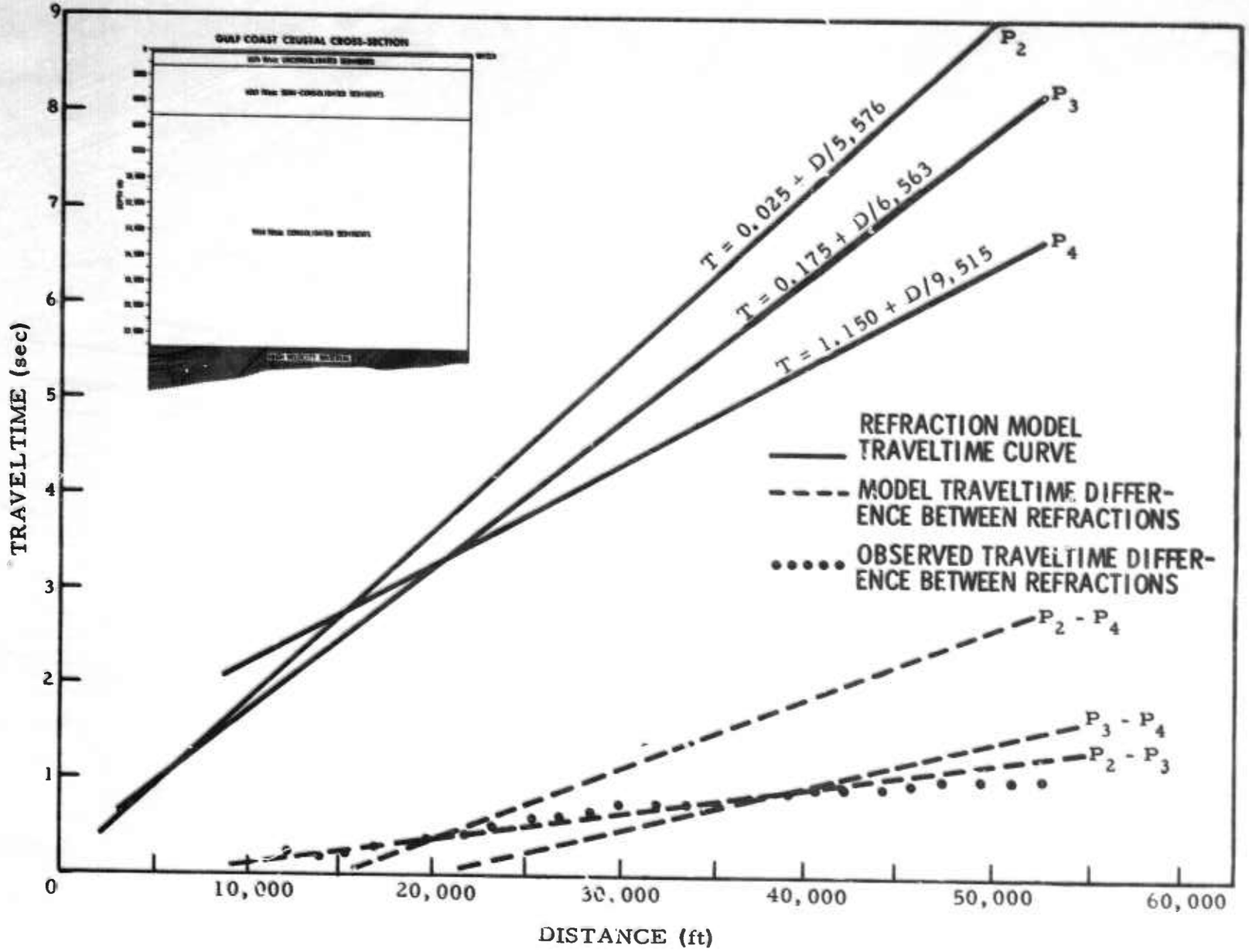


Figure II-23. Crustal Model Used for Data Analysis

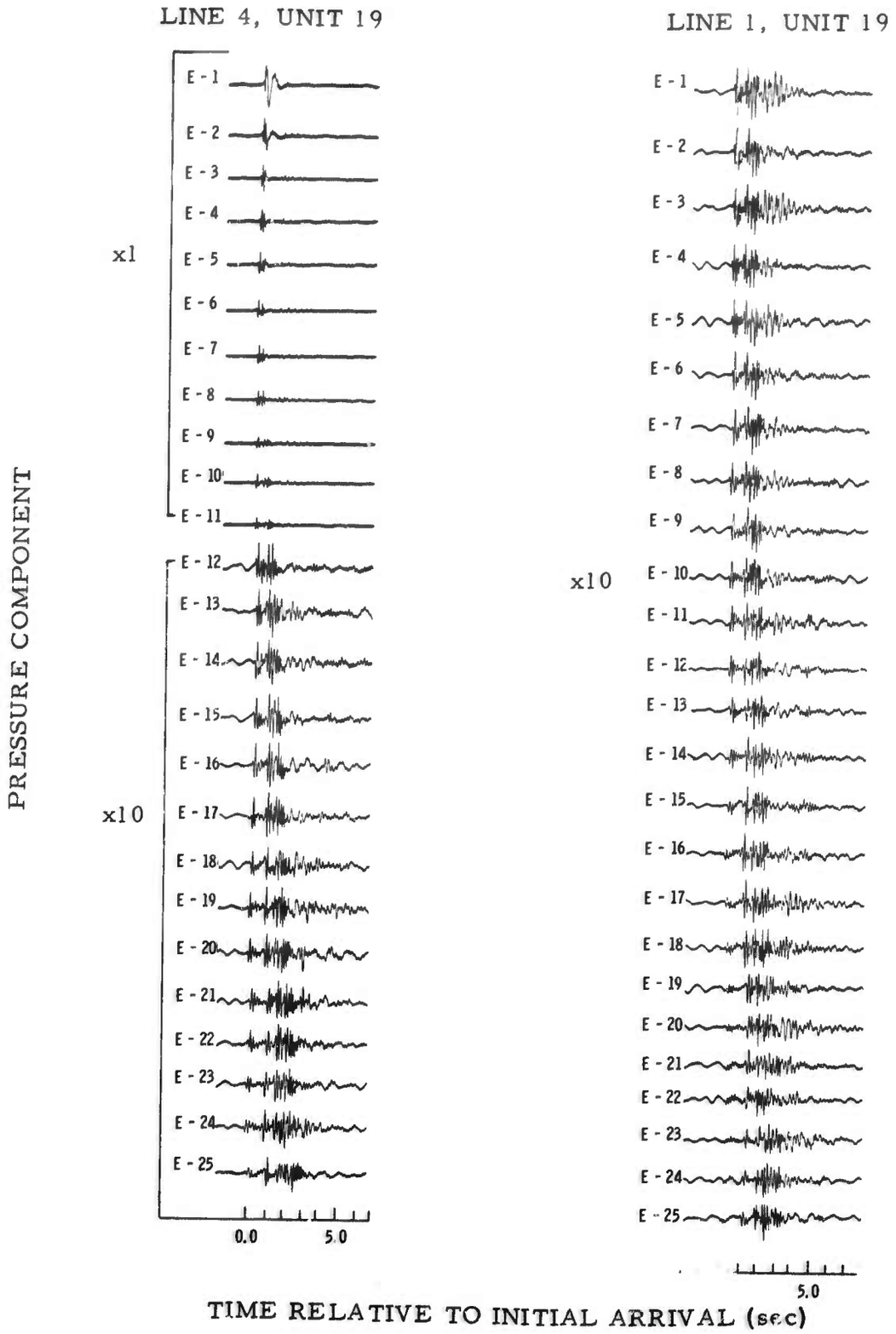


Figure II-24. Refraction Arrival-Time Difference, Model Verification

Table II-2

REFRACTION MODEL FOR UPPER CRUST, GULF OF MEXICO

| Layer Identification | Compressional Velocity (ft/sec) | Thickness (ft) |
|---|---|---|
| Water | 4,921 | 200 |
| Unconsolidated sediments | 5,576 | 1,117 |
| Semiconsolidated sediments | 6,563 | 3,937 |
| Consolidated sediments | 9,515 | 10,044 |

Figures II-25a and II-25b show several models having slightly different thicknesses for the unconsolidated (mud) layer and various compressional velocities. In the distance range of 10,000 to 20,000 ft, where the best dispersive waveforms are observed, the traveltimes predicted for the initial refraction arrival by the various models are within 0.25 sec of one another.

Using the traveltimes from Case I in Table II-3 for the $P_3$ refraction, group velocity as a function of period was measured; results are plotted in Figure II-26 for three shot-receiver distances. It is tacitly assumed here that sufficient dispersion occurred for the various frequencies being studied to be well-separated in time (i.e., assumption of stationary phase). These measurements are accurate to ±15 percent at each period, using

$$\mu(T_o) \cong \frac{X_o}{t_o} \left(1 \pm \frac{\Delta X}{X} \pm \frac{\Delta t}{t}\right) = \mu_o \left(1 \pm \frac{1}{20} \pm \frac{1}{10}\right)$$

The measurements were made from shots 5, 7, and 9 (line 4) at distances of 12,144, 15,312, and 20,064 ft, respectively. One case of inverse dispersion was observed; this was shot 1, line 1, at a distance of 25,872 ft (which will be discussed later in the report). The results presented here are preliminary; digitized data were limited for the low-velocity shear arrival, and Fourier analysis of its waveform possibly will yield an improved estimate of

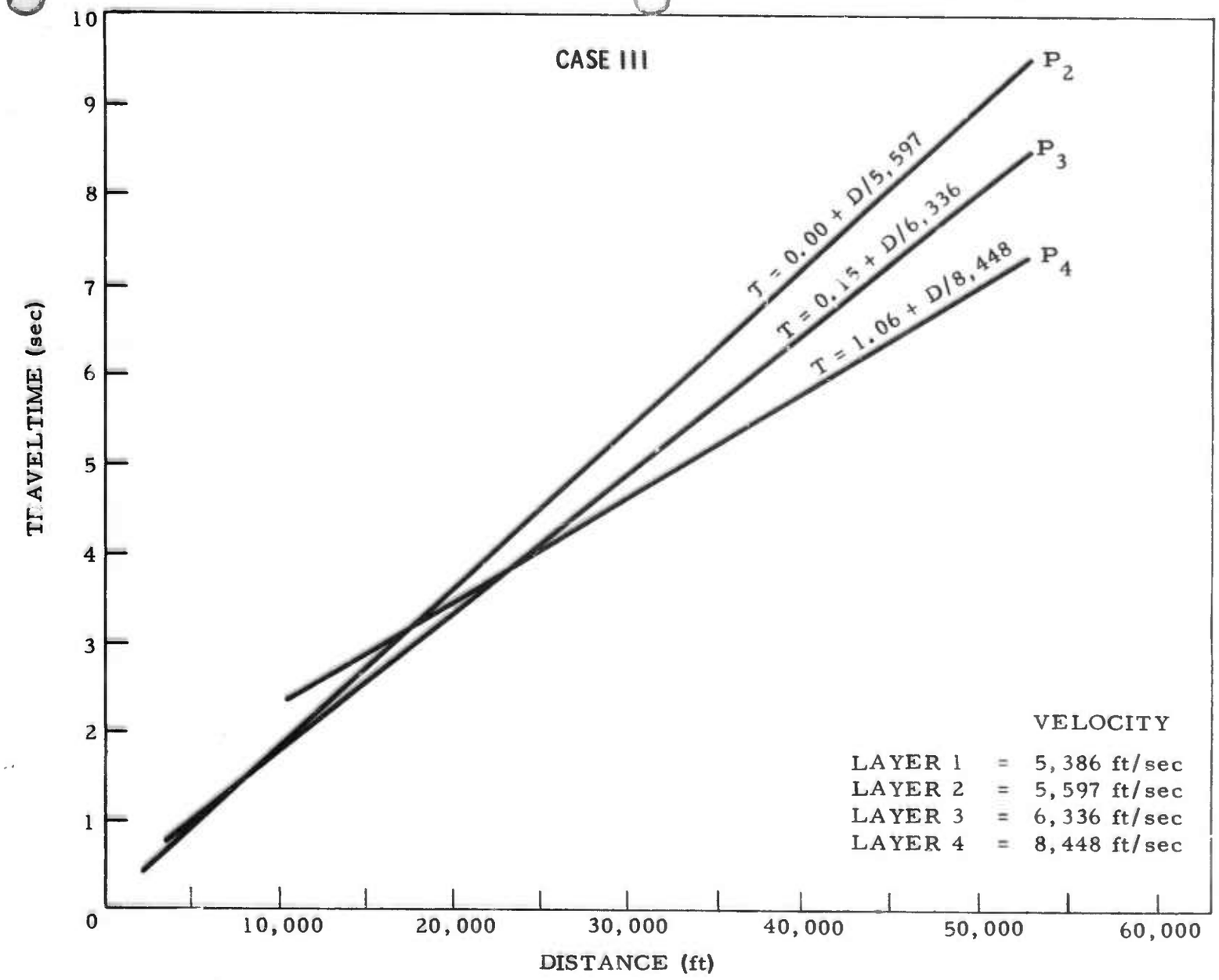


Figure II-25b. $P_3$ Refraction Traveltimes, Case III

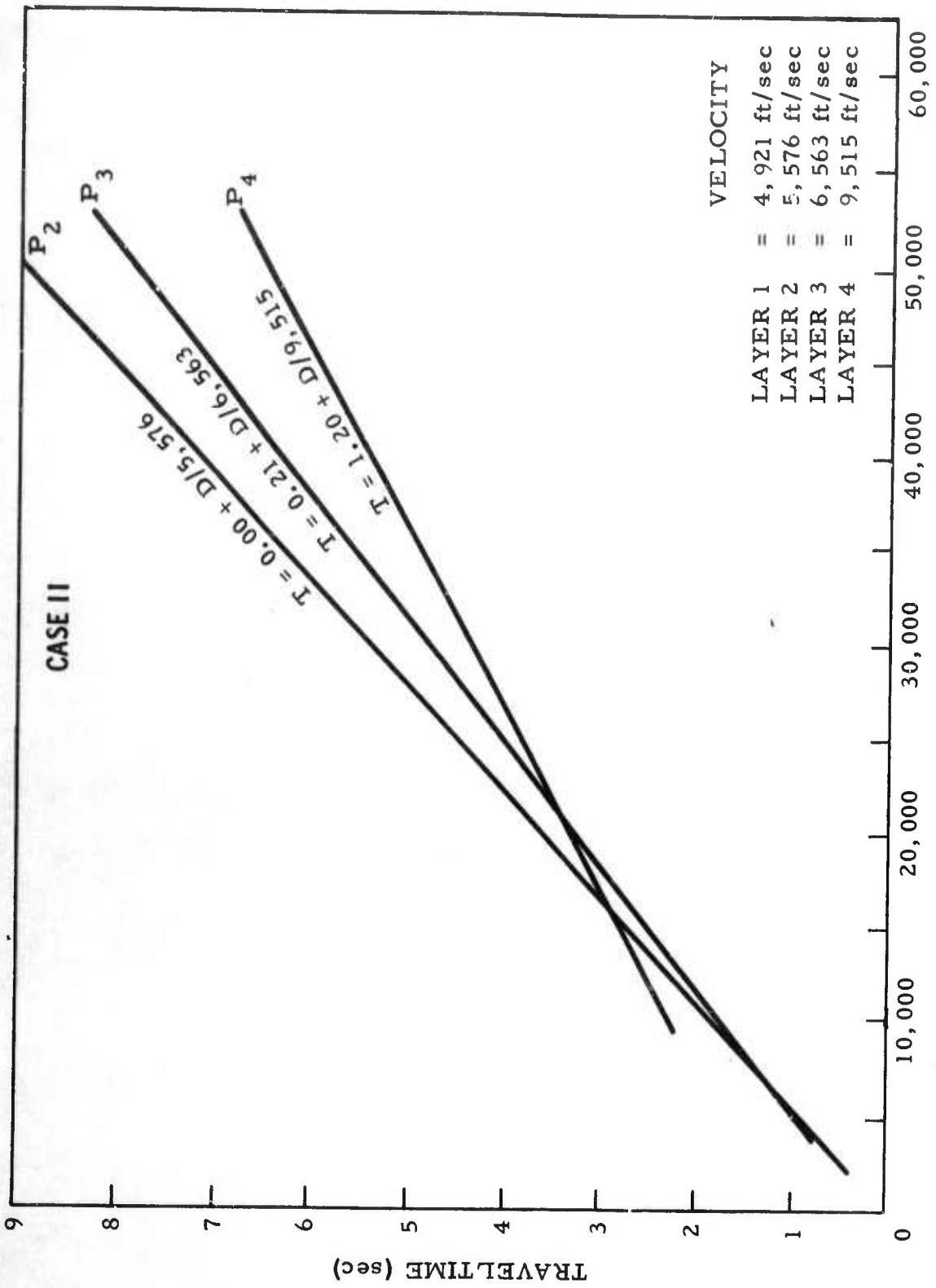


Figure II-25a. $P_3$ Refraction Traveltimes, Case II

Table II-3

$P_3$ REFRACTION TRAVELTIMES

| Source-Receiver Distance (ft) | Traveltimes (sec) | | |
|---|---|---|---|
| | Case I | Case II | Case III |
| 12,144 | 2.032 | 2.070 | 2.076 |
| 13,728 | 2.273 | 2.311 | 2.326 |
| 15,312 | 2.516 | 2.552 | 2.576 |
| 16,896 | 2.756 | 2.794 | 2.826 |
| 20,064 | 3.239 | 3.276 | 3.326 |
| 21,648 | 3.480 | 3.518 | 3.576 |
| 23,232 | 3.721 | 3.759 | 3.826 |
| 25,344 | 4.043 | 4.081 | 4.160 |
| Mud-layer thickness (ft) | 817 | 1017 | 817 |

Table II-4

EWING'S TRAVELTIME MODEL PARAMETERS, $P_3$ REFRACTOR

| Compressional Velocity ($\alpha$) (ft/sec) | Shear Velocity ($\beta$) (ft/sec) | Relative Density ($\rho$) (ft/sec) | Layer Thickness (H)- (ft) |
|---|---|---|---|
| 4,921 | — | 5,438 | 200 |
| 5,576 | 422 | 6,600 | 50 |
| 5,576 | 607 | 6,600 | 100 |
| 5,576 | 792 | 6,600 | 50 |
| 5,576 | 1,056 | 7,920 | — |

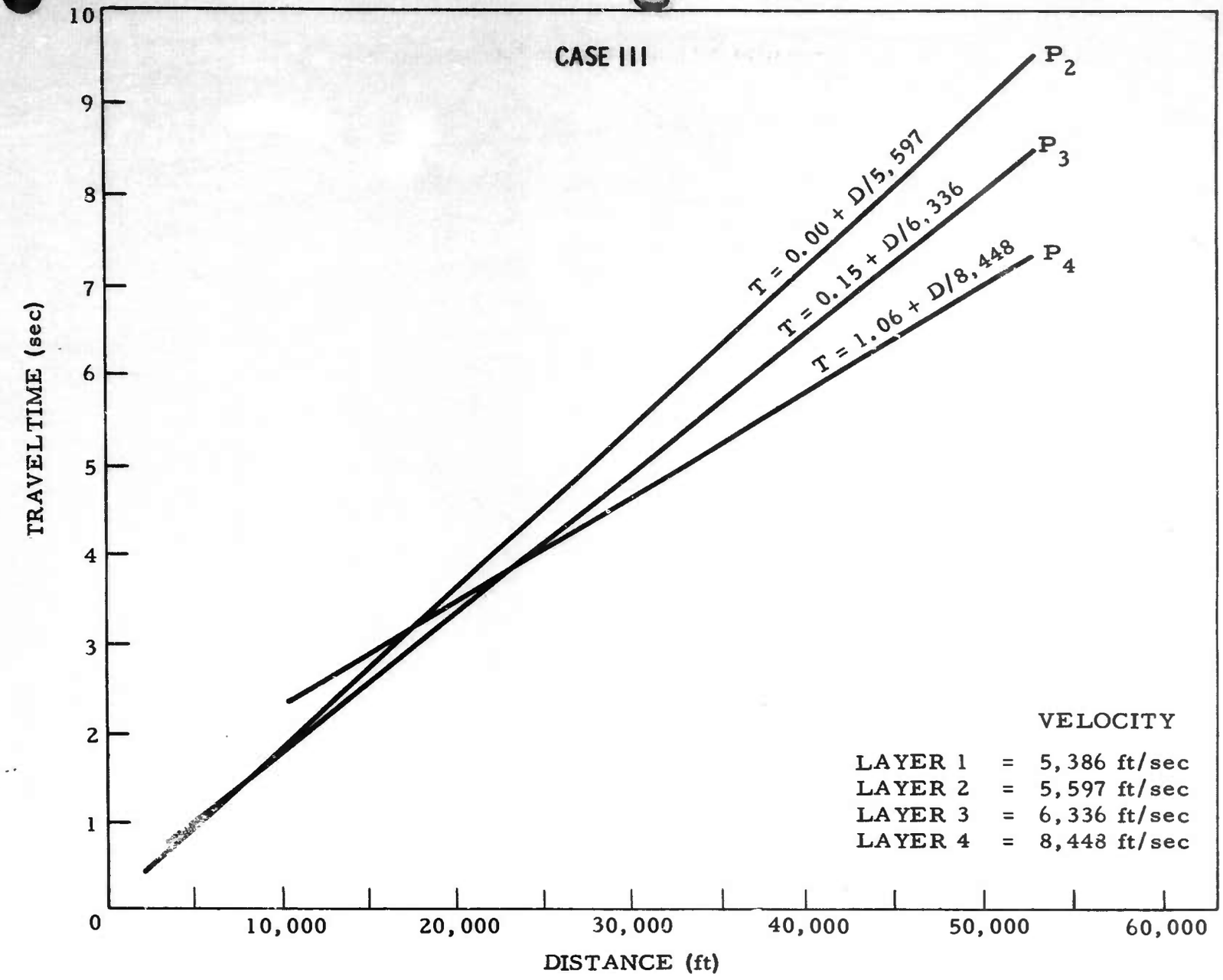


Figure II-25b. $P_3$ Refraction Traveltimes, Case III

Table II-3

$P_3$ REFRACTION TRAVELTIMES

| Source-Receiver Distance (ft) | Traveltimes (sec) | | |
|---|---|---|---|
| | Case I | Case II | Case III |
| 12,144 | 2.032 | 2.070 | 2.076 |
| 13,728 | 2.273 | 2.311 | 2.326 |
| 15,312 | 2.516 | 2.552 | 2.576 |
| 16,896 | 2.756 | 2.794 | 2.826 |
| 20,064 | 3.239 | 3.276 | 3.326 |
| 21,648 | 3.480 | 3.518 | 3.576 |
| 23,232 | 3.721 | 3.759 | 3.826 |
| 25,344 | 4.043 | 4.081 | 4.160 |
| Mud-layer thickness (ft) | 817 | 1017 | 817 |

Table II-4

EWING'S TRAVELTIME MODEL PARAMETERS, $P_3$ REFRACTOR

| Compressional Velocity ($\alpha$) (ft/sec) | Shear Velocity ($\beta$) (ft/sec) | Relative Density ($\rho$) (ft/sec) | Layer Thickness (H)- (ft) |
|---|---|---|---|
| 4,921 | — | 5,438 | 200 |
| 5,576 | 422 | 6,600 | 50 |
| 5,576 | 607 | 6,600 | 100 |
| 5,576 | 792 | 6,600 | 50 |
| 5,576 | 1,056 | 7,920 | — |

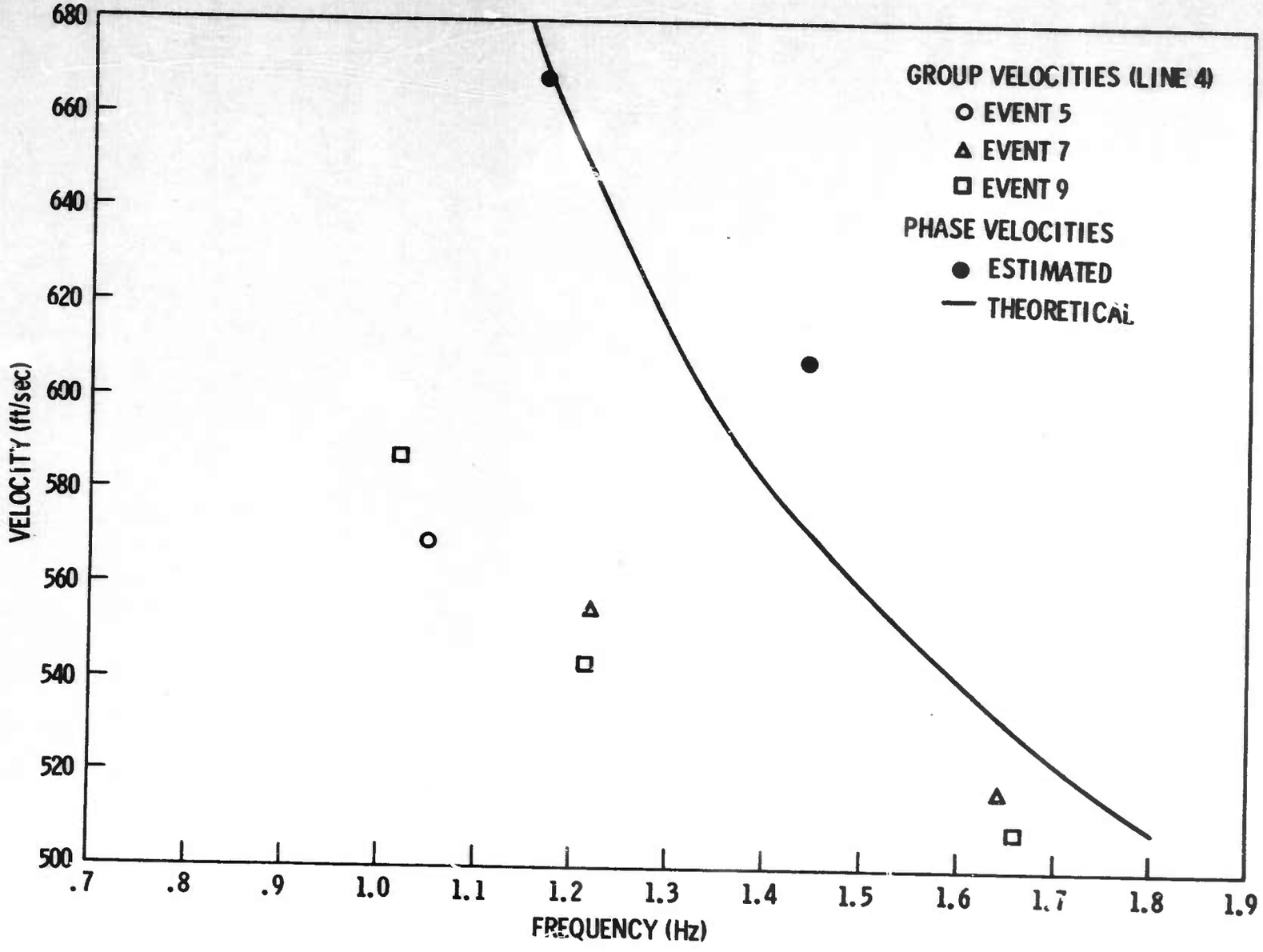


Figure II-26. Group and Phase Velocities (Observed and Theoretical)

the position of the various traveling wave components comprising the total wave motion. As Laster et al[5] have observed, the stationary phase approximation for moderate distances and times may be more in error in some cases than is realized.

As mentioned earlier, observed wavetrains indicate the presence of well-defined sedimentary layers. Shear-mode energy near 1.0 Hz would be confined primarily to the upper 240 ft of sediments ($\lambda = C/F \leq 800$ ft, $\sigma \approx \lambda/4 = 200$ ft). More than one mode of propagation may be excited, leading to complicated motion at distances sufficiently short that the separate modal waveforms overlap and interfere. This is apparently the case for the portions of the data traces denoted in Figure II-21 as Love and shear energy. The horizontals are responding to multiple-mode energy and are not readily interpreted. For the low-velocity wave, pressure and horizontal amplitudes are weak, while vertical amplitude is strong. This result has been predicted from mode-theory considerations.[5]

A model of sedimentary layering in the upper 300 ft of the OBS drop area was constructed to examine this low-velocity phenomenon further. Model parameters are given in Table II-4. Theoretical dispersion curves can be computed from this model and compared against experimental dispersion measurements. In this way, shear-velocity structure in the upper ocean-bottom sediments can be defined, making possible a better understanding of the role and importance of modal propagation of seismic energy through these very soft (low-rigidity) deposits. The theoretical phase-velocity dispersion curve obtained for the model in Table II-4 is displayed by the continuous curve in Figure II-26. Determination of the group-velocity dispersion curve is not possible at this time because the computer program has been hampered by accuracy problems over much of the frequency range of interest.

The behavior of the group-velocity curve is of great importance with regard to the branch of inverse dispersion that has been measured, since the existence of a group-velocity minimum is implied to satisfy such observations. Higher-order modes also could possibly contribute to part of the experimental dispersion curves. At present, the question is an open one, and further calculations are needed to resolve it.

An attempt was made to determine phase velocities by visual correlation of peaks between traces from adjacent shotpoints. In Figure II-26, the phase-velocity estimates are superimposed as data on the theoretically predicted curve. The general shear-velocity gradient and layer thicknesses are certainly correct; however, the model phase-velocity dispersion curve is quite sensitive to relatively small changes in the shear-velocity gradient in the upper 250 ft of sediment. Improvements in the match between experimental and theoretical dispersion curves depend on better estimates from the data. If more of the shot data were digitized, a more precise determination of the shear-velocity gradient in the Gulf Coast ocean-bottom sediments would be possible.

b. Signal Spectra and Coherence

Power spectra and 2-channel coherences were computed over two intervals of the shot-1 (line-1) explosion wavetrain. This record (No. 1) was the only one used for investigating the frequency-domain characteristics of the various seismic arrivals (signal) displayed in Figure II-21. The first gate consisted of 12.5 sec, beginning near the first refracted arrival.

Several refractions are visible on the vertical and pressure traces. Strong motion of long duration also occurs on the horizontal traces. Of the four instruments, the least excited is the vertical, with only the refractions and a very high-frequency low-amplitude arrival clearly present in most cases. On the pressure trace, a relatively large-amplitude more-or-less sinusoidal wave pattern (1 Hz to 5 Hz) can be seen. This phenomenon is identified as being predominantly a leaking mode, similar to that described by Su et al.[6]

Power spectra of the pressure and vertical components are shown in Figure II-27; their close similarity is apparent. Both the horizontal and vertical signal spectra, as well as the corresponding noise spectra, are displayed in Figure II-27, where strong narrowband energy is observed to be centered about 3.5 Hz, 4 Hz, 5 Hz, 5.3 Hz, and 6.2 Hz on the horizontal seismometers.

All instruments sense the relatively broadband noise peak around 1 Hz, but the vertical component additionally appears to have a small signal peak just below 1 Hz. The existence of long-lasting strong motion on the horizontal components can be partially interpreted using the normal-mode results of Sykes and Oliver;[7] they found that surface waves corresponding to propagation in Love modes and in certain shear modes are very sensitive to the shear velocity and thickness of a low-rigidity sedimentary layer. In particular, two families of shear modes exist: one, which includes the fundamental Rayleigh mode, is primarily sensitive to variations in water depth; the other, to the properties of a low-rigidity layer. Thus, the horizontal motion observed by the OBS units following the arrival of the leaky-mode energy may consist of a mixture of these two types of shear waves. At frequencies above 1 Hz, both families of shear modes can exhibit large horizontal-to-vertical motion at the water-sediment interface.

Figure II-28 gives the frequency-aligned power spectra and 2-channel coherences for the horizontal components of unit 19. This figure implies a strong similarity between horizontal waveforms within a unit. A notable degree of similarity across a very broad frequency band above 3 Hz is indicated by the 2-channel coherence for the pressure traces between units (Figure II-27). Such behavior is consistent with the presence of high-phase-velocity leaking-mode energy.

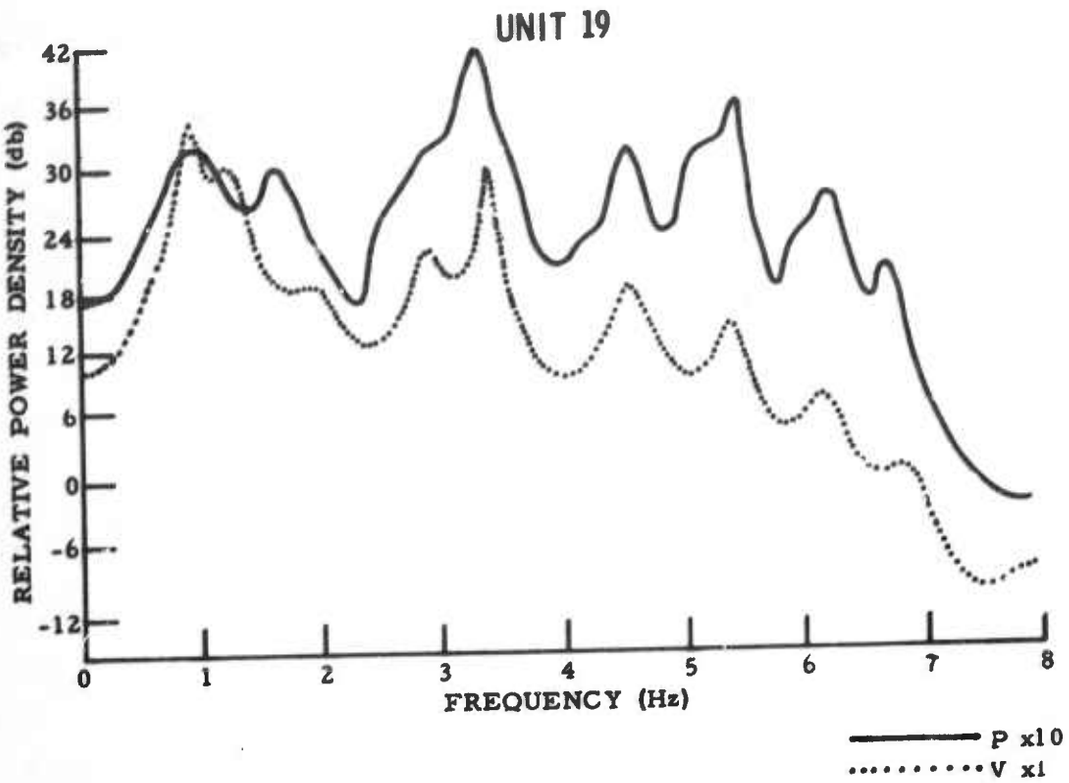


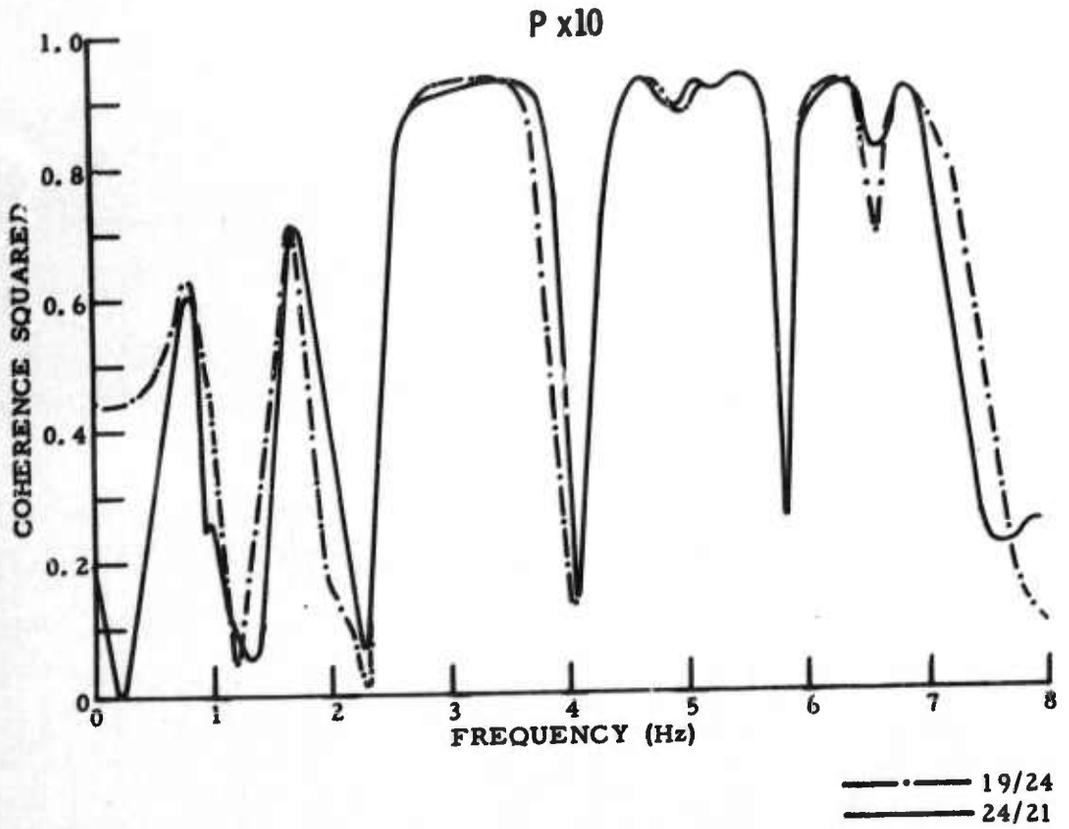


Figure II-27. Early-Arriving Signal Spectra: P x10 and V x1, Unit 19 (Top); P x10 and Noise Coherence (Bottom)

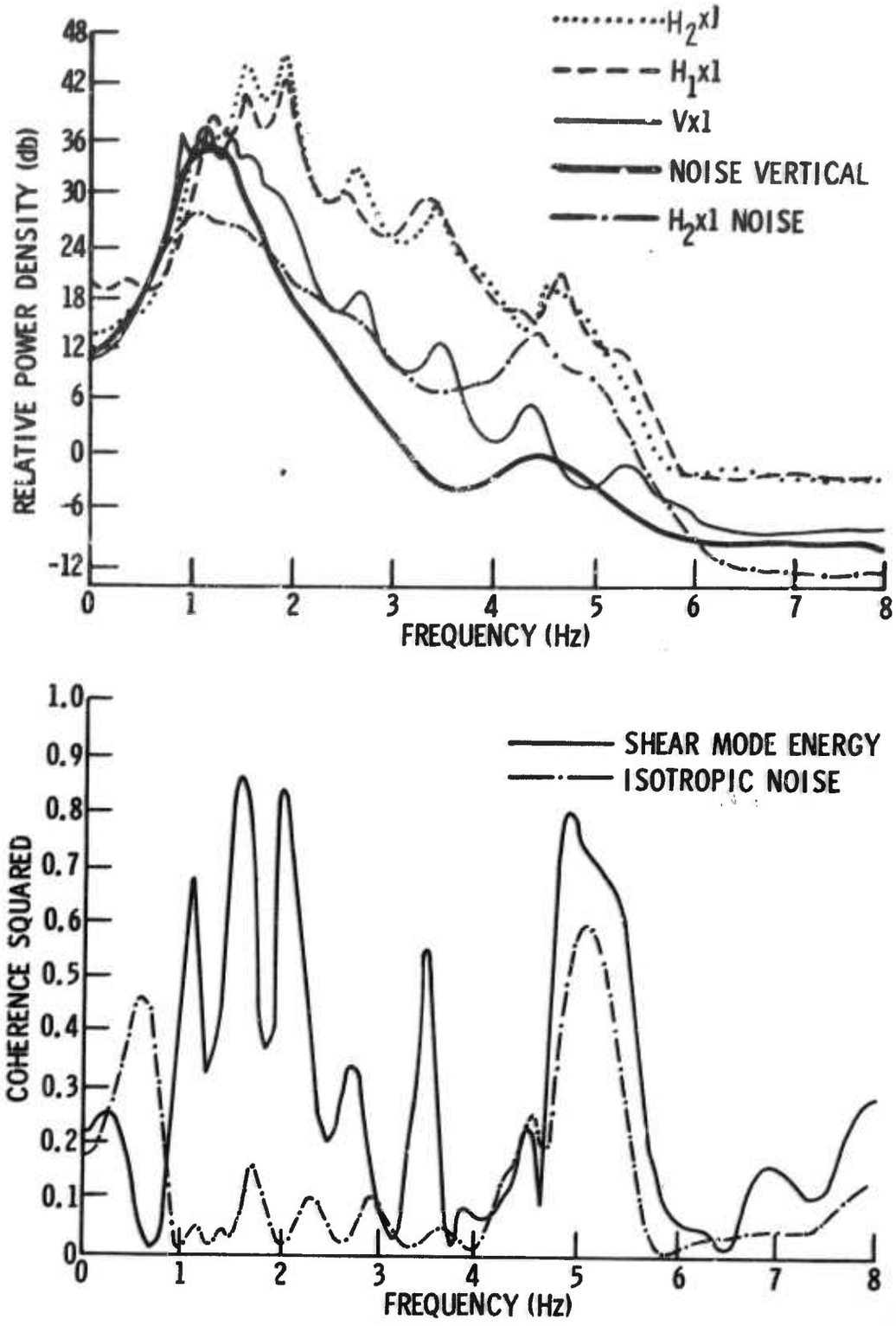


Figure II-28. Early-Arriving Signal Spectra: V, P, $H_1$, and $H_2$, Unit 19 (Top); Intraunit Coherence, $H_1$ x1/$H_2$ x1, Noise (Bottom)

The second data gate consisted of approximately 17.2 sec, beginning with the predominantly horizontal motion which precedes the large, slow, shear-wave arrival midway on the signal wavetrain. The first part of this interval may be partly occupied by Love-mode energy followed by at least one and probably several shear modes. An estimate of the group velocity near 1.4 Hz for the large-amplitude shear arrival is approximately 800 fps.

Figure II-29 gives vertical and horizontal signal and noise power spectra as observed on unit 19. Also in this figure are the corresponding 2-channel coherences computed between unit-19 horizontals. Again, the signal energy is concentrated in narrow frequency bands; the virtually identical horizontal power spectra peak around 1.5 Hz, 1.9 Hz, 2.7 Hz, 3.5 Hz, and 4.8 Hz, respectively, and the signal energy is strongly coherent. The vertical seismometer measures narrow energy bands around 2.7 Hz, 3.6 Hz, 4.5 Hz, and 5.5 Hz. There has been no attempt to derive a theoretical amplitude spectrum from normal-mode theory to compare with these experimental results. Proper definition of the seismic source will be one of the greatest uncertainties in any such calculations.

## D. CONCLUSIONS

The spectral analysis of the Gulf recorded data results in the following conclusions.

- System performance is not measurably affected by the described unit modifications (e.g., heavy anchor, anchor pads, different silastic).
- The Hall-Sears seismometer package is operationally similar to the EV-17 and more dependable since its horizontals are less sensitive to leveling problems.

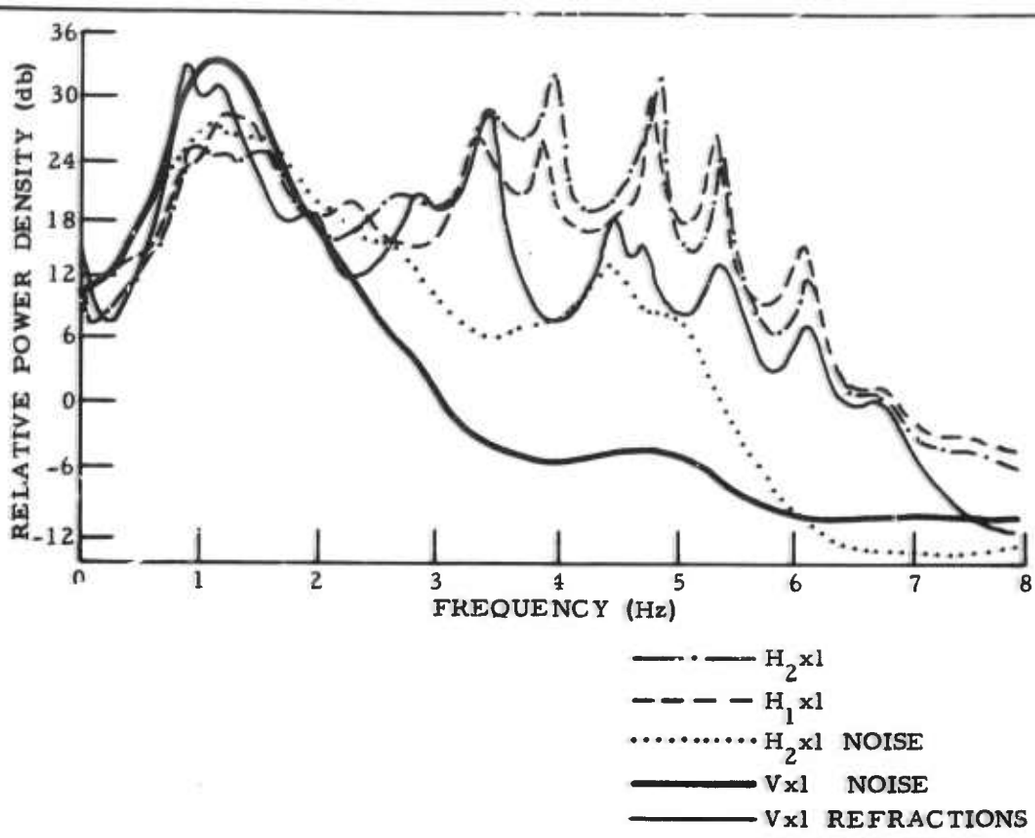


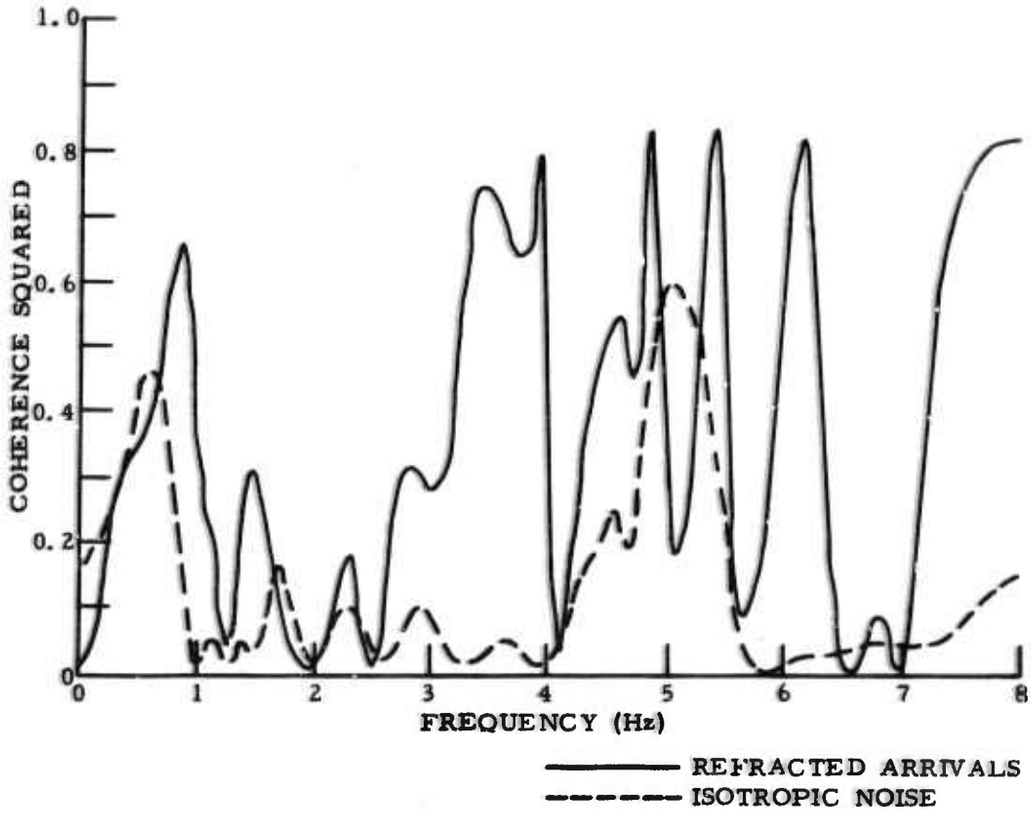


Figure II-29. Shear (Rayleigh) Mode and Noise Spectra: V x1, $H_1$ x1, $H_2$ x1, Unit 19 (Top); Shear (Rayleigh) Mode and Noise Coherence: $H_2$ x1 / $H_1$ x1 (Bottom)

- Shallow bottom sediments in the test area are highly layered, supporting several propagation modes. Shear velocities vary rapidly in these shallow sediments. Very low-velocity Rayleigh-type wave motion is observed from explosions, following refracted arrivals and higher-velocity normal modes; these low-velocity arrivals are probably dispersive Stoneley waves of the type described by Davies.[2]

- Signal energy on the horizontals immediately following the refracted arrivals is a combination of leaking modes and shear modes.

- The dominant ambient noise appears to be isotropic and of low velocity (approximately 600 fps); this results from unusually well-defined shallow mud layers and may serve to explain much of the difference between ocean-bottom and land recordings.

The degree to which these results, especially those pertaining to the noise field, can be extrapolated to other ocean-bottom areas is not known. Certainly, continued investigation in other oceanic areas is indicated. However, previous OBS experiments[8,9] indicate general agreement with these results, and ocean-bottom ambient noise appears likely to be generally isotropic; very low propagation velocity due to mud-layering also could exist.

## SECTION III

## REFERENCES


1. Texas Instruments Incorporated, 1968: Ocean-Bottom Seismograph System-Response Study, Contract F33657-67-C-1341, 31 Jan.

2. Davies, D., 1965, Dispersed Stoneley waves on the ocean bottom: Bull. Seis. Soc. Am., v. 55, n. 5, p. 903-918, Oct.

3. Ewing, J., J. Antoine, and M. Ewing, 1960: Geophysical Measurements in the Western Caribbean Sea and in the Gulf of Mexico, JGR65, p. 4087-4126.

4. Laster, S. J., J. G. Foreman, and A. F. Linville, 1965, Theoretical investigation of modal seismograms for a layer over a half-space: Geophysics, v. 30, p. 571-596.

5. Texas Instruments Incorporated, 1962: Ocean-Bottom Seismometer Data Analysis Program, Semiannual Tech. Rpt. No. 3, Contract AF 19(604)-8368, Appendix C, 15 Nov.

6. Su, S. S., and J. Dorman, 1965, The use of leaking modes in seismogram interpretation and in studies of crust-mantle structure: Bull. Seis. Soc. Am., v. 55, p. 989.

7. Sykes, Lynn R., and Jack Oliver, 1964, The propagation of short-period seismic surface waves across oceanic areas, part I-theoretical study: Bull. Seis. Soc. Am., v. 54, n. 5, part A, p. 1349-1372.

8. Texas Instruments Incorporated, 1961: Ocean-Bottom Seismometer Data Analysis Program, Contract AF 19(604)-8368, 15 Mar.

9. Texas Instruments Incorporated, 1964: Ocean-Bottom Seismometer Data Collection and Analysis, Final Rpt., Contract AF 19(604)-8368, 12 Oct.

10. Amos, D. G., and L. H. Koopmans, 1963: Tables of the Distribution of the Coefficient of Coherence for Stationary Bivariate Gaussian Processes, Sandia Corporation Monography, Mar.

11. Blackman, R. B., and J. W. Tukey, 1959: The Measurement of Power Spectra from the Point of View of Communications Engineering, Dover Publications, New York, N. Y.

12. Parzen, E., 1961, Mathematical considerations in the estimation of spectra: Technometrics, v. 3, p. 167-190.

# APPENDIX A

# ELECTRICAL AND MECHANICAL SPECIFICATIONS OF OCEAN-BOTTOM SEISMOGRAPHS

# APPENDIX A

## ELECTRICAL AND MECHANICAL SPECIFICATIONS OF OCEAN-BOTTOM SEISMOGRAPHS

| Unit | Dimensions (in.) | Weight (lb) | Electrical and/or Mechanical Specifications |
|---|---|---|---|
| Anchor | 42.5 diameter x 16 height | ≈ 335 | None |
| Sphere (upper and lower hemispheres and pressure ring) | 40.5 OD x 36.75 ID | ≈ 1000 | Spun from 7178 aluminum alloy<br>Maximum operating pressure: 11,500 psi |
| Release mechanism | 15.5 x 3.5 x 1.5 | 2.5 | 15-v dc input to burn fuse wire |
| Hydrophone | 5.5 diameter x 8.625 height | 12 | Capacitance: 0.0158 to 0.0168 μf<br>Sensitivity: 2.2 v/psi<br>Impedance: 20 MΩ negative to ground;<br>(minimum) 50 MΩ positive to ground;<br>100 MΩ positive to negative<br>Crystal type: Clevite PZT-4 |
| Radio beacon | 12.6 x 4.3 x 2.4<br>Antenna length: 48 | 2 | Power output: 3 w<br>Power input: 15 v dc at 1 amp (during ON time)<br>Frequency: 26.670 MHz (±0.005%)<br>Modulation: 90% with 400-Hz tone<br>Duty cycle: nominal 0.1-sec ON time every 0.5 sec<br>Standby power input: 15 v dc at 3 ma<br>Power source: B-1000 |
| Seismometers:<br>Mark III and Mark IV | 15 x 13 x 13 | 35<br>(Mass of suspension: 2760 gm) | Coil excursion: vertical - ±0.125 in.<br>horizontal - ±2 mm<br>Tilt angle: ±2° all directions with no more than 2% frequency change<br>Sensitivity: 480 v/m/sec open circuit;<br>384 v/m/sec at 0.6 critical damping<br>Coil resistance: 5000 Ω<br>Damping: 20,000 Ω for 0.6 critical<br>Natural frequency: 1(±0.05) Hz |
| Mark V | 15.75 x 6.875 x 6.875 | 35<br>(Mass of suspension: (941 gm) | Coil Excursion: vertical: ±0.250 in.<br>horizontal: ±0.250 in.<br>Tilt Angle: 3° all directions with no more than 2% frequency change.<br>Sensitivity: 258 v/m/sec at 0.6 critical damping<br>Coil resistance: 4100 (±25) ohms<br>Damping: 21,000 Ω for 0.6 critical<br>Natural frequency: 1(±0.03) Hz<br>Calibration coil sensitivity: 1.1 mμ/μa at 0.6 critical |
| Digital clock | 8.0 x 4.25 x 4.75 | 2.25 | Oscillator frequency: 1.6384 MHz<br>Outputs: 400-Hz square wave at 3 v pp;<br>12.5-Hz square wave at 1.5 v pp<br>Real-time and identification code: 1/min superposed over 1-sec timing pulses at 2.1 v pp<br>Anchor release pulse: 4 sec (Mark III);<br>9 sec (Mark IV and Mark V)<br>Timing accuracy: ±0.1 sec/30 days<br>Power input: 3 v dc at 100 ma from B-400;<br>15 v dc at 5 ma from B-200 |
| Backup clock | 7.75 x 5.5 x 2.0 | 1.50 | Power input: 3 v dc at 50 ma from B-500;<br>15 v dc from B-600<br>Output: relay closure and time signal to recorder<br>Release setting accuracy: ± 15 min<br>Clock drift: 2 sec/day maximum |

| Name | Dimensions (in.) | Weight (lb) | Electrical and/or Mechanical Specifications |
|---|---|---|---|
| Bias oscillator | 6.0 x 2.25 x 3.0 | 0.75 | Power input: 12 v dc (regulated) at 3.4 ma<br>Output: 1.5 v pp, 145-Hz sine wave<br>Temperature range: -20 to 130°F (ambient) |
| Sonar receiver | 9.7 x 4.5 x 2.25 | 2.0 | Power input: 3 v dc at 30 ma<br>Signal input capacitance: 0.0033 μf, resonant at 5.9 kHz, 6.5 kHz<br>Sensitivity: 1 μv rms for activation of release relay<br>Output relay closure: Relay with 2 amp SPST normally open contacts<br>Code frequencies: Code 1 - 5.9 kHz; Code 2 - 6.5 kHz |
| Release relay box | 4.5 x 2.25 x 2.5 | - - - | Inputs: Sonar coded; digital-clock preselected time; backup-clock preselected time; sump-switch emergency water leak |
| Battery power supply | | | Outputs: |
| B-100 | 10.75 x 7.0 x 4.0 | 14.4 | 15 v dc, 27 ma |
| B-200 | 10.75 x 7.0 x 4.0 | 14.4 | 15 v dc, 32 ma |
| B-300 | 6.0 x 3.25 x 7.5 | 7.7 | -12 v dc, 7 ma (except Mark III) |
| B-400 | 9.5 x 4.0 x 3.0 | 7.7 | 3 v dc, 100 ma |
| B-500 | 3.0 x 3.75 x 6.25 | 5.0 | 3 v dc, 80 ma |
| B-600 | 8.5 x 3.25 x 2.0 | 2.8 | 15 v dc |
| B-700 | 3.0 x 1.59 x 5.625 | 1.62 | 510 v dc |
| B-1000 | 10.75 x 7.0 x 4.0 | 14.4 | 15 v dc |
| Beacon light | 9.5 x 12.75 x 8.0 | 12 | Power input: 510 v dc from B-700<br>Flash rate: 0.25 sec each 5 sec |
| Recorder | 16.5 x 10.5 x 5.5 | 14 (with reels)<br>10 (without reels) | Tape speed: 0.0075 ips<br>Speed variation: wow and flutter <1%<br>Reel capacity: 1800 ft, 1 mil thick, 1 in. wide<br>Reel size: 8-in. diameter<br>Power input: 12 v dc at 30 ma (regulated)<br>Signal input impedance: 10 K, 5 v pp for full-level recording<br>Frequency response: 0.25 to 14 Hz<br>Magnetic head:<br>Inductance: 100 mH<br>dc resistance: 150 Ω<br>Tracks: 14 IRIG standard<br>Track width: 0.050 in.<br>Track spacing: 0.070 in. on centers<br>Dynamic range: 30 db<br>Type of recording: direct record<br>Number of tracks: 14 IRIG analog standard<br>Recording time: 33 days |
| Control box | 10 x 7 x 3 | - - - | None |
| Reactance amplifier (Mark IV and Mark V) | 12 x 6 x 5 | 5.06 | Input power: 15 v dc at 27 ma from B-200<br>Voltage gain: 106 db, 60-db attenuation provided in 6-db steps<br>Input impedance: 20 K to seismometer channels, 6 M to hydrophone channels<br>Frequency response: 1.5 to 8.5 Hz ±3 db (limited by filters) |
| Trilevel amplifier (Mark IV and Mark V) | 7.25 x 3.25 x 3.25 | 2 | Input power: +15 v dc from B-200<br>Voltage gain: preset at factory, no adjustment required; each gain labeled on the circuit board |

# APPENDIX B
# TEST SPECIFICATIONS

# APPENDIX B

## TEST SPECIFICATIONS

| TI Drawing | Name |
|---|---|
| 121900 | OBS System Test Procedure |
| 121901 | Pressure-Transducer Unit Test |
| 121903 | Seismometer-System Unit Test |
| 121904 | RA-6 Preamplifier Unit Test |
| 121905 | Trilevel-Amplifier Unit Test |
| 121906 | Bias-Oscillator Unit Test |
| 121908 | Sonar Receiver Unit Test |
| 121910 | Digital-Clock Unit Test |
| 121913 | Blinker-Light Unit Test |
| 121914 | Recorder Unit Test |
| 121915 | Recorder 30-Day Test |
| 121916 | Radio-Beacon Unit Test |
| 121918 | Trilevel-Amplifier Unit Test |
| 121917 | Operational-Amplifier Unit Test |
| 128982 | Backup-Clock Unit Test |

# APPENDIX C

# MATHEMATICAL DERIVATIONS OF COHERENCES

# APPENDIX C
## MATHEMATICAL DERIVATIONS OF COHERENCES

Defined are some of the mathematical forms used in the spectral analysis. Two types of spectra are considered: energy-density spectra and power-density spectra. Energy-density spectra measure the energy density of a transient waveform as a function of frequency. Power-density spectra are similar functions which estimate the power density of a random stochastic time series.

Both types of spectra may be obtained by Fourier-transforming an autocorrelation function of the transient or time-series sample under consideration. The autocorrelation function $\Phi_{kk}(\tau)$ is defined as

$$\Phi_{kk}(\tau) = \lim_{T\to\infty} \frac{1}{2T} \int_{-T}^{T} f_k(t)\, f_k(t+\tau)dt \qquad -T \le \tau \le T$$

where 2T is the length of the sample of time series $f_k(t)$ under consideration.

The Fourier transform $\Phi(\omega)$ of function $\Phi(\tau)$ is defined as

$$\Phi(\omega) = \int_{-\infty}^{\infty} \Phi(\tau)\, e^{-i\omega\tau} d\tau \qquad -\infty < \omega < \infty$$

where $\omega$ is angular frequency.

Estimates of the coherence $C(\omega)$ between any two time series (k and j, for instance) are obtained by computing

$$C(\omega) = \frac{\Phi_{kj}(\omega)\ \Phi_{kj}^{*}(\omega)}{\Phi_{kk}(\omega)\ \Phi_{jj}(\omega)} \qquad -\infty < \omega < \infty$$

where $\Phi_{kk}(\omega)$ and $\Phi_{jj}(\omega)$ are the power-density spectra at frequency $\omega$ of the $k^{th}$ and $j^{th}$ time series, respectively; $\Phi_{kj}(\omega)$ is the crosspower density spectrum for the same pair of time series; and the asterisk denotes complex conjugate. Crosspower-density spectra are estimated by Fourier-transforming the crosscorrelation function $\Phi_{kj}(\tau)$, which is defined as

$$\Phi_{kj}(\tau) = \lim_{T \to \infty} \frac{1}{2T} \int_{-T}^{T} f_k(t)\, f_j(t + \tau)\, dt \qquad -T < \tau < T$$

Coherence as a function of frequency is a measure of the similarity of two time series. This similarity does not require identical waveforms for the two time series but rather an unvarying phase or time dependence of one or the other. If there is complete phase dependence at a particular frequency $\omega$, one time series is completely predictable from the other at that frequency and $C(\omega)$ is identically 1. If the two time series have no constant phase relationship at a particular frequency $\omega$ (such as two random number series), no prediction is possible and $C(\omega)$ is identically 0. Values of $C(\omega)$ between 1 and 0 indicate that only a portion of the energy at frequency $\omega$ is coherent.

This definition for coherence (which is used in this report) is more properly termed coherence squared, when compared with the definition given by Amos and Koopmans,[10] which appears to be in more common usage:

$$C(\omega) = \frac{\Phi_{kj}(\omega)}{\sqrt{\Phi_{kk}(\omega)\, \Phi_{jj}(\omega)}} \qquad \begin{matrix} \Phi_{kk}(\omega) \pm o \\ \Phi_{jj}(\omega) \pm o \end{matrix}$$

The function is a normalized measure of coherence and, in general, is complex-valued. When written in the polar form, the modulus $\gamma(\omega)$ measures the intensity of the coherence and the argument $\theta(\omega)$ measures the average phase difference between $f_k(t)$ and $f_j(t)$ at frequency $(\omega)$.

In practice, infinitely long data samples and infinite frequency ranges are impossible to consider; therefore, many techniques have been developed to obtain valid power estimates from finite samples.[11,12]

This problem does not arise with transients since the interval 2T can be made sufficiently long to encompass the entire transient function. Transient functions are not often treated, however, but rather mixtures of transients and random time series.

The technique used in this report to obtain stabilized spectral estimates has involved computation of the autocorrelation of the time series and then design of a time-domain filter to "whiten" the autocorrelation (i.e., a filter, the frequency-domain response of which is the inverse of the Fourier transform of the autocorrelation). The filter's response (and ultimately its inverse) is exact and can be directly estimated without the distortion normally encountered when Fourier-transforming a truncated autocorrelation.

UNCLASSIFIED

Security Classification

**DOCUMENT CONTROL DATA - R&D**

*(Security classification of title, body of abstract and indexing annotation must be entered when the overall report is classified)*

1. ORIGINATING ACTIVITY (Corporate author)
Texas Instruments Incorporated
Science Services Division
P. O. Box 5621, Dallas, Texas 75222

2a. REPORT SECURITY CLASSIFICATION
Unclassified

2b. GROUP
—

3. REPORT TITLE
OCEAN-BOTTOM SEISMOGRAPH PRODUCTION AND GULF OF MEXICO DATA ANALYSIS – FINAL REPORT

4. DESCRIPTIVE NOTES (Type of report and inclusive dates)
Final Report

5. AUTHOR(S) (Last name, first name, initial)
BeAbout, Edgar G. Howard, R. Fred Johnson, William A.
Harris, Hugh K. Kimler, Benjamin F.

| 6. REPORT DATE | 7a. TOTAL NO. OF PAGES | 7b. NO. OF REFS |
|---|---|---|
| 31 July 1968 | 87 | 12 |

8a. CONTRACT OR GRANT NO.
F33657-68-C-0242

b. PROJECT NO.
VELA T/8701/ASD

c.

d.

9a. ORIGINATOR'S REPORT NUMBER(S)
—

9b. OTHER REPORT NO(S) (Any other numbers that may be assigned this report)
—

10. AVAILABILITY/LIMITATION NOTICES
This document is subject to special export controls and each transmittal to foreign governments or foreign nationals may be made only with prior approval of Chief, AFTAC

11. SUPPLEMENTARY NOTES
ARPA Order No. 624
ARPA Program Code No. 7F10

12. SPONSORING MILITARY ACTIVITY
Advanced Research Projects Agency
Department of Defense
The Pentagon, Washington, D.C. 20301

13. ABSTRACT

Six additional Ocean-Bottom Seismographs, similar in design and functionally interchangeable with existing units, were produced. Results of testing the new units showed that system performance is not measurably affected by the unit modifications and that the replacement Hall-Sears seismometer package is operationally similar to the EV-17 but is more dependable.

Shallow bottom sediments in the test area are highly layered, supporting several propagation modes. Shear velocities vary rapidly in these shallow sediments. Very low-velocity Rayleigh-type wave motion is observed from explosions, following refracted arrivals and higher-velocity normal modes; these low-velocity arrivals are probably dispersive Stoneley waves. Signal energy on the horizontals immediately following the refracted arrivals is a combination of leaking modes and shear modes. The dominant ambient noise appears to be isotropic and of low velocity; this results from unusually well-defined shallow mud layers and may serve to explain much of the difference between ocean-bottom and land recordings.

DD FORM 1 JAN 64 1473

UNCLASSIFIED

Security Classification

| 14. KEY WORDS | LINK A | | LINK B | | LINK C | |
|---|---|---|---|---|---|---|
| | ROLE | WT | ROLE | WT | ROLE | WT |
| Ocean-Bottom Sesimograph | | | | | | |
| Highly-Layered Shallow-Bottom Sediments | | | | | | |
| Low-Velocity Rayleigh-Type Wave Motion | | | | | | |
| Isotropic Ambient Noise | | | | | | |

## INSTRUCTIONS

1. ORIGINATING ACTIVITY: Enter the name and address of the contractor, subcontractor, grantee, Department of Defense activity or other organization *(corporate author)* issuing the report.

2a. REPORT SECURITY CLASSIFICATION: Enter the overall security classification of the report. Indicate whether "Restricted Data" is included. Marking is to be in accordance with appropriate security regulations.

2b. GROUP: Automatic downgrading is specified in DoD Directive 5200.10 and Armed Forces Industrial Manual. Enter the group number. Also, when applicable, show that optional markings have been used for Group 3 and Group 4 as authorized.

3. REPORT TITLE: Enter the complete report title in all capital letters. Titles in all cases should be unclassified. If a meaningful title cannot be selected without classification, show title classification in all capitals in parenthesis immediately following the title.

4. DESCRIPTIVE NOTES: If appropriate, enter the type of report, e.g., interim, progress, summary, annual, or final. Give the inclusive dates when a specific reporting period is covered.

5. AUTHOR(S): Enter the name(s) of author(s) as shown on or in the report. Enter last name, first name, middle initial. If military, show rank and branch of service. The name of the principal author is an absolute minimum requirement.

6. REPORT DATE: Enter the date of the report as day, month, year, or month, year. If more than one date appears on the report, use date of publication.

7a. TOTAL NUMBER OF PAGES: The total page count should follow normal pagination procedures, i.e., enter the number of pages containing information.

7b. NUMBER OF REFERENCES: Enter the total number of references cited in the report.

8a. CONTRACT OR GRANT NUMBER: If appropriate, enter the applicable number of the contract or grant under which the report was written.

8b, 8c, & 8d. PROJECT NUMBER: Enter the appropriate military department identification, such as project number, subproject number, system numbers, task number, etc.

9a. ORIGINATOR'S REPORT NUMBER(S): Enter the official report number by which the document will be identified and controlled by the originating activity. This number must be unique to this report.

9b. OTHER REPORT NUMBER(S): If the report has been assigned any other report numbers *(either by the originator or by the sponsor)*, also enter this number(s).

10. AVAILABILITY/LIMITATION NOTICES: Enter any limitations on further dissemination of the report, other than those imposed by security classification, using standard statements such as:

(1) "Qualified requesters may obtain copies of this report from DDC."

(2) "Foreign announcement and dissemination of this report by DDC is not authorized."

(3) "U. S. Government agencies may obtain copies of this report directly from DDC. Other qualified DDC users shall request through

_____."

(4) "U. S. military agencies may obtain copies of this report directly from DDC. Other qualified users shall request through

_____."

(5) "All distribution of this report is controlled. Qualified DDC users shall request through

_____."

If the report has been furnished to the Office of Technical Services, Department of Commerce, for sale to the public, indicate this fact and enter the price, if known.

11. SUPPLEMENTARY NOTES: Use for additional explanatory notes.

12. SPONSORING MILITARY ACTIVITY: Enter the name of the departmental project office or laboratory sponsoring *(paying for)* the research and development. Include address.

13. ABSTRACT: Enter an abstract giving a brief and factual summary of the document indicative of the report, even though it may also appear elsewhere in the body of the technical report. If additional space is required, a continuation sheet shall be attached.

It is highly desirable that the abstract of classified reports be unclassified. Each paragraph of the abstract shall end with an indication of the military security classification of the information in the paragraph, represented as *(TS), (S), (C), or (U)*.

There is no limitation on the length of the abstract. However, the suggested length is from 150 to 225 words.

14. KEY WORDS: Key words are technically meaningful terms or short phrases that characterize a report and may be used as index entries for cataloging the report. Key words must be selected so that no security classification is required. Identifiers, such as equipment model designation, trade name, military project code name, geographic location, may be used as key words but will be followed by an indication of technical context. The assignment of links, rules, and weights is optional.